

Tensor Density Estimator by Convolution-Deconvolution

Yifan Peng¹, Siyao Yang^{*2}, Yuehaw Khoo³, and Daren Wang⁴

^{1,2}Committee on Computational and Applied Mathematics, University of Chicago

³Committee on Computational and Applied Mathematics and Department of Statistics,
University of Chicago

⁴Department of Applied and Computational Mathematics and Statistics, University of
Notre Dame

Abstract

We propose a linear algebraic framework for performing density estimation. It consists of three simple steps: convolving the empirical distribution with certain smoothing kernels to remove the exponentially large variance; compressing the empirical distribution after convolution as a tensor train, with efficient tensor decomposition algorithms; and finally, applying a deconvolution step to recover the estimated density from such tensor-train representation. Numerical results demonstrate the high accuracy and efficiency of the proposed methods.

1 Introduction

Density estimation is a fundamental problem in data science with wide-ranging applications in fields such as science (Cranmer (2001); Chen (2017)), engineering (Chaudhuri et al. (2014)), and economics (Zambom and Dias (2013)). More precisely, given N data points $\{x^{(i)}\}_{i=1}^N \sim p^*$, where each $x^{(i)}$ is an independent and identically distributed (i.i.d.) sample from an unknown ground truth distribution $p^* : \mathbb{R}^d \rightarrow \mathbb{R}$, the goal is to estimate p^* based on empirical distribution

$$\hat{p}(x) = \frac{1}{N} \sum_{i=1}^N \delta_{x^{(i)}}(x) \quad (1)$$

where $\delta_{x^{(i)}}(x)$ is the Dirac delta function centered at $x^{(i)}$. In general, one cannot use the empirical distribution as an estimator of the density p^* , due to the lack of absolute continuity or exponentially large variance.

1.1 Our contributions:

In this paper, we propose a natural approach to density estimation, entirely based on linear algebra. Our goal is to achieve computational complexity that is linear in dimensionality. This is accomplished by viewing the density estimation process as applying a low-dimensional orthogonal projector in function space onto the noisy \hat{p} . Due to the dimension reduction, the exponentially

*Corresponding author

large variance in \hat{p} is suppressed. Additionally, we leverage tensor-train (TT) algebra to perform this projection with linear computational complexity in terms of both dimensionality and sample size. This approach also yields a final density estimator in the form of a tensor train. Furthermore, we theoretically show that, in addition to achieving linear scaling in computational complexity, the estimation error also enjoys linear scaling under certain assumptions. Numerical experiments demonstrate that our estimator outperforms deep learning methods on several tasks, including Boltzmann sampling and generative modeling for real-world datasets. Here we list two remarkable results in Figure 1. More details on the numerical experiments can be found in Section 9.

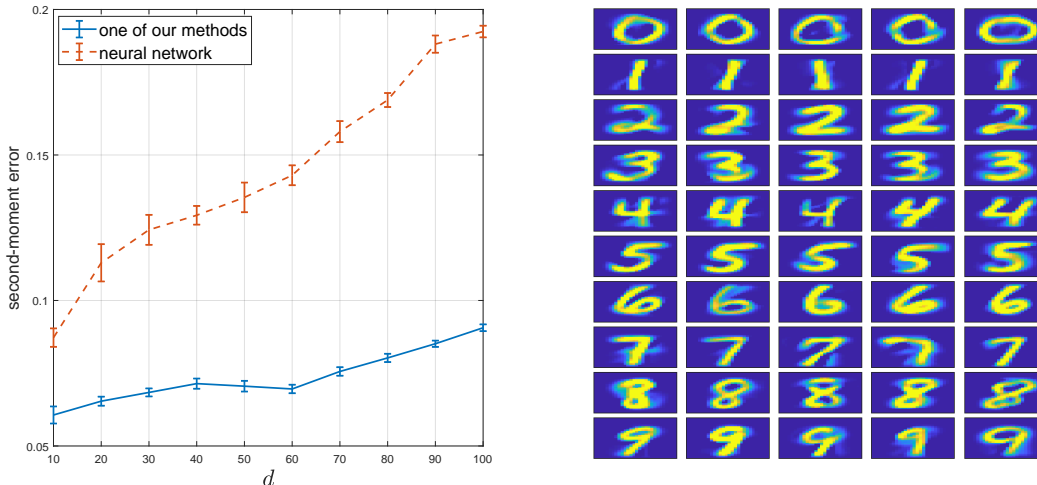


Figure 1: Left: density estimation for data sampled from a Boltzmann distribution. Figure visualizes the second-moment error for different dimensionality d . We compare the result of one of our proposed tensor-train-based method called TT-SVD-kn (see Section 4) with that of one neural network approach (Masked Autoregressive Flow); Right: images generated by another proposed algorithm called TT-rSVD-t (see Section 6) on the MNIST dataset.

1.2 Main idea:

In this subsection, we outline the main idea of the proposed method. Our method is based on a crucial assumption about the true density:

$$p^*(x) = \mu(x) \left(1 + \sum_{j_1=1}^d \sum_{l_1=2}^n b_{l_1}^{j_1} \phi_{l_1}^{j_1}(x_{j_1}) + \sum_{(j_1, j_2) \in \binom{d}{2}} \sum_{l_1, l_2=2}^n b_{l_1 l_2}^{j_1 j_2} \phi_{l_1}^{j_1}(x_{j_1}) \phi_{l_2}^{j_2}(x_{j_2}) \right), \quad (2)$$

where $\mu(x) = \mu_1(x_1) \cdots \mu_d(x_d)$ is a mean-field density, i.e., a separable density. $\{\phi_l^j\}_{l=1}^n$ are orthogonal basis functions with respect to μ_j and $\phi_1^j \equiv 1$, i.e.,

$$\int \phi_{l_1}^j(x_j) \phi_{l_2}^j(x_j) \mu_j(dx_j) = \delta_{l_1, l_2}, \quad (3)$$

and $b_{l_1}^{j_1}, b_{l_1 l_2}^{j_1 j_2}$ are the corresponding coefficients. The indices $(j_1, j_2) \in \binom{d}{2}$ denote all unordered pairs of distinct dimensions. In other words, we view p^* as a perturbative expansion around a mean-field

density μ , where each term in the perturbation series involves only a few variables (up to two variables in (2)). Although it is straightforward to generalize (2) to an expansion that includes higher-order interactions involving more than two variables with decaying coefficients, for clarity of presentation, we use (2) as our default model. Such an expansion is common in perturbation and cluster expansion theory in statistical mechanics.

Based on this setting, we discuss several estimators with increasing levels of sophistication. The first approach to estimate p^* is based on a simple and natural subspace projection:

$$\tilde{p} = \mu \odot (\Phi \text{diag}(w_K) \Phi^T \hat{p}). \quad (4)$$

For notational simplicity, we treat all functions and operators above as discrete matrices and vectors: we regard the concatenation of basis functions

$$\Phi := [\Phi_l(x)]_{x,l}$$

as a matrix with rows indexed by x and columns indexed by l . The operation $\Phi^T \hat{p}$ corresponds to convolution between basis functions and \hat{p} , i.e., summing or integrating out the variable x . The vector w_K , indexed by l , contains the weights associated with the basis functions and depends on a chosen positive integer K . $\text{diag}(\cdot)$ is the operator producing diagonal matrix with the elements of the input vector on the main diagonal. The mean-field μ is also treated as a vector, indexed by x , and \odot denotes the Hadamard (entrywise) product. Intuitively, the operator $\mu \odot (\Phi \text{diag}(w_K) \Phi^T \cdot)$ resembles a projector that projects \hat{p} onto a function space that only involves a small number of variables determined by the chosen integer K . More precisely, let the complete (up to a certain numerical precision) set of k -variable basis functions be defined as:

$$\mathcal{B}_{k,d} = \left\{ \phi_{l_1}^{j_1}(x_{j_1}) \cdots \phi_{l_k}^{j_k}(x_{j_k}) \mid 1 \leq j_1 < \cdots < j_k \leq d \text{ and } 2 \leq l_1, \dots, l_k \leq n \right\}. \quad (5)$$

which we refer to as the k -cluster basis throughout the paper. In particular, $\mathcal{B}_{0,d} = \{1\}$ only contains the constant basis. Furthermore, we say a function is k -cluster if it can be expanded by up to k -cluster basis. For example, the perturbed part of p^* in (2) is 2-cluster. Based on these definitions, Φ can be formulated as the concatenation of the k -cluster basis across different k :

$$\Phi(x) := [\mathcal{B}_{k,d}(x)]_{k=0}^d. \quad (6)$$

Furthermore, we define the weight vector w_K as:

$$w_K(j) := \begin{cases} 1 & j \in \binom{d}{K}, \\ 0 & \text{otherwise,} \end{cases} \quad (7)$$

which is an indicator vector that selects the 0- to K -cluster basis. With these definitions, one can verify that if p^* takes the form of (2), and if the univariate basis functions $\{\phi_l^j\}_{l=1}^n$ satisfy the orthogonality condition (3), then we can recover

$$p^* = \mu \odot (\Phi \text{diag}(w_K) \Phi^T p^*) \quad (8)$$

as long as $K \geq 2$. This fact motivates the proposed density estimator in (4). Moreover, unlike \hat{p} , whose variance scales as $O(n^d)$, Lemma 1 shows that the variance of \tilde{p} in (4) is significantly reduced,

scaling as polynomially dependent term $O(d^K)$ due to the projection onto a lower-dimensional function space. This substantial reduction in variance is a key advantage of our method.

While the estimator in (4) is intuitive, it is possible to further reduce the variance by imposing additional assumptions on p^* . Specifically, we assume that the low-order cluster coefficients $\text{diag}(w_K)\Phi^T p^*$ can be represented as a low-rank tensor train. The details of such a representation are provided in Section 1.5. Under this assumption, our estimation procedure can be modified as:

$$\tilde{p} = \mu \odot (\Phi (\text{TT-compress} (\text{diag}(w_K)\Phi^T \hat{p}))), \quad (9)$$

where we apply certain tensor-train compression algorithm, denoted as **TT-compress**, to the tensor $\text{diag}(w_K)\Phi^T \hat{p}$. The singular value thresholding involved in the compression procedure (**TT-compress**) can further suppress noise in $\text{diag}(w_K)\Phi^T \hat{p}$, leading to a more accurate density estimator.

While the estimator in (9) is expected to achieve a lower variance, a major drawback is that the projection $\text{diag}(w_K)\Phi^T \hat{p}$ onto the cluster basis up to order K has a computational complexity of $O(d^K n^K)$, corresponding to the number of cluster basis functions. This scaling quickly becomes prohibitive as d and K increase. To address this computational bottleneck, we propose a final estimator, which can be viewed as a more efficient variant of (9):

$$\tilde{p} = \mu \odot (\text{diag}(\tilde{w}_\alpha)^{-1} \Phi (\text{TT-compress} (\text{diag}(\tilde{w}_\alpha)\Phi^T \hat{p}))), \quad (10)$$

where $\tilde{w}_\alpha \in \mathbb{R}^{n^d}$ represents a soft down-weighting of the cluster basis. This approach differs from using w_K , which applies a hard threshold that entirely discards cluster bases involving more than K variables. A key advantage of using such \tilde{w}_α is that it can be designed as a rank-1 tensor, allowing the sequence of operations in (10) to be executed with a computational complexity of only $O(dn)$. This drastically reduces the cost compared to the $O(d^K n^K)$ complexity in (9). Furthermore, the final density estimator \tilde{p} naturally takes the form of a tensor train, allowing essential tasks such as moment computation, sample generation, and pointwise evaluation of the density to scale linearly in d . In Section 2.3, we present a simple example demonstrating that the estimator in (10) yields accurate results comparable to those of (9), thereby illustrating their similar compression capabilities. The study of (10) will be the focus of this paper.

1.3 Related work

In this subsection, we survey several lines of works that are most closely related to the proposed method.

Density estimation literature. Classical density estimation methods such as histograms (Scott (1979, 1985)), kernel density estimators (Parzen (1962); Davis et al. (2011)) and nearest neighbor density estimates (Mack and Rosenblatt (1979)) are known for their statistical stability and numerical robustness in low-dimensional cases. But they often struggle with the curse of dimensionality, even in moderately high-dimensional spaces. More recently, deep generative modeling has emerged as a powerful tool for generating new samples, particularly in the context of image, based on neural network architecture. This approach includes energy-based models (Kim and Bengio (2016); Du and Mordatch (2019); Song and Ermon (2019)) generative adversarial networks (GANs) (Goodfellow et al. (2020); Liu et al. (2021)), normalizing flows (Dinh et al. (2014); Rezende and Mohamed (2015); Dinh et al. (2016)), and autoregressive models (Germain et al. (2015); Uria et al. (2016); Papamakarios et al. (2017)). While the numerical performance for these modern methods is impressive, statistical guarantees and non-convex optimization convergence analysis remain

challenging areas of research. Furthermore, for some of these models (e.g. energy based model), generating i.i.d. samples can still be expensive. For methods like GANs, while it can generate samples efficiently, it does not provide a way to evaluate the value of a density at any given point. In short, it is difficult for a method to enjoy all the desirable properties such as easy to train, easy to generate samples, can support evaluation of density values, and can be estimated without the curse of dimensionality.

Tensor train from partial sensing of a function. Tensor train, also known as the matrix product state (MPS) (White (1993); Perez-Garcia et al. (2006)) in the physics literature, has recently been used when to uncover a function, when only limited number of observations of this function are given. Methods for this include TT-cross (Oseledets and Tyrtshnikov (2010)), DMRG-cross (Savostyanov and Oseledets (2011)), TT completion (Liu et al. (2012); Song et al. (2019)), and others (Sun et al. (2020); Kressner et al. (2023); Shi et al. (2023)). It has broad applications in high-dimensional scientific computing problems (Kressner and Uschmajew (2016); Bachmayr et al. (2016) and machine learning (Stoudenmire and Schwab (2016); Huggins et al. (2019); Sengupta et al. (2022)).

Tensor train for density estimation. In a density estimation setting, we are not given observed entries of a density function, but just an empirical distribution of it. The key challenge lies in the randomness of the observed object, i.e. the empirical histogram, which contains an exponentially large variance in terms of the dimensionality. Therefore, reducing variance in a high-dimensional setting is crucial to design effective algorithms. Recently, work (Hur et al. (2023)) and subsequent studies (Tang et al. (2022); Peng et al. (2023); Chen and Khoo (2023); Tang and Ying (2023); Khoo et al. (2024)) employ sketching techniques in tensor decomposition step for density estimation problems, which originates from randomized linear algebra literature. However, most existing algorithms in these works do not have a general way to ensure a linear computational complexity when sketching, in terms of dimensionality. Another approach for density estimation with tensors is through optimization-based method. Works (Bradley et al. (2020); Han et al. (2018); Novikov et al. (2021)) implement gradient descent methods and optimize tensor-network representations according to some loss functions. However, the performance strongly depends on the initialization and often suffers from the problem of local minima due to the highly non-convex nature of the optimization landscape. Furthermore, these iterative procedures require multiple iterations over N data points, resulting in higher computational complexity compared to the previous tensor decomposition algorithms.

1.4 Organization

Here we summarize the organization of the paper. In Section 1.5, we introduce the tensor notation and diagram conventions used throughout. In Section 2, we present the core ideas behind our proposed “convolution–deconvolution” framework, highlighting its three key steps. The central component is the TT-compress algorithm as discussed previously that compresses cluster coefficients into a tensor train. Section 3 – 6 introduce various of such TT-compress algorithms: Section 3 presents a baseline algorithm based on sequential truncated singular value decomposition (SVD), along with its fast implementation for density estimation problems. Section 4 includes an algorithm that utilizes the Nyström approximation to further accelerate the algorithm in Section 2. In Section 5, we study an algorithm that performs SVD efficiently by truncating the elements in the tensor, and then introduce a further acceleration by employing a hierarchical matrix factorization. Section 6 proposes an algorithm utilizing random sketching matrices with low-rank tensor structures. Sec-

tion 7 presents a pre-processing procedure based on principal component analysis (PCA), enabling our compression algorithms to handle very high-dimensional problems. Theoretical analysis for the algorithms is provided in Section 8. In Section 9, we showcase the comprehensive numerical results to demonstrate the high accuracy and efficiency for our proposed algorithms. Finally, in Section 10, we summarize our findings.

1.5 Tensor notations and diagrams

We begin with some definitions regarding tensors. A d -dimensional tensor $A \in \mathbb{R}^{n_1 \times n_2 \cdots \times n_d}$ is a collection of entries denoted by $A(i_1, i_2, \dots, i_d)$ with $1 \leq i_j \leq n_j$ for $1 \leq j \leq d$. Diagrammatically, a tensor can be denoted as a node whose dimensionality is indicated by the number of the “legs” of the node. In Figure 2(a), the diagrams for a three-dimensional tensor A and a two-dimensional matrix B are plotted as an example. We use i_1, i_2, i_3 to denote the three legs in tensor A . We may also use a rectangle to denote a tensor when it has many legs in this paper.

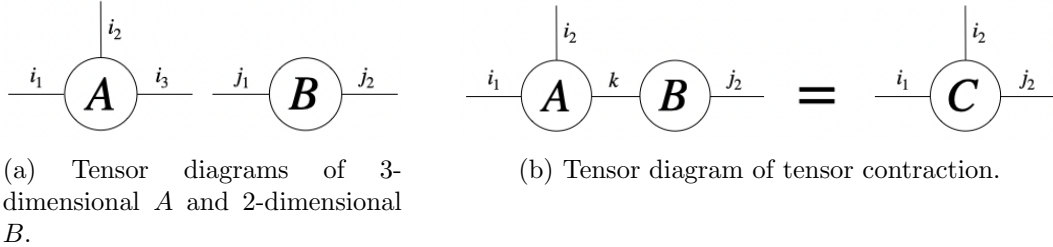


Figure 2: Basic tensor diagrams and operations.

Based on the definition of tensor, we list several tensor operations that will be used frequently in the paper:

1. **“o” contraction.** We use \circ to represent the tensor cores contraction $(A \circ B)(i_1, i_2, j_2) = \sum_k A(i_1, i_2, k)B(k, j_2)$. Such operation is denoted as diagram in Figure 2 (b) which combines the last leg of A and the first leg of B . The resulting $C = A \circ B$ is a three-dimensional tensor.
2. **Unfolding matrix.** Given a d -dimensional tensor with entries $A(i_1, i_2, \dots, i_d)$, if we group the first j indices into a multi-index $i_{1:j}$ and group the rest into another multi-index $i_{j+1:d}$, we will obtain a j -th *unfolding matrix* $A^{(j)} \in \mathbb{R}^{(n_1 \cdots n_j) \times (n_{j+1} \cdots n_d)}$ (also called j -th unfolding of A) satisfying

$$A^{(j)}(i_{1:j}, i_{j+1:d}) = A(i_1, i_2, \dots, i_d). \quad (11)$$

In particular, $A^{(0)} \in \mathbb{R}^{1 \times n_1 \cdots n_d}$ and $A^{(d)} \in \mathbb{R}^{n_1 \cdots n_d \times 1}$ are respectively the row and column vectors reshaped from the tensor.

In general, the memory cost of a high-dimensional tensor suffers from curse of dimensionality. Tensor-train representation is a way to decompose the whole exponential large d -dimensional tensor with underlying low-rank structure into d number of components:

$$A = G_1 \circ G_2 \circ \cdots \circ G_d \in \mathbb{R}^{n_1 \times \cdots \times n_d} \quad (12)$$

where $G_1 \in \mathbb{R}^{n_1 \times r_1}$, $G_2 \in \mathbb{R}^{r_1 \times n_2 \times r_2}$, \dots , $G_{d-1} \in \mathbb{R}^{r_{d-2} \times n_{d-1} \times r_{d-1}}$, $G_d \in \mathbb{R}^{r_{d-1} \times n_d}$ are called tensor cores and $\{r_j\}_{j=1}^{d-1}$ are the ranks. The TT representation can be visualized as the left panel of Figure

3. Throughout the paper, we denote the largest rank by

$$r = \max_j r_j.$$

Then the memory cost for storing A in TT form is at $O(dnr^2)$, which has no curse of dimensionality if r is small. In addition, a TT can also be used to represent a continuous function $f(x_1, \dots, x_d)$ formulated as a tensor product basis function expansion:

$$f(x_1, x_2, \dots, x_d) = \sum_{l_1, l_2, \dots, l_d=1}^n A(l_1, l_2, \dots, l_d) \phi_{l_1}(x_1) \phi_{l_2}(x_2) \dots \phi_{l_d}(x_d)$$

where the coefficient A takes the TT format as (12). Such functional tensor-train representation is illustrated in the right panel of Figure 3.

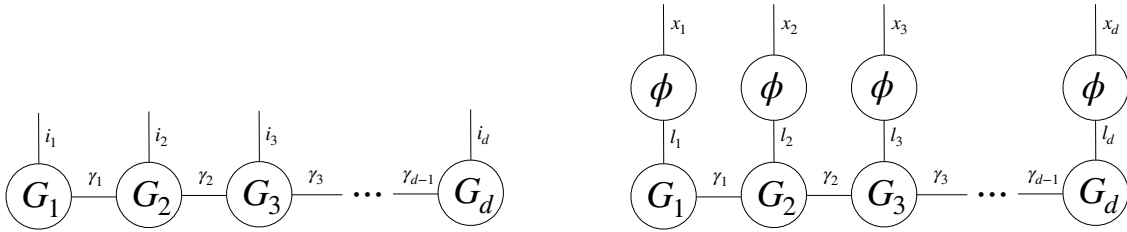


Figure 3: Diagram for tensor-train representation. Left: discrete case. Right: continuous case.

2 Main approach

In this section, we detail the framework of our main approach. In order to perform (10), we perform the following three steps:

1. **Convolution.** Project the empirical distribution \hat{p} to “coefficients” \hat{c} under certain basis expansion with $O(dN)$ computational cost:

$$\hat{c} = \text{diag}(\tilde{w}_\alpha) \Phi^T \hat{p} = \text{diag}(\tilde{w}_\alpha) \int \Phi(x)^T \hat{p}(x) dx. \quad (13)$$

2. **Tensor compression.** Approximate \hat{c} as a TT $\tilde{c} = \text{TT-compress}(\hat{c})$. This step can be done by several proposed algorithms listed in Table 1. Notably, several of these algorithms achieve $O(dN)$ complexity. These complexity estimates will be further validated through numerical experiments in Section 9.

Algorithm	Corresponding section	Computational complexity
TT-SVD	§3	$O(\min(dn^{d+1}, dN^2n))$
TT-SVD-kn	§4	$O(dNn)$
TT-SVD-c (K -cluster)	§5	$O(d^{K+1}Nn^{K+1})$
TT-SVD-c (hierarchical)	§5.1	$O(d \log(d)Nn)$
TT-rSVD-t	§6	$O(dNn)$

Table 1: Computational complexity of proposed TT-compress.

3. **Deconvolution.** Get the desired density estimator based on the TT coefficient \tilde{c} with $O(dN)$ computational cost:

$$\tilde{p} = \mu \odot (\Phi \text{diag}(\tilde{w}_\alpha)^{-1} \tilde{c}). \quad (14)$$

Here \tilde{p} is also a TT, if $\Phi \text{diag}(\tilde{w}_\alpha)^{-1}$ has an appropriate low-rank tensor structure.

Overall, the computational cost our approach (with proper choices of **TT-compress**) can achieve computational complexity that scales linearly with both the dimensionality d and sample size N , demonstrating the high efficiency. In the rest of this section, we will further elaborate convolution (Step 1) and deconvolution (Step 3). We defer the details of tensor compression (Step 2) to Section 3 – 6.

2.1 Convolution step

The key part of this step is the choice of $\tilde{w}_\alpha \in \mathbb{R}^{n^d}$, the soft down-weighting of the cluster basis (6). In this work, we choose the weight of any k -cluster basis $\phi_{l_1}^{j_1}(x_{j_1}) \cdots \phi_{l_k}^{j_k}(x_{j_k})$ to be

$$\alpha^k, \text{ where parameter } \alpha \in (0, 1]. \quad (15)$$

In this way, the coefficient tensor $\hat{c} = \text{diag}(\tilde{w}_\alpha) \Phi^T \hat{p}$ has entries

$$\hat{c}(l_1, l_2, \dots, l_d) = \frac{1}{N} \sum_{i=1}^N \alpha^{\|l-\mathbf{1}\|_0} \prod_{j=1}^d \phi_{l_j}^j(x_j^{(i)}).$$

where $\|\cdot\|_0$ is the zero norm counting the number of non-zero entries of a vector, and $\mathbf{1}$ is the all-one d -dimensional vector. $\|l-\mathbf{1}\|_0$ is then the number of non-constant univariate basis functions among $\phi_{l_1}^{j_1}(x_{j_1}) \cdots \phi_{l_k}^{j_k}(x_{j_k})$. Under such choice, $\text{diag}(\tilde{w}_\alpha)$ can be formulated as a rank-1 tensor operator, allowing the fast convolution (and also fast deconvolution later) with only $O(dN)$ computational cost. In fact, given samples $\{x^{(i)}\}_{i=1}^N$, \hat{c} is formulated as

$$\hat{c} = \frac{1}{N} \sum_{i=1}^N \tilde{\Phi}_1^{(i)} \otimes \tilde{\Phi}_2^{(i)} \otimes \cdots \otimes \tilde{\Phi}_d^{(i)} \quad (16)$$

where $\tilde{\Phi}_j^{(i)} = [1, \alpha \phi_2^j(x_j^{(i)}), \dots, \alpha \phi_n^j(x_j^{(i)})] \in \mathbb{R}^n$. This expression is plotted as tensor diagrams in Figure 4. For future use, we introduce

$$\tilde{\Phi}_j \in \mathbb{R}^{N \times n} \quad (17)$$

to denote the matrix whose rows are $\tilde{\Phi}_j^{(i)}$.

The idea of such choice is to assign smaller weights for higher-order cluster basis to suppress the variance. The parameter α describes the denoising strength — a smaller α produces stronger denoising and thus smaller variance. In particular when $\alpha = 1$, this soft-thresholding method (10) reduces to the hard-thresholding (9) using all cluster bases. We point out that by choosing sufficiently small α , this soft-thresholding strategy has smaller variance compared to the hard-thresholding approach (9). The following lemma considers a toy model to show the variance of the hard-thresholding approach:

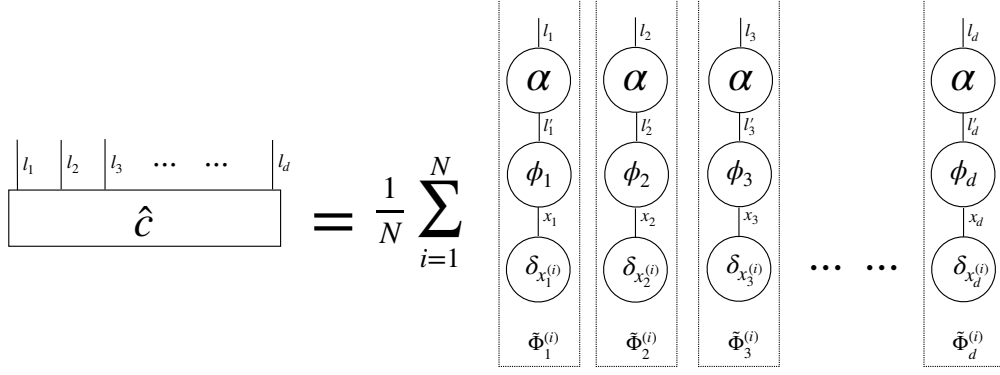


Figure 4: Tensor diagram of $\hat{c} = \text{diag}(\tilde{w}_\alpha)\Phi^T\hat{p}$. “ α ” denotes diagonal matrix $\text{diag}(1, \alpha, \dots, \alpha) \in \mathbb{R}^{n \times n}$; “ ϕ_j ” denotes “matrix” $[\phi_l^j(x)]_{x,l}$.

Lemma 1. Suppose $\{\phi_l\}_{l=1}^n$ are Legendre polynomials and the ground truth density p^* satisfies (8) with the mean-field component $\mu \sim \text{Unif}([0, 1]^d)$, the following variance estimation holds

$$\mathbb{E}\|\Phi \text{diag}(w_K)\Phi^T\hat{p} - \Phi \text{diag}(w_K)\Phi^T p^*\|_{L_2}^2 = \mathcal{O}\left(\frac{d^K n^{2K}}{N}\right). \quad (18)$$

Proof. Note that the error $\|\text{diag}(w_K)\Phi^T\hat{p} - \text{diag}(w_K)\Phi^T p^*\|_F^2$ has at most $\binom{d}{K}n^K$ terms, where each term follows

$$\left(\int \left(\prod_{k=1}^K \phi_{l_k}^{j_k}(x_{j_k}) \right) (\hat{p}(x) - p^*(x)) dx \right)^2 \quad (19)$$

for indices $(j_1, \dots, j_K) \in \binom{d}{K}$ and $l_1, \dots, l_K \in \{2, \dots, n\}$. Since Legendre polynomial satisfies $\|\phi_{l_k}^{j_k}\|_\infty \leq \sqrt{n}$, then

$$\mathbb{E} \left(\int \left(\prod_{k=1}^K \phi_{l_k}^{j_k}(x_{j_k}) \right) (\hat{p}(x) - p^*(x)) dx \right)^2 = \frac{1}{N} \int \left(\prod_{k=1}^K \phi_{l_k}^{j_k}(x_{j_k}) \right)^2 p^*(x) dx \leq \frac{n^K}{N} \int p^*(x) dx = \frac{n^K}{N} \quad (20)$$

Therefore, the total variance is bounded by

$$\mathbb{E}\|\Phi \text{diag}(w_K)\Phi^T\hat{p} - \Phi \text{diag}(w_K)\Phi^T p^*\|_{L_2}^2 = \mathbb{E}\|\text{diag}(w_K)\Phi^T\hat{p} - \Phi^T p^*\|_F^2 \leq \binom{d}{K} n^K \frac{n^K}{N} = \mathcal{O}\left(\frac{d^K n^{2K}}{N}\right). \quad (21)$$

□

On the other hand, the variance of the soft-thresholding approach under the model assumption

in Lemma 1 is estimated by

$$\begin{aligned}
& \mathbb{E} [\|\Phi \text{diag}(\tilde{w}_\alpha) \Phi^T \hat{p} - \Phi \text{diag}(\tilde{w}_\alpha) \Phi^T p^*\|_{L_2}^2] \\
&= \mathbb{E} [\|\text{diag}(\tilde{w}_\alpha) \Phi^T \hat{p} - \text{diag}(\tilde{w}_\alpha) \Phi^T p^*\|_F^2] \\
&= \sum_{l_1, \dots, l_d=1}^n \alpha^{2\|l-1\|_0} \mathbb{E} \left[\int (\hat{p}(x) - p^*(x)) \left(\prod_{j=1}^d \phi_{l_j}^j(x_j) \right) dx \right]^2 \\
&= \frac{1}{N} \sum_{l_1, \dots, l_d=1}^n \alpha^{2\|l-1\|_0} \int \prod_{j=1}^d (\phi_{l_j}^j(x_j))^2 p^*(x) dx \\
&\leq \frac{1}{N} \sum_{l_1, \dots, l_d=1}^n \alpha^{2\|l-1\|_0} n^{\|l-1\|_0} \int p^*(x) dx \\
&= \frac{1}{N} \sum_{l_1, \dots, l_d=1}^n (\alpha^2 n)^{\|l-1\|_0} = \frac{1}{N} (1 + (n-1)n\alpha^2)^d \tag{22}
\end{aligned}$$

where the inequality follows $\|\phi_{l_j}^j\|_\infty \leq \sqrt{n}$ for $l_j \geq 2$ and we use the binomial theorem for the last equality. With this estimation, we conclude that if we set $\alpha = 1$, the variance scales at least $O(n^d)$, indicating the curse of dimensionality. To avoid this, we choose

$$\alpha = \sqrt{\frac{C}{(n-1)nd}}$$

for some constant C without d -dependency. Under this choice, (22) can be bounded by

$$\mathbb{E} [\|\Phi \text{diag}(\tilde{w}_\alpha) \Phi^T \hat{p} - \Phi \text{diag}(\tilde{w}_\alpha) \Phi^T p^*\|_{L_2}^2] \leq \frac{1}{N} \left(1 + \frac{C}{d}\right)^d \leq \frac{1}{N} e^C \tag{23}$$

The resulting error has no curse of dimensionality. However, we also point out that α should not be chosen to be too small, which might lead to instability in our later operations. This will be further elaborated in Section 2.2.

2.2 Deconvolution step

After we have received the approximated coefficient \tilde{c} in TT format:

$$\tilde{c} = \hat{G}_1 \circ \hat{G}_2 \circ \dots \circ \hat{G}_d \in \mathbb{R}^{n \times n \times \dots \times n}.$$

in tensor compression step, the last step then obtains the final density estimator in TT format by implementing the deconvolution

$$\tilde{p} = \mu \odot (\Phi \text{diag}(\tilde{w}_\alpha)^{-1} \tilde{c}). \tag{24}$$

The structure of $\Phi \text{diag}(\tilde{w}_\alpha)^{-1} \tilde{c}$ is illustrated in Figure 5. Since \tilde{c} is a low-rank tensor train, the complexity of the evaluation on a single point x is only $O(dn)$.

Remark 1. *In practice, as dimensionality d grows, some elements in $\text{diag}(\tilde{w}_\alpha)$ become exponentially small, which potentially lead to instability when computing the inverse. One solution is to implement inverse with given threshold: $\tilde{p} = \Phi(\text{diag}(\alpha) + \lambda I)^{-1} \tilde{c}$. Here λ is a small thresholding constant to avoid instability issues and I is identity matrix. In practice, we find that even without this post-procedure, the tensor-train estimator does not suffer from such an instability.*

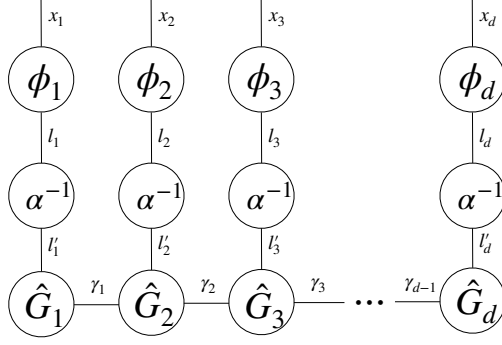


Figure 5: Tensor diagram for the final density estimator \tilde{p} . “ α^{-1} ” denotes diagonal matrix $\text{diag}(1, 1/\alpha, \dots, 1/\alpha) \in \mathbb{R}^{n \times n}$; “ ϕ_j ” denotes “matrix” $[\phi_l^j(x)]_{x,l}$.

2.3 Motivation: mean-field example

In this subsection, we walk through the main steps of the proposed approach using a mean-field example of the ground truth density, i.e., $p^* = \mu$ in (2). This toy example is used to illustrate why the soft-thresholding strategy in (10) effectively projects an empirical density onto the space spanned by low-order cluster bases, providing a similar effect as (9). The analysis can be extended to general examples.

For convenience, we first introduce some notations for moments: we define the first-order moment $\hat{q}_j \in \mathbb{R}^{(n-1) \times 1}$ as

$$\hat{q}_j(l_j) = \int \phi_{l_j+1}^j(x_j) \hat{p}(x) dx, \quad l_j = 1, \dots, n-1, \quad (25)$$

and the second-order moment $\hat{q}_{j,j'} \in \mathbb{R}^{(n-1) \times (n-1)}$

$$\hat{q}_{j,j'}(l_j, l'_{j'}) = \int \phi_{l_j+1}^j(x_j) \phi_{l'_{j'}+1}^{j'}(x_{j'}) \hat{p}(x) dx, \quad l_j, l'_{j'} = 1, \dots, n-1. \quad (26)$$

Higher-order moments can be defined following the same logic.

We consider to compress the tensor $\text{diag}(\tilde{w}_\alpha) \Phi^T \hat{p}$ into a tensor train using one specific approach called CUR approximation (Mahoney and Drineas (2009)). Specifically, a given matrix $A \in \mathbb{R}^{m \times n}$ can be approximated by the following rank- r factorization

$$A = CU^+R$$

where $C \in \mathbb{R}^{m \times r}$ and $R \in \mathbb{R}^{r \times n}$ respectively consist of selected r columns and rows. U is the intersection (cross) submatrix formed by the selected rows and columns, and U^+ is the Moore-Penrose generalized inverse of U . To ensure a good approximation, the columns and rows are typically chosen to maximize the determinant of U . Repeating the procedure for all dimensions, we can receive a tensor-train decomposition eventually. Further details will be discussed in Section 4. Based on the notations above, we first unfold the weighted projection tensor $\text{diag}(\tilde{w}_\alpha) \Phi^T \hat{p}$ as

$$(\text{diag}(\tilde{w}_\alpha) \Phi^T \hat{p})^{(1)} = \begin{bmatrix} 1 & \alpha[\hat{q}_j^{(0)}]_{j=2}^d & \alpha^2[\hat{q}_{j,j'}^{(0)}]_{j,j'=2}^d & \cdots \\ \alpha\hat{q}_1 & \alpha^2[\hat{q}_{1,j}^{(1)}]_{j=2}^d & \alpha^3[\hat{q}_{1,j,j'}^{(1)}]_{j,j'=2}^d & \cdots \end{bmatrix} =: B_1 \quad (27)$$

in terms of the order of α , where we use $[\cdot]$ to represent the concatenation of those inside terms through the column. Since the ground truth density p^* is mean-field (rank-1), we choose only $r = 1$ column and row for CUR approximation of $(\text{diag}(\tilde{w}_\alpha)\Phi^T\hat{p})^{(1)}$. With α chosen to be sufficiently small, the $(1, 1)$ -entry is the largest in B_1 . Therefore, first row and first column are chosen for the CUR approximation:

$$B_1 \approx \begin{bmatrix} 1 \\ \alpha\hat{q}_1 \end{bmatrix} \underbrace{\begin{bmatrix} 1 & \alpha[\hat{q}_j^{(0)}]_{j=2}^d & \alpha^2[\hat{q}_{j,j'}^{(0)}]_{j,j'=2}^d & \cdots \end{bmatrix}}_{=:B_2} \quad (28)$$

The left vector $\begin{bmatrix} 1 \\ \alpha\hat{q}_1 \end{bmatrix}$ is the resulting first TT core (before normalization). Next, we continue to implement the cross approximation on the unfolding of remaining tensor B_2 . First row and first column are again chosen following the same logic:

$$B_2 = \begin{bmatrix} 1 & \alpha[\hat{q}_j^{(0)}]_{j=3}^d & \alpha^2[\hat{q}_{j,j'}^{(0)}]_{j,j'=3}^d & \cdots \\ \alpha\hat{q}_2 & \alpha^2[\hat{q}_{2,j}^{(1)}]_{j=3}^d & \alpha^3[\hat{q}_{2,j,j'}^{(1)}]_{j,j'=3}^d & \cdots \end{bmatrix} \approx \begin{bmatrix} 1 \\ \alpha\hat{q}_2 \end{bmatrix} \underbrace{\begin{bmatrix} 1 & \alpha[\hat{q}_j^{(0)}]_{j=3}^d & \alpha^2[\hat{q}_{j,j'}^{(0)}]_{j,j'=3}^d & \cdots \end{bmatrix}}_{=:B_3}. \quad (29)$$

We repeat this procedure until decomposing the tensor into the product of d rank-1 cores:

$$\text{diag}(\tilde{w}_\alpha)\Phi^T\hat{p} \approx \begin{bmatrix} 1 \\ \alpha\hat{q}_1 \end{bmatrix} \otimes \begin{bmatrix} 1 \\ \alpha\hat{q}_2 \end{bmatrix} \otimes \cdots \otimes \begin{bmatrix} 1 \\ \alpha\hat{q}_d \end{bmatrix} =: \text{TT-compress}(\text{diag}(\tilde{w}_\alpha)\Phi^T\hat{p}). \quad (30)$$

Furthermore, we try to estimate the difference between the representation in (30) and hard truncation $\text{TT-compress}(\text{diag}(w_K)\Phi^T\hat{p})$ in (9), which are the summation of all k -cluster terms for $k > K$. Since ground truth density p^* is mean-field, the expectation of empirical one-marginal is $\mathbb{E}[\hat{q}_j] = \mu$. Besides, variance $\text{Var}[\hat{q}_j] = O(\frac{n-1}{N})$ for each j due to the orthogonality of $\{\phi_l^j\}_{l=1}^n$ with respect to μ . Therefore, we can have an upper bound of k -cluster, $\alpha^k \|\hat{q}_{j_1} \otimes \cdots \otimes \hat{q}_{j_k}\|_F \leq C\alpha^k (\frac{n}{N})^{k/2}$ for some constant $C > 0$. Then compared to the hard-thresholding K -cluster estimator in (9), the difference towards the soft-thresholding estimator (10) is upper bounded by

$$\begin{aligned} & \| (\text{TT-compress}(\text{diag}(w_K)\Phi^T\hat{p})) - (\text{TT-compress}(\text{diag}(\tilde{w}_\alpha)\Phi^T\hat{p})) \|_F \leq C \sum_{k=K+1}^d \binom{d}{k} \alpha^k \left(\frac{n}{N}\right)^{k/2} \\ & \leq C \sum_{k=K+1}^d \left(\frac{\alpha de}{K} \sqrt{\frac{n}{N}}\right)^k \leq Cd \left(\frac{\alpha de}{K} \sqrt{\frac{n}{N}}\right)^{K+1} \end{aligned} \quad (31)$$

when $\frac{\alpha de}{K} \sqrt{\frac{n}{N}} < 1$ for sufficient large N . The difference between two estimators is polynomially small with respect to sample size N . This turns out to be a clear example to demonstrate the reliability of soft-thresholding approach (10).

3 Tensor-train SVD (TT-SVD)

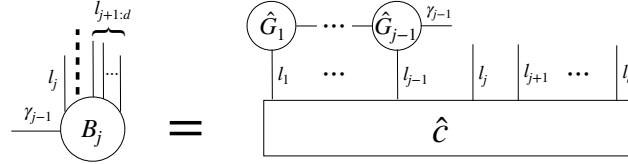
Starting from this section, we focus on Step 2 of the main approach — tensor compression. To this end, we first propose to use the tensor-train SVD (TT-SVD) algorithm. The TT-SVD algorithm is originally proposed in Oseledets (2011), which compresses a high-dimensional tensor into a low-rank tensor train by performing truncated SVD sequentially. For our problem, we use TT-SVD to

find the approximation \tilde{c} in TT format of \hat{c} depicted in Figure 4, which can be obtained following the procedures in Algorithm 1.

Algorithm 1 TT-SVD

INPUT: Tensor $\hat{c} \in \mathbb{R}^{n \times n \times \dots \times n}$. Target rank $\{r_1, \dots, r_{d-1}\}$.

- 1: **for** $j \in \{1, \dots, d-1\}$ **do**
- 2: Perform SVD to $B_j \in \mathbb{R}^{nr_{j-1} \times n^{d-j}}$, which is formed by the following tensor contraction



In particular, $B_1 = \hat{c}^{(1)}$ which is the first unfolding matrix of \hat{c} defined in (11). With SVD $B_j = U_j \Sigma_j V_j^T$, we obtain the j -th core $\hat{G}_j \in \mathbb{R}^{r_{j-1} \times n \times r_j}$, which is reshaped from the first r_j principle left singular vectors in U_j .

3: **end for**

- 4: Obtain the last core $\hat{G}_d = B_d \in \mathbb{R}^{r_{d-1} \times n}$.

OUTPUT: Tensor train $\tilde{c} = \hat{G}_1 \circ \hat{G}_2 \circ \dots \circ \hat{G}_d \in \mathbb{R}^{n \times n \times \dots \times n}$.

Below, we briefly outline the idea behind this algorithm. When $j = 1$, we want to obtain the first core \hat{G}_1 by performing SVD to $\hat{c}^{(1)}$ (which is B_1 in Algorithm 1). Then we let $\hat{G}_1 \in \mathbb{R}^{n \times r_1}$ to be first r_1 principle left singular vectors. The rationale of the first step is to approximate $\hat{c}^{(1)}$ as $\hat{c}^{(1)} \approx \hat{G}_1 (\hat{G}_1^T \hat{c}^{(1)})$. In the $j = 2$ step, we want to obtain \hat{G}_2 , which gives a further approximation to $\hat{G}_1 (\hat{G}_1^T \hat{c}^{(1)})$. The way we do this is to factorize $\hat{G}_1^T \hat{c}^{(1)} \in \mathbb{R}^{r_1 \times n^{d-1}}$, by applying SVD to B_2 , which is the reshaping of $\hat{G}_1^T \hat{c}^{(1)}$. This completes the $j = 2$ step. Then we do the above procedure recursively till $j = d - 1$. After implementing sequential SVD for $d - 1$ times, the remaining $B_d \in \mathbb{R}^{r_{d-1} \times n}$ is a matrix and we take it as the final core in the tensor-train representation since no more decomposition is required.

Naively, the computational cost from SVD in Algorithm 1 scales exponentially large as $O(dn^{d+1})$ in terms of dimensionality. However, for the density estimation problem, we can take advantage of the structure of \hat{c} as depicted in Figure 4 to achieve a fast implementation of Algorithm 1. We will use the next subsection to elaborate such fast implementation.

3.1 Fast implementation of TT-SVD

In this subsection, we present a fast implementation of Algorithm 1 with a complexity of $O(dN^2nr)$, which scales linearly with d and is therefore well-suited for high-dimensional cases. Notably, this efficient implementation introduces no additional approximations and produces the same output as the vanilla implementation in Algorithm 1.

The key of the fast implementation lies in fast calculations of SVD of B_j in Algorithm 1. Instead of performing SVD to B_j directly to get its left singular vectors as in Line 2 of Algorithm 1, we consider computing the eigenvectors of $B_j B_j^T$, which is a relatively small matrix of size $nr_{j-1} \times nr_{j-1}$. However, one concern is that the cost of forming $B_j B_j^T$ can in principle scale exponentially with dimensionality, since the column size of B_j is n^{d-j} as indicated by multiple legs between the two

nodes in Figure 6. Fortunately, by using the structure of \hat{c} as shown in Figure 4, one can form $B_j B_j^T$ much more efficiently. This is shown in Line 2 of Algorithm 2, which summarizes the TT-SVD procedure that is implemented in a computationally feasible manner.

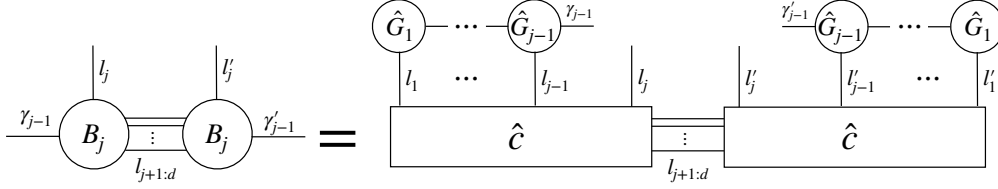


Figure 6: Tensor components for forming $B_j B_j^T$.

In Algorithm 2, the main computation lies in forming D_j and E_j in Line 2. A naive way is to compute them independently, leading to $O(dN^2)$ complexity. However, D_j and E_j can be computed in a recursive way efficiently, where computations can be reused. More specifically, one can precompute E_j by

$$E_j = E_{j+1} \odot (\tilde{\Phi}_j \tilde{\Phi}_j^T) \quad (32)$$

starting from $E_d = I_{N \times N}$ which is $N \times N$ the identity matrix. D_j is computed recursively based on core \hat{G}_{j-1} starting from $D_1 = \tilde{\Phi}_1^T$ according to Figure 7. The last core \hat{G}_d is assigned as the matrix B_d in algorithm 1, which is equal to the average of $D_d^{(i)}$ over sample index i . Therefore, we compute \hat{G}_d as the average of $D_d^{(i)}$ in Algorithm 2. In this way, the computational cost of E_j , D_j and $B_j B_j^T$ is $O(N^2 nr)$ which has no dependency on dimensionality. Afterwards, one can solve the core by eigen-decomposition of $B_j B_j^T \in \mathbb{R}^{nr_{j-1} \times nr_{j-1}}$ with a minor cost as $O((nr)^3)$. Overall, the computational cost of this fast implementation is $O(dN^2 nr)$.

While this fast implementation significantly reduces the computational complexity from exponential to linear in d , we point out that such implementation still requires $O(N^2)$ computations to form each E_j , which can make it challenging with a large number of samples even in low dimensional cases. In Section 4, we will further improve Algorithm 2 using kernel Nyström approximation, which will bring computational cost to $O(dN)$ only.

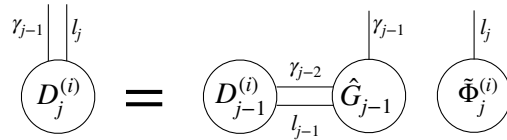


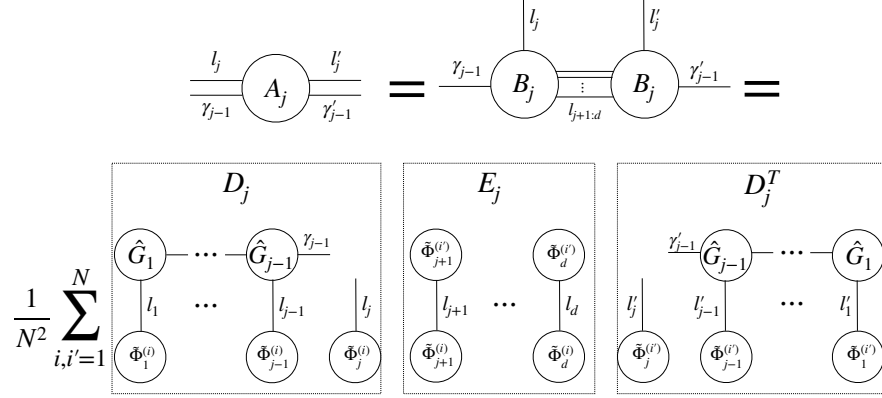
Figure 7: Tensor diagram illustrating the recursive calculation of $D_j^{(i)}$, which is the i -th column of the matrix D_j in Algorithm 2.

Algorithm 2 Fast implementation of TT-SVD

INPUT: Samples $\{x^{(i)}\}_{i=1}^N$. Target rank $\{r_1, \dots, r_{d-1}\}$.

1: **for** $j \in \{1, \dots, d-1\}$ **do**

2: Perform eigen-decomposition to $A_j := B_j B_j^T \in \mathbb{R}^{nr_{j-1} \times nr_{j-1}}$, which is computed by $A_j = \frac{1}{N^2} D_j E_j D_j^T$ where $D_j \in \mathbb{R}^{nr_{j-1} \times N}$ and $E_j \in \mathbb{R}^{N \times N}$ are the resulting matrices by contraction in the boxes of the below figure:



In particular, $D_1 = \tilde{\Phi}_1^T$ defined in (17). Here D_j and E_j should be computed recursively to reuse calculations. With eigen-decomposition $A_j = U_j \Lambda_j U_j^T$, we obtain the j -th core $\hat{G}_j \in \mathbb{R}^{r_{j-1} \times n \times r_j}$, which is reshaped from the first r_j principle eigenvectors in U_j .

3: **end for**

4: Obtain the last core:

$$\hat{G}_d = \frac{1}{N} \sum_{i=1}^N D_d^{(i)} \in \mathbb{R}^{r_{d-1} \times n}$$

where $D_d^{(i)}$ is the reshaping of i -th column of D_d .

OUTPUT: Tensor train $\tilde{c} = \hat{G}_1 \circ \hat{G}_2 \circ \dots \circ \hat{G}_d \in \mathbb{R}^{n \times n \times \dots \times n}$.

4 TT-SVD with kernel Nyström approximation (TT-SVD-kn)

In this section, we propose a further modification based on the fast implementation of TT-SVD developed in Section 3.1. This modification accelerates Algorithm 2 using kernel Nyström approximation to reduce the complexity from $O(dN^2)$ to $O(dN)$. As we have pointed out at the end of Section 3.1, the $O(N^2)$ complexity of Algorithm 2 is the consequence of exact evaluation of the $N \times N$ matrix E_j in the step of eigen-decomposition for $B_j B_j^T$. The proposed modification in this section will utilize kernel Nyström approximation (Williams and Seeger (2000)) to form E_j efficiently.

To begin with, we briefly introduce the idea of kernel Nyström method to approximate a symmetric matrix as shown in Figure 8. Given a symmetric matrix $A \in \mathbb{R}^{m \times m}$, the kernel Nyström method chooses \tilde{r} columns of A uniformly at random without replacement and approximates A by the following low-rank cross approximation

$$A \approx MW^+M^T \tag{33}$$

where $M \in \mathbb{R}^{m \times \tilde{r}}$ consists of the \tilde{r} chosen columns, $W \in \mathbb{R}^{\tilde{r} \times \tilde{r}}$ is the intersection of the chosen \tilde{r} columns and the corresponding \tilde{r} rows and W^+ is the Moore-Penrose generalized inverse of W .

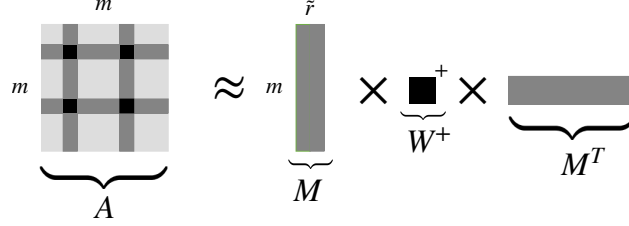


Figure 8: Cross approximation of a symmetric matrix.

Such approximation can be applied to the symmetric matrix E_j in Algorithm 2, resulting in the more efficient TT-SVD-kn algorithm summarized in Algorithm 4. By the recurrence relation (32), E_j is formulated as

$$E_j = (\tilde{\Phi}_d \tilde{\Phi}_d^T) \odot (\tilde{\Phi}_{d-1} \tilde{\Phi}_{d-1}^T) \odot \cdots \odot (\tilde{\Phi}_{j+1} \tilde{\Phi}_{j+1}^T), \quad (34)$$

which is depicted by the first equation in Figure 9. To apply kernel Nyström method, we randomly sample \tilde{r} rows in E_j with index $\mathcal{I} \subset \{1, 2, \dots, N\}$, and we define $\tilde{\Phi}_m^{(\mathcal{I})} \in \mathbb{R}^{\tilde{r} \times n}$, which is denoted by the blocks in each $\tilde{\Phi}_m$ in Figure 9, as the resulting submatrices formed by the sampled rows.

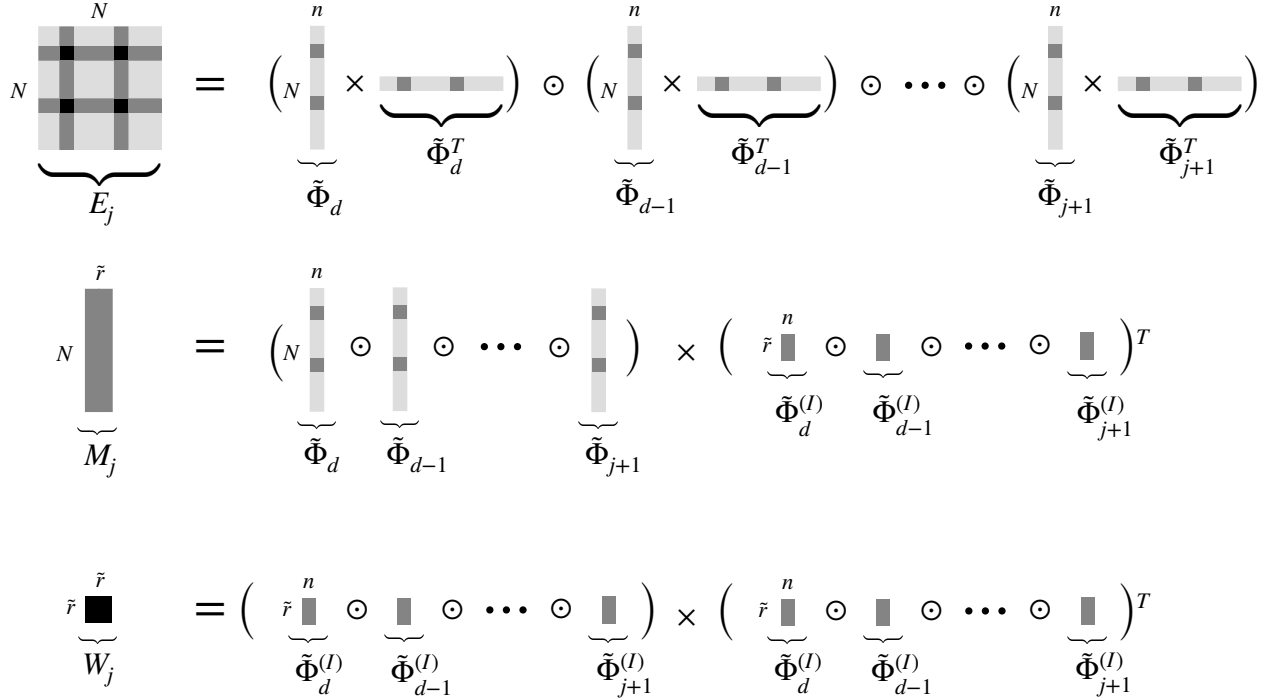


Figure 9: Cross approximation of E_j , the most expensive component in Algorithm 2.

At this point, we perform the cross approximation for E_j :

$$E_j \approx M_j W_j^+ M_j^T$$

where $M_j \in \mathbb{R}^{N \times \tilde{r}}$ is the submatrix formed by the chosen columns in E_j and $W_j \in \mathbb{R}^{\tilde{r} \times \tilde{r}}$ is the corresponding intersection. Using the expression (34), M_j and W_j are respectively formulated as the second and third equation in Figure 9. The structures of M_j and W_j allow us to compute them in a recursive manner as in Line 2 of Algorithm 3: suppose we have already obtained $\tilde{\Phi}_{j+2:d}$ and $\tilde{\Phi}_{j+2:d}^{(\mathcal{I})}$, M_j and W_j can be evaluated with complexity $O(Nn)$ (direct computations based on their definitions in Figure 9 is $O(dNn)$). Consequently, $B_j B_j^T$ in the previous Algorithm 2 can now be approximated by

$$B_j B_j^T = \frac{1}{N^2} D_j E_j D_j^T \approx \frac{1}{N^2} D_j M_j W_j^+ M_j^T D_j^T$$

as in Line 4 of Algorithm 4. The computational cost for the above matrix multiplications is $O(Nnr \max(nr, \tilde{r}))$, which is significantly smaller compared to the original $O(N^2 nr)$ complexity in Algorithm 2. By considering the calculations for all d tensor cores, the total computational cost is $O(dNnr \max(nr, \tilde{r}))$. Here we remark that we have employed the same indices \mathcal{I} for computing all E_j . Such practice is the key to reuse the calculations in this recursive implementation so that we can achieve a complexity that is only linear in sample size.

Algorithm 3 TT-SVD-kn

INPUT: Samples $\{x^{(i)}\}_{i=1}^N$. Target rank $\{r_1, \dots, r_{d-1}\}$. Number of sampled columns \tilde{r} .

- 1: Sample \tilde{r} integers from $\{1, \dots, N\}$ and let \mathcal{I} be the set of sampled integers.
- 2: Pre-compute $\{W_j\}_{j=1}^{d-1}$ and $\{M_j\}_{j=1}^{d-1}$ based on sampled indices \mathcal{I} recursively by Figure 9.
- 3: **for** $j \in \{1, \dots, d-1\}$ **do**
- 4: Perform eigen-decomposition to $B_j B_j^T \in \mathbb{R}^{nr_{j-1} \times nr_{j-1}}$, which is approximated by

$$B_j B_j^T \approx A_j := \frac{1}{N^2} D_j M_j W_j^+ M_j^T D_j^T$$

where D_j is computed recursively as Figure 7. With eigen-decomposition $A_j = U_j \Lambda_j U_j^T$, we obtain the j -th core $\hat{G}_j \in \mathbb{R}^{r_{j-1} \times n \times r_j}$, which is reshaped from the first r_j principle eigenvectors in U_j .

- 5: **end for**
- 6: Obtain the last core:

$$\hat{G}_d = \frac{1}{N} \sum_{i=1}^N D_d^{(i)} \in \mathbb{R}^{r_{d-1} \times n}$$

where $D_d^{(i)}$ is the i -th column of D_d .

OUTPUT: Tensor train $\tilde{c} = \hat{G}_1 \circ \hat{G}_2 \circ \dots \circ \hat{G}_d \in \mathbb{R}^{n \times n \times \dots \times n}$.

5 TT-SVD with truncated cluster basis (TT-SVD-c)

In this section, we introduce the TT-SVD-c algorithm (Algorithm 4), which is a modified TT-SVD algorithm based on truncated cluster basis sketching. The central idea is to utilize sketching technique to approximate the full SVDs of $B_j \in \mathbb{R}^{nr_{j-1} \times n^{d-j}}$ in Line 2 of Algorithm 1. More specifically, each step when we compute the left singular vectors U_j from B_j in Algorithm 1, we

instead compute the left singular vectors from a sketched B_j :

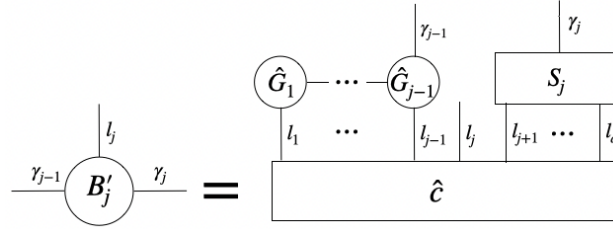
$$B'_j = B_j S_j, \quad (35)$$

where S_j is some appropriately chosen sketching matrix with size $n^{d-j} \times \tilde{r}_j$, with sketching size \tilde{r}_j much smaller than n^{d-j} (Line 2 of Algorithm 4). In this way, we can reduce the exponential complexity of full SVD for B_j to $O(\max(nr\tilde{r}_j^2, n^2r^2\tilde{r}_j))$ complexity of SVD for B'_j .

Algorithm 4 TT-SVD-c

INPUT: Samples $\{x^{(i)}\}_{i=1}^N$. Target rank $\{r_1, \dots, r_{d-1}\}$. Cluster order K .

- 1: **for** $j \in \{1, \dots, d-1\}$ **do**
- 2: Perform SVD to $B'_j \in \mathbb{R}^{nr_{j-1} \times \tilde{r}_j}$, which is formed by the following tensor contraction



where $S_j \in \mathbb{R}^{n^{d-j} \times \tilde{r}_j}$ is the sketching matrix depending on cluster order K . The contraction of the right-hand side is done efficiently as shown in Figure 10. With SVD $B'_j = U_j \Sigma_j V_j^T$, we obtain the j -th core $\hat{G}_j \in \mathbb{R}^{r_{j-1} \times n \times r_j}$, which is reshaped from the first r_j principle left singular vectors in U_j .

3: **end for**

4: Obtain the last core $\hat{G}_d = B'_d \in \mathbb{R}^{r_{d-1} \times n}$.

OUTPUT: Tensor train $\tilde{c} = \hat{G}_1 \circ \hat{G}_2 \circ \dots \circ \hat{G}_d \in \mathbb{R}^{n \times n \times \dots \times n}$.

The key of this approach is to choose good sketching matrix S_j such that B'_j retains the same range, and thus the same left singular space, as B_j . Here, we follow a specific way to construct sketching matrix S_j (Chen and Khoo (2023); Peng et al. (2023)), where we only include the low-order cluster basis. We first introduce the set of k -cluster indices:

$$\mathcal{J}_{k,d} = \{(l_1, \dots, l_d) \mid l_1, \dots, l_d \in \{1, \dots, n\} \text{ and } \|l - \mathbf{1}\|_0 = k\},$$

which are the basis indices of those cluster bases in $\mathcal{B}_{k,d}$ defined in (5) since $\phi_1^j \equiv 1$.

Our choice of sketching matrix is based on the low-order cluster indices. To sketch B_j , we construct $S_j \in \mathbb{R}^{n^{d-j} \times \tilde{r}_j}$ as follows: each column of S_j is defined based on a multivariate index $l \in \bigcup_{k=0}^K \mathcal{J}_{k,d-j}$ where K is the chosen cluster order:

$$\mathbf{1}_{l_1} \otimes \mathbf{1}_{l_2} \otimes \dots \otimes \mathbf{1}_{l_{d-j}}$$

where $\mathbf{1}_l$ is a $n \times 1$ column vector evaluating as 1 on the l th component and 0 elsewhere. Under this construction, S_j is a sparse matrix with column size

$$\tilde{r}_j = \sum_{k=0}^K |\mathcal{J}_{k,d-j}| = O(d^K n^K).$$

At this point, the only concern is that forming $B'_j = B_j S_j$ has exponential complexity by direct matrix multiplication. Similar to Algorithm 2, we utilize the structure of \hat{c} (16):

$$B'_j = B_j S_j = \frac{1}{N} D_j (E_j)^T = \frac{1}{N} \sum_{i=1}^N D_j^{(i)} (E_j^{(i)})^T \in \mathbb{R}^{nr_{j-1} \times \tilde{r}_j} \quad (36)$$

where D_j, E_j are defined in Figure 10 (c) and $D_j^{(i)}, E_j^{(i)}$ represent the i -th column of matrix D_j, E_j , respectively. According to the structure of D_j, E_j , their computation can be done in a recursive way following the diagram in Figure 10 (a) and (b).

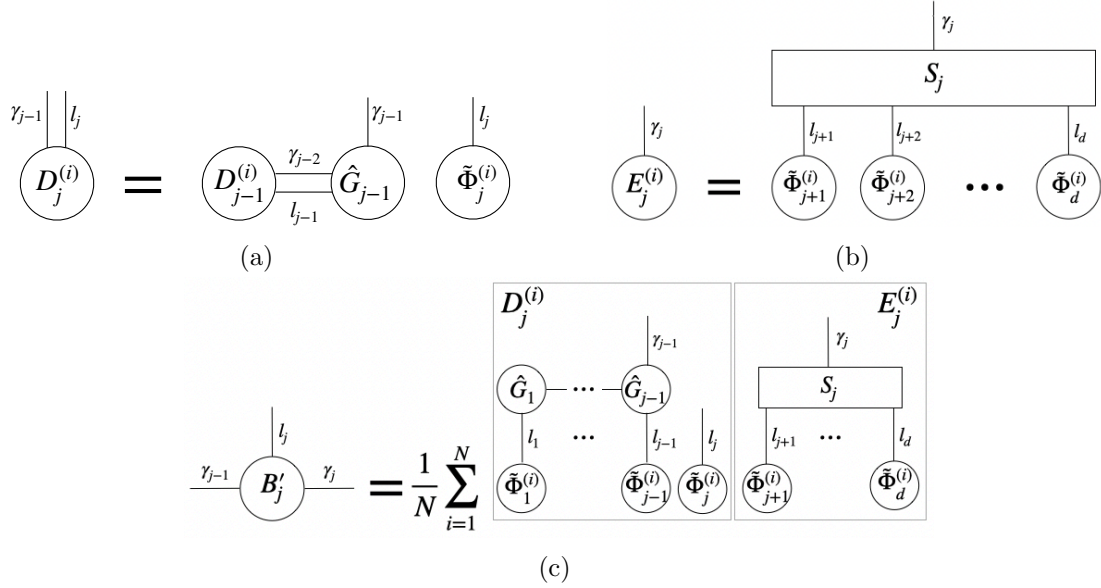


Figure 10: Tensor diagrams illustrating recursive computation of B'_j in Line 2 of Algorithm 4. (a) recursive calculation of $D_j^{(i)}$, which is the i -th column of the matrix D_j ; (b) recursive calculation of $E_j^{(i)}$, which is the i -th column of the matrix E_j ; (c) calculation of B'_j based on $D_j^{(i)}$ and $E_j^{(i)}$.

In terms of the computational complexity of Algorithm 4, the cost for $\{E_j\}_{j=1}^{d-1}$ is $O(d^{K+1} N n^K)$ for k -cluster truncation. Besides, the cost for $\{D_j\}_{j=1}^{d-1}$ follows the analysis in Figure 7 and Algorithm 2, which is $O(d N n r^2)$. Furthermore, the computational complexity of multiplication in B'_j and the following SVD step requires $O(d^{K+1} N n^{K+1})$. To summarize, the dominant term in computational complexity is $O(d^{K+1} N n^{K+1})$. The reduction is from standard TT-SVD algorithm $O(\min(d n^{d+1}, d N^2 n))$ to $O(d^{K+1} N n^{K+1})$, which is significant especially for a large sample size N and low-order K . In the following subsection, we further propose a modification of TT-SVD-c which constructs sketching matrix S_j based on hierarchical matrix decomposition. This acceleration can achieve a lower computational complexity as $O(d \log(d))$.

5.1 Acceleration of TT-SVD-c via hierarchical matrix decomposition

In this subsection, we propose a modification that further accelerates TT-SVD-c method with cluster order $K = 1$. The key insight of this acceleration lies in the assumption that the ground truth

density p^* has high correlations between nearby variables (such as x_1 and x_2) and low correlation between distant variables (such as x_1 and x_d), which is satisfied by many real cases. In Algorithm 4, the sketching matrix S_j considers all correlations equally without taking the distance into account, which includes redundant correlations with distant variables and leads to a large column size of S_j . In fact, even if cluster order $K = 1$, the column size is $O(d)$, which results in the overall computational cost of $O(d^2)$. This motivates us to further sketch S_j , which is done by hierarchical matrix decomposition (Hackbusch (1999); Hackbusch and Khoromskij (2000); Bebendorf (2008)) of covariance matrix M , whose (j_1, j_2) -block is formulated as

$$M_{j_1, j_2} = [\mathbb{E}_p[\phi_{l_1}^{j_1}(x_{j_1})\phi_{l_2}^{j_2}(x_{j_2})]]_{l_1, l_2} \in \mathbb{R}^{n \times n} \quad (37)$$

for all $1 \leq j_1, j_2 \leq d$.

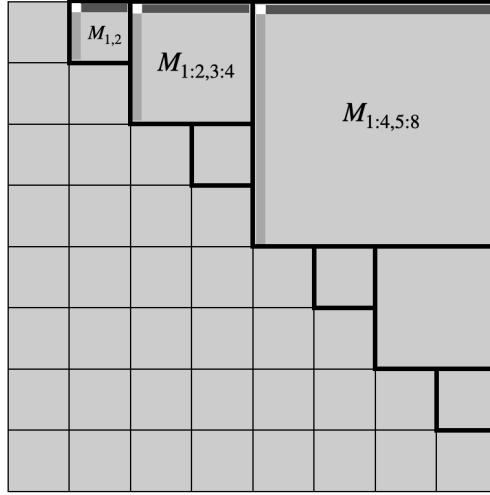


Figure 11: Hierarchical matrix decomposition of covariance matrix for $d = 8$. The figure depicts the three block matrices $M_{1:4,5:8}$, $M_{1:2,3:4}$, $M_{1,2}$ whose top \tilde{r} right singular vectors (visualized as dark gray matrix in each block matrix).

To illustrate the idea, we consider an example with $d = 8$. Covariance matrix M is depicted in Figure 11, where we use $M_{j_1:j_2, j_3:j_4}$ to represent the submatrix formed by blocks with row index from j_1 to j_2 and column index from j_3 to j_4 . To implement hierarchical matrix decomposition, we perform SVD on upper triangular off-diagonal blocks $M_{1:4,5:8}$, $M_{1:2,3:4}$, $M_{1,2}$ and get top \tilde{r} right singular vectors V'_1, V'_2, V'_3 , respectively. Here the sketching size \tilde{r} (different from that in Algorithm 4) is chosen as a constant. V'_1, V'_2, V'_3 respectively capture correlations with variables $x_{5:8}$, $x_{3:4}$ and x_2 .

Once the singular vectors V'_1, V'_2, V'_3 are obtained, we can use them to construct sketching matrices with smaller column sizes. When computing the first core \hat{G}_1 , we form $Q_1 = \text{diag}[V'_1, V'_2, V'_3] \in \mathbb{R}^{7n \times 3\tilde{r}}$ which captures the weighted correlation between x_1 and $x_{2:8}$, and we use S_1 and Q_1 to sketch B_1 as $B'_1 = B_1 S_1 Q_1 \in \mathbb{R}^{n \times 3\tilde{r}}$. Once this is done, we perform SVD to B'_1 to obtain \hat{G}_1 . For the second core, we form $Q_2 = \text{diag}[V'_1, V'_2] \in \mathbb{R}^{6n \times 2\tilde{r}}$ to capture the weighted correlation between variables x_2 and variables $x_{3:8}$. Then we sketch $B'_2 = B_2 S_2 Q_2$, and perform SVD to B'_2 to obtain \hat{G}_2 . Note that we can reuse V'_1, V'_2 in the second step since both of them were already computed in the first step. By repeating the procedure and generating new sketch $B'_j = B_j S_j Q_j$ for the remaining j , this hierarchical approach enables the efficient computation of all cores $\{\hat{G}_j\}_{j=1}^d$.

In terms of computational complexity, there are two major sources of computations. The first is the SVD of off-diagonal block matrices ($M_{1:4,5:8}, M_{1:2,3:4}, M_{1,2}$ for $d = 8$). For each block, we first apply kernel Nyström approximation (33) with \tilde{r} sampled rows and columns, followed by SVD. The cost for this part of computations is $O(d \log(d) N n \tilde{r})$. The second major computation is forming $B'_j = B_j S_j Q_j$. The number of columns in the weight matrix Q_j is at most $\log_2(d) \tilde{r}$. Since S_j is a sparse matrix, the computation of $B'_j = B_j S_j Q_j$ for all j needs $O(d \log(d) N n \tilde{r})$ computational cost upon leveraging a similar strategy for computing (36). The computational costs discussed above are the dominant cost in Algorithm 4. We can replace S_j with $S_j Q_j$ in Algorithm 4 and follow the operations in Figure 10, the method achieves a reduced computational complexity $O(d \log(d) N n)$ compared to the original complexity $O(d^2 N n^2)$ for TT-SVD-c with cluster order $K = 1$.

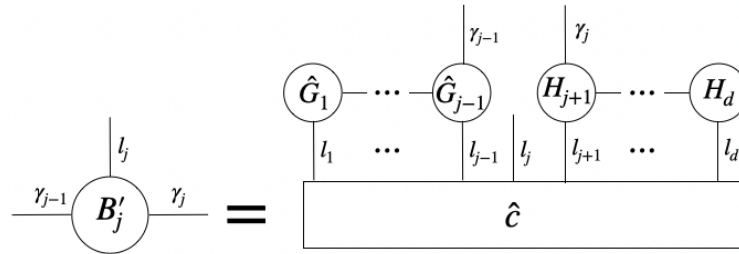
6 TT-SVD with random tensorized sketching (TT-rSVD-t)

In this section, we propose another modification for TT-SVD algorithm via sketching. This approach follows the randomized sketching technique (Huber et al. (2017)), originated from randomized linear algebra literature (Halko et al. (2011)), to accelerate SVD. The key idea is to choose sketching matrix $S_j \in \mathbb{R}^{n^{d-j} \times \tilde{r}}$ as some random matrix, where \tilde{r} is a given sketching size, which is usually chosen to be reasonably larger than target rank r of the output tensor-train estimator. Afterwards, similar as TT-SVD-c, we perform SVD to $B'_j = B_j S_j$. In general, the matrix multiplication $B_j S_j$ has exponentially large computational cost. Our solution to this curse of dimensionality is to form S_j by a set of random tensor trains, leading to the TT-rSVD-t algorithm summarized in Algorithm 5.

Algorithm 5 TT-rSVD-t

INPUT: Samples $\{x^{(i)}\}_{i=1}^N$. Target rank $\{r_1, \dots, r_{d-1}\}$. Sketching size \tilde{r} .

- 1: Generate random tensor train with cores $\{H_j\}_{j=1}^d$, where $H_1 \in \mathbb{R}^{n \times \tilde{r}}, H_2, \dots, H_{d-1} \in \mathbb{R}^{\tilde{r} \times n \times \tilde{r}}, H_d \in \mathbb{R}^{\tilde{r} \times n}$.
- 2: **for** $j \in \{1, \dots, d-1\}$ **do**
- 3: Perform SVD to $B'_j \in \mathbb{R}^{n r_{j-1} \times \tilde{r}_j}$, which is formed by the following tensor contraction



The contraction of the right-hand side is done efficiently as shown in Figure 12. With SVD $B'_j = U_j \Sigma_j V_j^T$, we obtain the j -th core $\hat{G}_j \in \mathbb{R}^{r_{j-1} \times n \times r_j}$, which is reshaped from the first r_j principle left singular vectors in U_j .

4: **end for**

5: Obtain the last core $\hat{G}_d = B'_d \in \mathbb{R}^{r_{d-1} \times n}$.

OUTPUT: Tensor train $\tilde{c} = \hat{G}_1 \circ \hat{G}_2 \circ \dots \circ \hat{G}_d \in \mathbb{R}^{n \times n \times \dots \times n}$.

To implement Algorithm 5, we first generate a d -dimensional random tensor train with fixed rank \tilde{r} whose cores are H_1, H_2, \dots, H_d (Line 1). In practice, we can set each core as i.i.d. random Gaussian matrix/tensor or random uniform matrix/tensor. When sketching B_j , we construct sketching matrix $S_j \in \mathbb{R}^{n^{d-j} \times \tilde{r}}$ as the reshaping of $H_{j+1} \circ H_{j+2} \circ \dots \circ H_d$ (Line 3). Afterwards, we contract B_j with S_j and perform SVD to solve the j -th core \hat{G}_j .

Similar to (36) for TT-SVD-c, B'_j is computed recursively as illustrated in Figure 12(c). The key difference lies in the new formulation of E_j , which arises from the new choice of sketching matrix S_j . Leveraging the tensor-train structure, E_j can also be computed recursively as shown in Figure 12(b). The total computational cost for $\{E_j\}_{j=1}^{d-1}$ is $O(dNn\tilde{r}^2)$. The computation of $\{D_j\}_{j=1}^{d-1}$, depicted in Figure 12(a), follows the same approach used in Algorithm 2 and incurs a computational cost of $O(dNn\tilde{r}^2)$. Overall, the SVD step required to compute all tensor cores has a total complexity of $O(dNn\tilde{r}^2)$, which is linear with respect to both dimensionality and sample size.

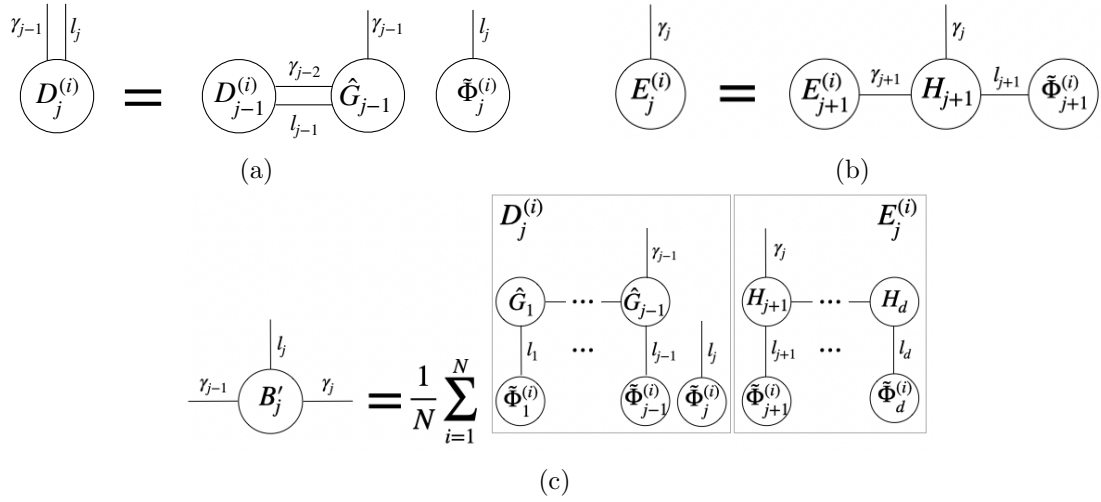


Figure 12: Tensor diagrams illustrating recursive computation of B'_j in Line 2 of Algorithm 5. (a) recursive calculation of $D_j^{(i)}$, which is the i -th column of the matrix D_j ; (b) recursive calculation of $E_j^{(i)}$, which is the i -th column of the matrix E_j ; (c) calculation of B'_j based on $D_j^{(i)}$ and $E_j^{(i)}$.

7 Pre-processing steps for general distributions

In this section, we propose several pre-processing steps to extend the discussed framework to general distributions. The pre-processing procedure consists of a dimension-reduction step using principal component analysis (PCA), followed by a step to determine the mean-field and the univariate bases. The full algorithm is summarized in Algorithm 6.

Algorithm 6 Tensor density estimator after variable re-ordering.

INPUT: Samples $\{x^{(i)}\}_{i=1}^N$. Embedding dimension d' , $d' \leq d$. Target rank $\{r_1, \dots, r_{d-1}\}$.

- 1: Apply PCA to the samples $\{x^{(i)}\}_{i=1}^N$. Denote the top d' orthonormal principal components as $Q \in \mathbb{R}^{d \times d'}$. Define the new variables as $z^{(i)} = Q^T x^{(i)}$, $i = 1, \dots, N$, with the associated empirical distribution denoted by \hat{p}_z .
- 2: Estimate the 1-marginals $\mu'_1(z_1) \cdots \mu'_{d'}(z_{d'})$ using one-dimensional kernel density estimation. The product of these 1-marginals forms the mean-field $\mu' = \prod_{j=1}^{d'} \mu'_j$ in the reduced coordinate system.
- 3: Compute the orthogonal basis $\{\phi_l^j(z_j)\}_{l=1}^n$ for each $j = 1, \dots, d'$, where the basis functions are orthogonalized with respect to $\mu'_j(z_j)$.
- 4: Obtain the d' -dimensional tensor density estimator in the reduced coordinate system:

$$\tilde{p}_z = \mu' \odot \text{diag}(\tilde{w}_\alpha)^{-1} \Phi (\text{TT-compress}(\text{diag}(\tilde{w}_\alpha) \Phi^T \hat{p}_z)),$$

where **TT-compress** is any tensor-train compression algorithm detailed in Section 3 – 6. The final density estimator in the original space is obtained as:

$$\tilde{p}(x) = \frac{1}{Z} \tilde{p}_z(Q^T x),$$

where Z is the normalization factor.

OUTPUT: Tensor density estimator \tilde{p} .

When dealing with a general distribution, the optimal ordering of variables is generally unknown. A poor variable ordering may lead to a high-rank TT representation, significantly increasing computational complexity. To address this, Step 1 of Algorithm 6 applies PCA to simultaneously decorrelate the variables and reduce the dimensionality. The resulting reduced-coordinate variables $\{z^{(i)}\}_{i=1}^N$ often exhibit simpler dependence structures, allowing a more compact TT representation. The eigen-decomposition in PCA can be performed through a “streaming approach”, as in [Henriksen and Ward \(2019\)](#); [Hoskins et al. \(2024\)](#); [Khoo et al. \(2024\)](#) with a complexity of $O(Ndd')$.

In Step 2 of Algorithm 6, we aim to perform the projection (10) on the empirical distribution \hat{p}_z . However, to do so, we require knowledge of the mean-field $\mu'(z) = \prod_{j=1}^{d'} \mu'_j(z_j)$. To approximate this, we apply a kernel density estimator to each of the one-dimensional marginals of \hat{p}_z . This step ensures that μ' captures the product structure of the new coordinate system.

In Step 3, we construct orthonormal basis functions with respect to each one-dimensional marginal. This can be achieved using a Gram-Schmidt procedure or a stable three-term recurrence method (see [Gautschi \(2004\)](#)) for polynomial basis functions.

Finally, in Step 4, we estimate the density \hat{p}_z in the reduced-coordinate system using the tensor-train density estimator. This involves applying any tensor-train compression algorithms **TT-compress** detailed in Section 3 – 6 to $\text{diag}(\tilde{w}_\alpha) \Phi^T \hat{p}_z$. The resulting density estimator \tilde{p}_z is then mapped back to the original space via the transformation $\tilde{p}(x) = \tilde{p}_z(Q^T x)$ followed by normalization.

8 Theoretical results

In this section, we present an error analysis of our proposed methods. For simplicity, we focus primarily on the hard-thresholding approach described in (9). Based on Section 2.3, we know the estimator from hard-thresholding approach in (9) is close to the primarily discussed soft-thresholding approach in (10). The detailed analysis of the soft-thresholding approach in (10) will be deferred to future work.

We again use the notations $\hat{c} = \text{diag}(w_K)\Phi^T\hat{p}$ and $c^* = \text{diag}(w_K)\Phi^T p^*$ to denote the coefficient tensors. For simplicity, we assume the mean-field component $\mu \sim \text{Unif}([0, 1]^d)$. In this way, the univariate basis functions $\{\phi_l\}_{l=1}^n$ are orthonormal, and we take Legendre polynomials as an example in our analysis. In addition, we propose the following assumptions on the ground truth density:

Assumption 1. *Suppose the ground truth density function $p^* : [0, 1]^d \rightarrow \mathbb{R}^+$ satisfies is an additive model (1-cluster):*

$$p^*(x_1, \dots, x_d) = 1 + q_1^*(x_1) + \dots + q_d^*(x_d), \quad (38)$$

where $q_j^* \in H^{\beta_0}([0, 1])$ for some integer $\beta_0 \geq 1$ satisfies the regularity

$$\min_j \|q_j^*\|_{L_2([0,1])} \geq b^* \quad \text{and} \quad \max_j \|q_j^*\|_{H^{\beta_0}([0,1])} \leq B^*$$

for two $O(1)$ positive constants b^* and B^* . Under this assumption, we can immediately obtained that $\|p^*\|_\infty \leq 1 + B^*d$ according to Sobolev embedding theorem.

Assumption 1 consider only the 1-cluster model and include the regularity constraint for each one-dimensional component. This motivation stems from the fact that the left/right subspaces are computationally straightforward, allowing for an efficient tensor-train representation of p^* . This specific structure, in turn, yields a favorable estimation error rate with respect to the dimensionality.

We state our main theorem under these assumptions:

Theorem 1. *Suppose the ground truth p^* satisfies Assumption 1, the empirical coefficient tensor $\hat{c} = \text{diag}(w_K)\Phi^T\hat{p}$, and*

$$N \geq C_0 d^{2K-1} n^{4K-2} \log(dn), \quad (39)$$

where C_0 is some sufficiently large constant independent of N , n and d . When we use TT-SVD (Algorithm 1) as TT-compress with \tilde{c} being the output with target rank $r = 2$, the following bound holds with high probability:

$$\frac{\|\tilde{c} - c^*\|_F}{\|c^*\|_F} = O\left(\sqrt{\frac{dnB^* \log(dn)}{N} \sum_{j=1}^{d-1} \frac{1}{\sigma_2^2(c^{*(j)})}}\right) \quad (40)$$

where $\sigma_2(\cdot)$ denotes the second largest singular value.

The theorem states that the relative error of the coefficient decreases at Monte Carlo rate $O(\frac{1}{\sqrt{N}})$ with respect to samples size N . Moreover, under the assumption that p^* is 1-cluster, the relative error grows only linearly with the dimensionality d , up to a logarithmic factor, if the second largest (also the smallest since $r = 2$) singular values of all the unfolding matrices of c^* are uniformly lower bounded.

For the error with respect to density, the following corollary presents the error bound, including additional approximation error. Both proofs are shown in the appendix.

Corollary 1. *Suppose all the conditions in Theorem 1 hold, the following bound for density estimator \tilde{p} (24) by TT-SVD (Algorithm 1) with target rank $r = 2$ holds with high probability:*

$$\frac{\|\tilde{p} - p^*\|_{L_2([0,1]^d)}}{\|p^*\|_{L_2([0,1]^d)}} = O\left(\sqrt{n^{-\beta_0} + \frac{dnB^* \log(dn)}{N} \sum_{j=1}^{d-1} \frac{1}{\sigma_2^2(c^*(j))}}\right), \quad (41)$$

where β_0 is the regularity parameter specified in Assumption 1.

9 Numerical results

In this section, we carry out numerical experiments to examine the performance of our proposed density estimation algorithms. In specific, we use TT-SVD-kn (Algorithm 3), TT-SVD-c (Algorithm 4) with hierarchical matrix decomposition and TT-rSVD-t (Algorithm 5). Unless otherwise noted, we use the following parameter settings throughout: we set the number of sampled columns in Nyström approximation $\tilde{r} = 100$ in TT-SVD-kn, sketching size $\tilde{r} = 10$ in TT-SVD-c with hierarchical matrix decomposition, sketching size $\tilde{r} = 30$ in TT-rSVD-t and the kernel parameter $\alpha = 0.01$. These parameter choices are based on empirical observations.

For simplicity, we choose the mean-field density μ as a uniform distribution, so that $\{\phi_l^j\}_{l=1}^n$ can be chosen as any orthonormal basis functions. Here we use the Fourier basis

$$\phi_l(x) = \begin{cases} \frac{1}{\sqrt{2L}}, & \text{for } l = 1, \\ \frac{1}{\sqrt{L}} \cos\left(\frac{l\pi x}{2L}\right) & \text{for even } l > 1 \\ \frac{1}{\sqrt{L}} \sin\left(\frac{(l+1)\pi x}{2L}\right) & \text{for odd } l > 1 \end{cases} \quad (42)$$

as the univariate basis function for all $j = 1, \dots, d$.

9.1 Gaussian mixture model

We first consider the d -dimensional Gaussian mixture model which is defined as :

$$\frac{1}{6}\mathcal{M}(0.18) + \frac{1}{3}\mathcal{M}(0.2) + \frac{1}{2}\mathcal{M}(0.22)$$

where

$$\mathcal{M}(\sigma) = \frac{2}{3}\mathcal{N}(-0.5, \sigma^2 I_{d \times d}) + \frac{1}{3}\mathcal{N}(0.5, \sigma^2 I_{d \times d}).$$

We set the domain as the hypercube $[-L, L]^d$ where $L = 1.5$ with mesh size 0.1 in each direction.

We first fix dimension $d = 10$. We draw N i.i.d samples from the mixture model, and use proposed three algorithms to fit a TT approximation for the empirical distribution of these samples. For the algorithms, we set fixed target rank $r = 3$ and use $n = 17$ Fourier bases. In the left panel of Figure 13, we test different sample sizes N and plot the relative L_2 -error defined by

$$\|\tilde{p} - p^*\|_{L_2} / \|p^*\|_{L_2}$$

in logarithm scale. One can observe that the relative error decays with Monte Carlo rate $O(1/\sqrt{N})$. Here we remark that the ground truth p^* for this Gaussian mixture model can be formulated as a

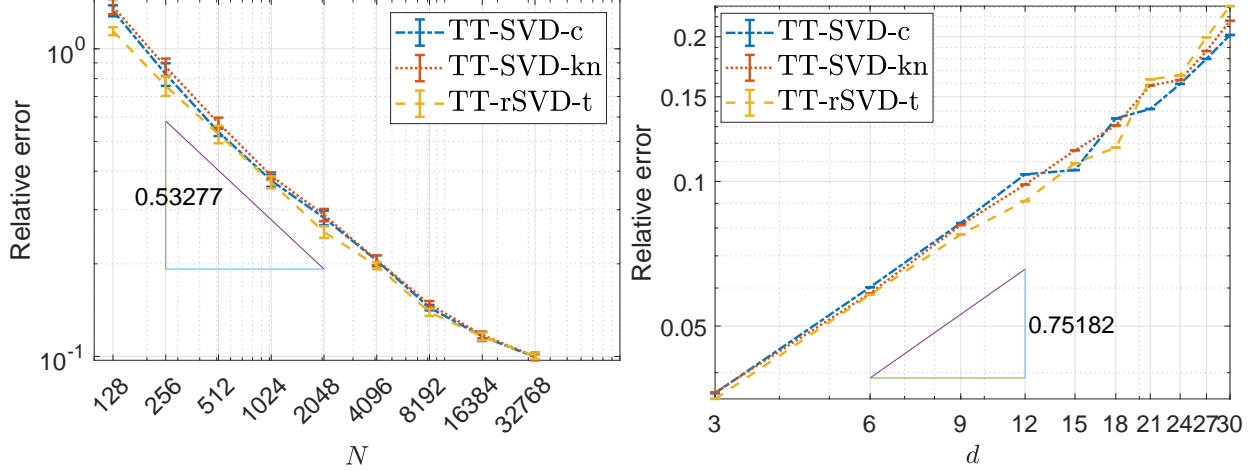


Figure 13: Gaussian mixture model: relative L_2 -error for proposed algorithms. Left: $d = 10$ and sample number $N = 2^7, 2^8, \dots, 2^{15}$. Right: $N = 10^6$ and dimension $d = 3, 6, 9, \dots, 30$.

TT without approximation error, and the numerical L_2 -norm based on quadrature of TTs can be easily computed with $O(d)$ complexity [Oseledets and Tyrtyshnikov \(2010\)](#).

Next, we fix the sample size $N = 10^6$ and test our algorithms with various dimensions d . The relative L_2 -error is plotted in right panel of Figure 13, which exhibits sublinear growth with increasing dimensionality according to the curves. In particular, with $N = 10^6$ samples, our algorithms can achieve two-digit relative L_2 -error up to $d = 12$. For dimensionality higher than that, we can expect that the error can also be controlled below 0.1 for a sufficiently large sample size, as suggested by the Monte Carlo convergence observed in the previous experiment.

Finally, we verify the time complexity of the algorithms. In Figure 14, we plot the wall clock time of three algorithms for fixed $d = 5$ with various N (left panel) and fixed $N = 10000$ with various d (right panel). The rates of wall clock time verify the theoretical computational complexity at listed in Table 1.

9.2 Ginzburg-Landau model

Now we consider a more practical problem in statistical physics as the Ginzburg-Landau model [Hoffmann and Tang \(2012\)](#). In particular, we consider the density estimation for the Boltzmann distribution

$$p^*(x) = \frac{1}{Z} e^{-\beta V(x)}$$

where β is the inverse temperature, Z is the normalization factor such that $\int p^*(x) dx = 1$, and V is the Ginzburg-Landau potential energy.

9.2.1 1D Ginzburg-Landau model

We first consider a 1D Ginzburg-Landau model where the potential energy is formulated as

$$V(x_1, \dots, x_d) = \sum_{i=1}^{d+1} \frac{\lambda}{2} \left(\frac{x_i - x_{i-1}}{h} \right)^2 + \frac{1}{4\lambda} (1 - x_i^2)^2 \text{ for } x \in [-L, L]^d \quad (43)$$

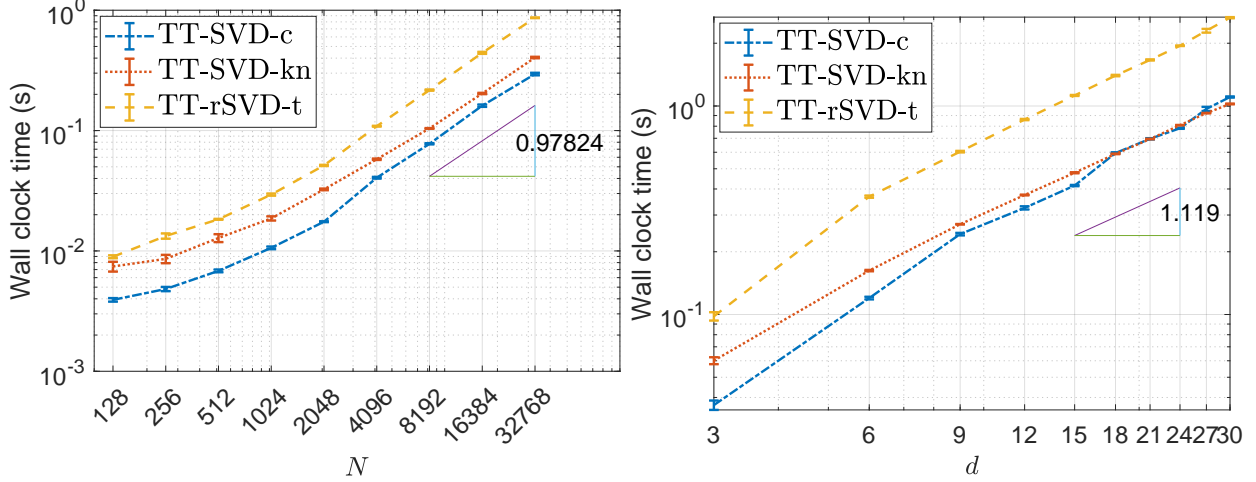


Figure 14: Gaussian mixture model: average wall clock time (seconds) for proposed algorithms. Left: $d = 5$ and sample number $N = 2^7, 2^8, \dots, 2^{15}$. Right: $N = 10000$ and dimension $d = 3, 6, 9, \dots, 30$.

where $x_0 = x_{d+1} = 0$, $h = 1/(1+d)$, $\lambda = 0.03$ and $\beta = 1/8$. We consider hypercube domain $[-L, L]^d$ with $L = 2.5$ and mesh size 0.05 in each direction. For the ground truth p^* , we use DMRG-cross algorithm (see [Savostyanov and Oseledets \(2011\)](#)) to get p^* in TT form, which is known to provide highly accurate approximations with arbitrarily prescribed precision. The samples of p^* are generated by running Langevin dynamics for sufficiently long time.

In Table 2, we list the relative L_2 -error of the approximated densities estimated by $N = 10^6$ samples with different number of univariate basis functions. For this example, we set fixed target rank $r = 4$. One can observe that the approximation improves as we use more basis functions. Such improvement can be further visualized in Figure 15, where we plot the marginal distribution of the approximated solutions solved by three algorithms when $d = 20$. All of them give accurate match to the sample histograms when a sufficient number of basis functions are used.

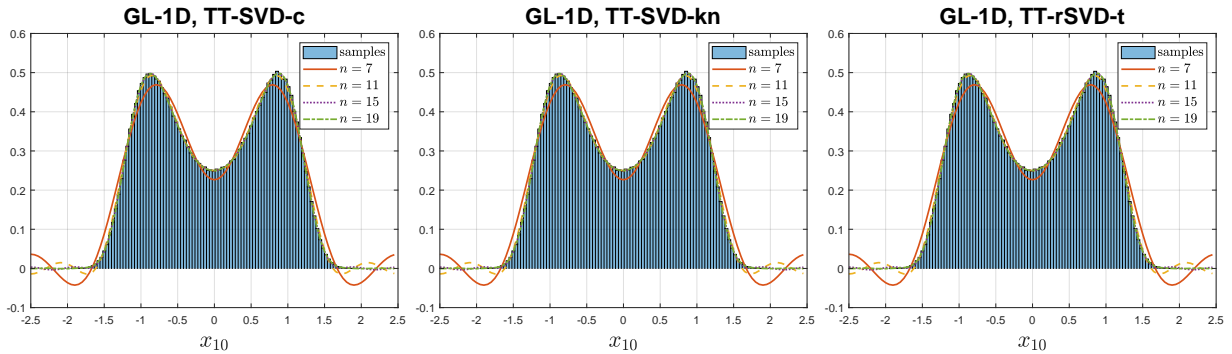


Figure 15: 1D G-L model: x_{10} -marginal of approximated solutions for $d = 20$ and $N = 10^6$ under different numbers of univariate basis functions used.

n	$d = 5$			$d = 10$		
	TT-SVD-c	TT-SVD-kn	TT-rSVD-t	TT-SVD-c	TT-SVD-kn	TT-rSVD-t
7	0.2810	0.2809	0.2810	0.4304	0.4304	0.4305
11	0.0782	0.0781	0.0781	0.1365	0.1365	0.1378
15	0.0305	0.0304	0.0301	0.0488	0.0483	0.0533
19	0.0275	0.0273	0.0289	0.0449	0.0404	0.0526
n	$d = 15$			$d = 20$		
	TT-SVD-c	TT-SVD-kn	TT-rSVD-t	TT-SVD-c	TT-SVD-kn	TT-rSVD-t
7	0.6342	0.6342	0.6343	0.7897	0.7897	0.7898
11	0.2169	0.2167	0.2186	0.3017	0.3016	0.3037
15	0.0733	0.0740	0.0836	0.1126	0.1125	0.1158
19	0.0613	0.0602	0.0716	0.0884	0.0874	0.1099

Table 2: 1D G-L model: comparison of L_2 relative errors with $N = 10^6$ and $d = 5, 10, 15, 20$ under different numbers of univariate basis functions used.

9.2.2 2D Ginzburg-Landau model

Next, we consider the 2D Ginzburg-Landau model which is defined on a $m \times m$ lattice. The potential energy is formulated as

$$V(x_{1,1}, \dots, x_{m,m}) = \frac{\lambda}{2} \sum_{i=1}^{m+1} \sum_{j=1}^{m+1} \left[\left(\frac{x_{i,j} - x_{i-1,j}}{h} \right)^2 + \left(\frac{x_{i,j} - x_{i,j-1}}{h} \right)^2 \right] + \frac{1}{4\lambda} \sum_{i=1}^m \sum_{j=1}^m (1 - x_{i,j}^2)^2$$

with the boundary condition

$$x_{0,j} = x_{m+1,j} = 1, \quad x_{i,0} = x_{i,m+1} = -1 \quad \forall i, j = 1, \dots, m$$

where we choose parameter $h = 1/(1+m)$, $\lambda = 0.1$ and inverse temperature $\beta = 1$. We set $L = 2$ with mesh size 0.05 for the domain. We consider a test example where $m = 16$ and thus the total number of dimensionality is $m^2 = 256$. For this 2D model, we apply the PCA pre-processing steps described in Section 7 to order the dimensions and also reduce the dimensionality, where we choose embedding dimension $d' = 100$. In terms of the algorithms, we set target rank $r = 10$, $\alpha = 0.001$ and we use $N = 10^4$ samples and $n = 21$ Fourier bases.

We evaluate the performance of our fitted tensor-train density estimators as generative models. Specifically, we first fit tensor-train density estimators \tilde{p} from the given $N = 10^4$ samples $\{x_i\}_{i=1}^N$ using proposed algorithms, then generate new samples $\{\tilde{x}_i\}_{i=1}^N$ from the learned tensor trains. Sampling each $\tilde{x}_i \sim \tilde{p}$ can be done via tensor-train conditional sampling

$$\tilde{p}(x_1, x_2, \dots, x_d) = \tilde{p}(x_1) \tilde{p}(x_2|x_1) \tilde{p}(x_3|x_2, x_1) \cdots \tilde{p}(x_d|x_{d-1}, \dots, x_1) \quad (44)$$

where each

$$\tilde{p}(x_i|x_{i-1}, \dots, x_1) = \frac{\tilde{p}(x_1, \dots, x_i)}{\tilde{p}(x_1, \dots, x_{i-1})}$$

is a conditional distribution of \tilde{p} , and $\tilde{p}(x_1), \dots, \tilde{p}(x_1, \dots, x_{d-1})$ are the marginal distributions. We point out each conditional sampling can be done in $O(d)$ complexity using the TT structure of \tilde{p} [Dolgov et al. \(2020\)](#).

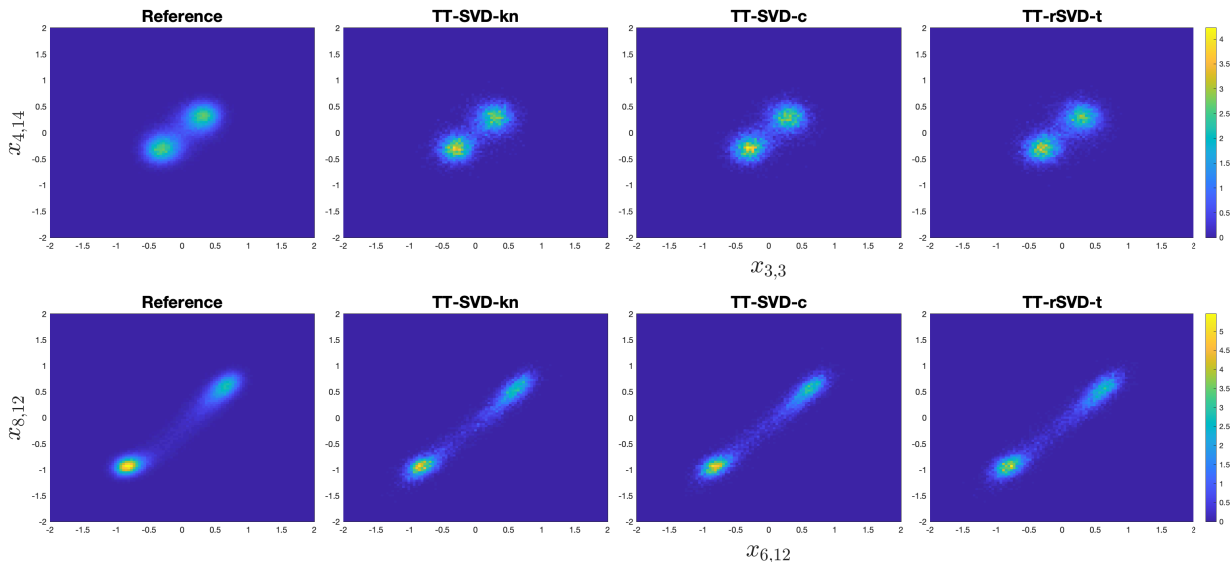


Figure 16: 2D G-L model on a 16×16 lattice: visualization of $(x_{3,3}, x_{14,14})$ -marginal (first row) and $(x_{6,12}, x_{8,12})$ -marginal (second row). Left to right: reference sample histograms, samples from tensor trains fitted by proposed algorithms.

Figure 16 illustrates the $(x_{3,3}, x_{14,14})$ -marginal and $(x_{6,12}, x_{8,12})$ -marginal distributions of the generated samples. For comparison, we also show results for $N^* = 10^5$ reference samples. The visualizations reveal that samples generated from tensor trains learned by all three proposed algorithms can capture local minima accurately. To quantify the accuracy, we compute the second-moment error

$$\|\tilde{X}^T \tilde{X} - X^{*T} X^*\|_F / \|X^{*T} X^*\|_F \quad (45)$$

where $\tilde{X} \in \mathbb{R}^{N \times d}$ is the matrix formed by the generated samples, and $X^* \in \mathbb{R}^{N^* \times d}$ are reference samples. The second-moment errors for TT-SVD-kn, TT-SVD-c and TT-rSVD-t algorithms are respectively 0.0278, 0.0252, 0.0264.

9.3 Comparison with neural network approaches

In this section, we compare the performance of generative models fitted by our proposed tensor-train algorithms with one example of neural network-based generative methods ([Papamakarios et al. \(2017\)](#)). For neural network details, we use 5 transforms and each transform is a 3-hidden layer neural network with width 128. We use Adam optimizer to train the neural network. The experiments are based on selected examples from previous subsections as well as real data from MNIST.

9.3.1 1D Ginzburg-Landau model

We first consider the Boltzmann distribution of 1D Ginzburg-Landau potential defined in (9.2.1) where we choose model parameters $\lambda = 0.005$ and $\beta = 1/20$. We use $N = 10^4$ samples as training data to fit tensor trains, and then generate $N = 10^4$ new samples from the learned tensor trains by conditional sampling (44).

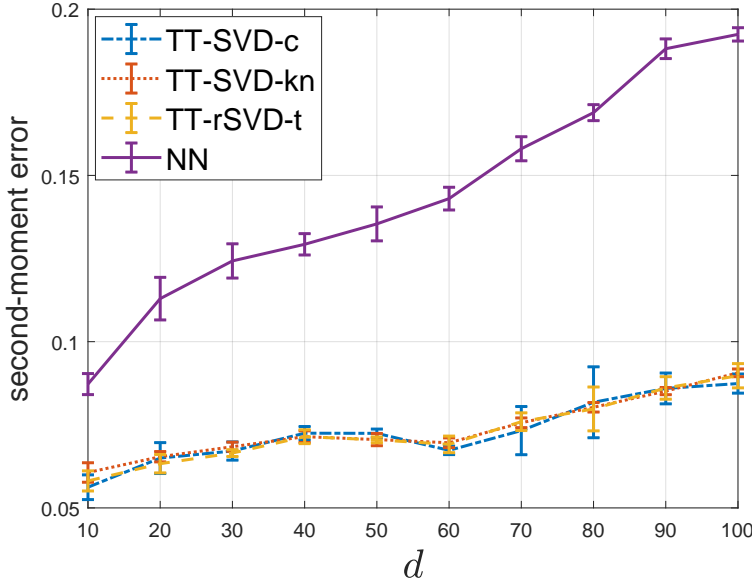


Figure 17: Comparison of second-moment errors of generated samples.

In Figure 17, we plot the second-moment errors of the samples generated by tensor-train algorithms and a neural network, compared against a reference set of $N^* = 10^6$ samples across various dimensions $d = 10, 20, \dots, 100$. Here we choose target rank $r = 4$ and use $n = 17$ Fourier bases for all simulations. The three proposed tensor-train algorithms exhibit similar performance and consistently achieve two-digit accuracy across all dimensions. Moreover, they are considerably more accurate than the neural network. To visualize this accuracy gap, Figure 18 further shows histograms of two selected marginal distributions from the generated samples for $d = 100$. It can be observed that samples generated by the tensor-train estimators more accurately capture local minima compared to those produced by the neural network.

9.3.2 Real data: MNIST

We also evaluate our algorithms on the MNIST dataset, which consists of 70,000 images of handwritten digits (0 through 9), each labeled with its corresponding digit. Each image is represented as a 28×28 pixel matrix. To learn the generative models, we treat the dataset as a collection of 70000×28^2 samples. For each digit class, we apply the TT-rSVD-t algorithm with parameters $\alpha = 0.05$, sketching rank $\tilde{r} = 40$, target rank $r = 10$ and $n = 15$ Fourier bases, to learn tensor-train representations from the corresponding samples of dimension $d = 28^2 = 784$. Again, the PCA pre-processing steps are applied to reduce dimensionality, where embedding dimension is set to $d' = 8$. After training, we independently sample five images for each digit from the learned TT, as shown in Figure 19(b). For comparison, Figure 19(a) displays five randomly selected images

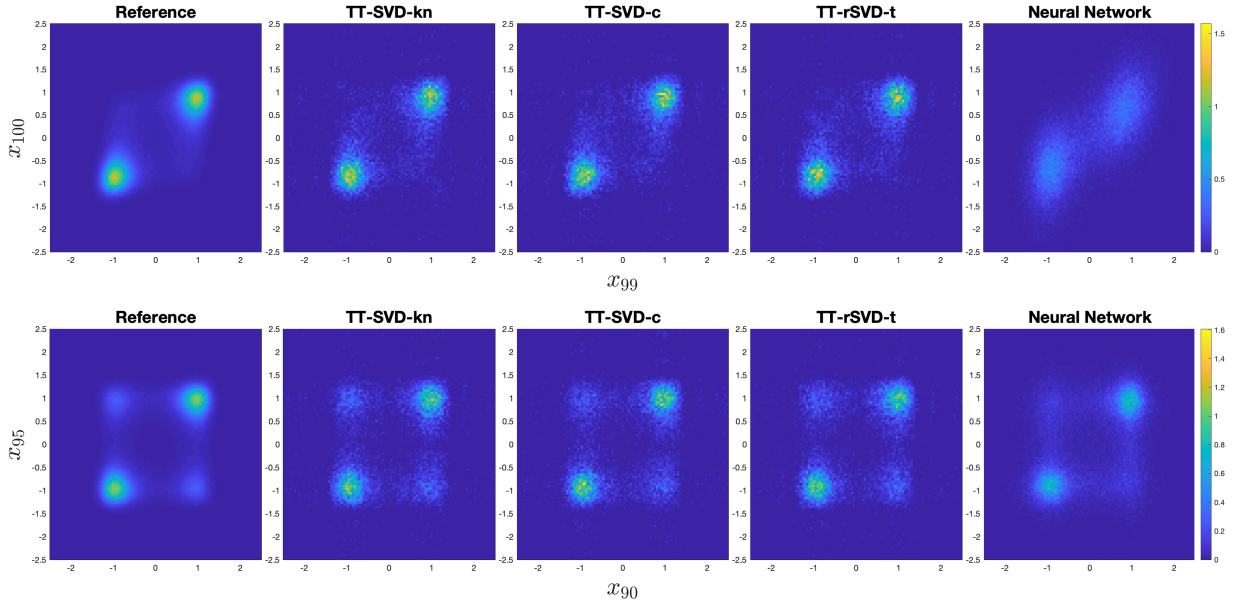


Figure 18: 1D G-L model for $d = 100$: visualization of (x_{99}, x_{100}) -marginal (first row) and (x_{90}, x_{95}) -marginal (second row) of samples from generative models. Left to right: reference samples, samples from tensor trains under three proposed algorithms, and samples from neural network.

per digit from the original MNIST dataset. The generated images from the tensor train exhibit well-preserved digit structures and visually plausible variations across classes.

10 Conclusion

In this paper, we propose a natural approach to high-dimensional density estimation entirely based on linear algebra, which allows the construction of a density estimator as a low-rank functional tensor train. To this end, we provide four tensor decomposition algorithms. The first one is based on direct TT-SVD algorithm with fast implementation in a density estimation setting. The second algorithm follows a Nystöm approximation. The third approach modifies the first approach by thresholding certain elements in the tensor and employing a hierarchical matrix factorization to accelerate computational efficiency. The last algorithm employs a tensorized sketching technique. Several of these proposed algorithms can achieve linear computational complexity both in dimension d and in sample size N . Theoretical analysis demonstrates that tensor-train estimators can also achieve linear scaling of the estimation error with respect to the dimensionality d under some specific conditions. Comprehensive numerical experiments validate the accuracy of all proposed algorithms, in comparison to other density estimators based on neural networks.

References

Markus Bachmayr, Reinhold Schneider, and André Uschmajew. Tensor networks and hierarchical tensors for the solution of high-dimensional partial differential equations. *Foundations of Computational Mathematics*, 16:1423–1472, 2016.

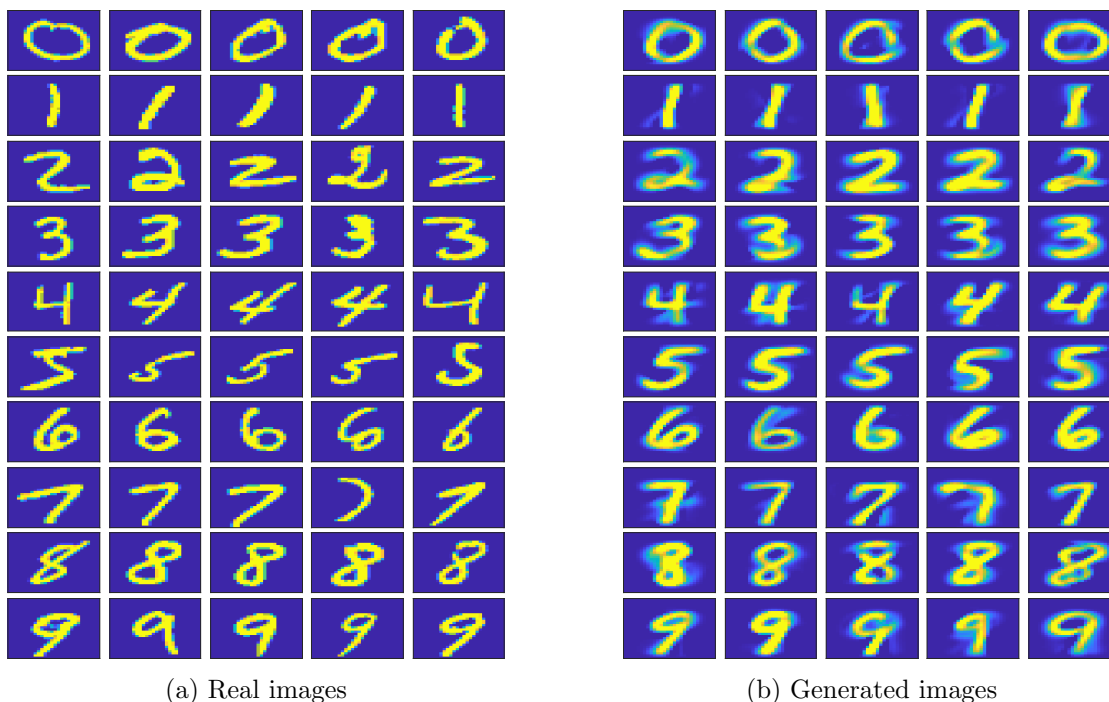


Figure 19: Generated and real images from MNIST. For each digit class, five images are randomly selected for illustration.

Mario Bebendorf. *Hierarchical matrices*. Springer, 2008.

Tai-Danae Bradley, E Miles Stoudenmire, and John Terilla. Modeling sequences with quantum states: a look under the hood. *Machine Learning: Science and Technology*, 1(3):035008, 2020.

T Tony Cai and Anru Zhang. Rate-optimal perturbation bounds for singular subspaces with applications to high-dimensional statistics. 2018.

Kamalika Chaudhuri, Sanjoy Dasgupta, Samory Kpotufe, and Ulrike Von Luxburg. Consistent procedures for cluster tree estimation and pruning. *IEEE Transactions on Information Theory*, 60(12):7900–7912, 2014.

Yen-Chi Chen. A tutorial on kernel density estimation and recent advances. *Biostatistics & Epidemiology*, 1(1):161–187, 2017.

Yian Chen and Yuehaw Khoo. Combining particle and tensor-network methods for partial differential equations via sketching. *arXiv preprint arXiv:2305.17884*, 2023.

Kyle Cranmer. Kernel estimation in high-energy physics. *Computer Physics Communications*, 136(3):198–207, 2001.

Richard A Davis, Keh-Shin Lii, and Dimitris N Politis. Remarks on some nonparametric estimates of a density function. *Selected Works of Murray Rosenblatt*, pages 95–100, 2011.

- Ronald A DeVore and George G Lorentz. *Constructive approximation*, volume 303. Springer Science & Business Media, 1993.
- Laurent Dinh, David Krueger, and Yoshua Bengio. Nice: Non-linear independent components estimation. *arXiv preprint arXiv:1410.8516*, 2014.
- Laurent Dinh, Jascha Sohl-Dickstein, and Samy Bengio. Density estimation using real nvp. *arXiv preprint arXiv:1605.08803*, 2016.
- Sergey Dolgov, Karim Anaya-Izquierdo, Colin Fox, and Robert Scheichl. Approximation and sampling of multivariate probability distributions in the tensor train decomposition. *Statistics and Computing*, 30:603–625, 2020.
- Yilun Du and Igor Mordatch. Implicit generation and modeling with energy based models. *Advances in Neural Information Processing Systems*, 32, 2019.
- Walter Gautschi. *Orthogonal polynomials: computation and approximation*. OUP Oxford, 2004.
- Mathieu Germain, Karol Gregor, Iain Murray, and Hugo Larochelle. Made: Masked autoencoder for distribution estimation. In *International conference on machine learning*, pages 881–889. PMLR, 2015.
- Ian Goodfellow, Jean Pouget-Abadie, Mehdi Mirza, Bing Xu, David Warde-Farley, Sherjil Ozair, Aaron Courville, and Yoshua Bengio. Generative adversarial networks. *Communications of the ACM*, 63(11):139–144, 2020.
- Wolfgang Hackbusch. A sparse matrix arithmetic based on-matrices. part i: Introduction to-matrices. *Computing*, 62(2):89–108, 1999.
- Wolfgang Hackbusch and Boris N Khoromskij. A sparse h-matrix arithmetic. part ii: Application to multi-dimensional problems. *Computing*, 64:21–47, 2000.
- Nathan Halko, Per-Gunnar Martinsson, and Joel A Tropp. Finding structure with randomness: Probabilistic algorithms for constructing approximate matrix decompositions. *SIAM review*, 53(2):217–288, 2011.
- Zhao-Yu Han, Jun Wang, Heng Fan, Lei Wang, and Pan Zhang. Unsupervised generative modeling using matrix product states. *Physical Review X*, 8(3):031012, 2018.
- Amelia Henriksen and Rachel Ward. Adaoja: Adaptive learning rates for streaming pca. *arXiv preprint arXiv:1905.12115*, 2019.
- Karl-Heinz Hoffmann and Qi Tang. *Ginzburg-Landau Phase Transition Theory and Superconductivity*. Birkhäuser Basel, 2012.
- Jeremy Hoskins, Yuehaw Khoo, Oscar Mickelin, Amit Singer, and Yuguan Wang. Subspace method of moments for ab initio 3-d single-particle cryo-em reconstruction. *arXiv preprint arXiv:2410.06889*, 2024.
- Benjamin Huber, Reinhold Schneider, and Sebastian Wolf. A randomized tensor train singular value decomposition. In *Compressed Sensing and its Applications: Second International MATHEON Conference 2015*, pages 261–290. Springer, 2017.

- William Huggins, Piyush Patil, Bradley Mitchell, K Birgitta Whaley, and E Miles Stoudenmire. Towards quantum machine learning with tensor networks. *Quantum Science and technology*, 4(2):024001, 2019.
- Yoonhaeng Hur, Jeremy G Hoskins, Michael Lindsey, E Miles Stoudenmire, and Yuehaw Khoo. Generative modeling via tensor train sketching. *Applied and Computational Harmonic Analysis*, 67:101575, 2023.
- Yuehaw Khoo, Yifan Peng, and Daren Wang. Nonparametric estimation via variance-reduced sketching. *arXiv preprint arXiv:2401.11646*, 2024.
- Taesup Kim and Yoshua Bengio. Deep directed generative models with energy-based probability estimation. *arXiv preprint arXiv:1606.03439*, 2016.
- Daniel Kressner and André Uschmajew. On low-rank approximability of solutions to high-dimensional operator equations and eigenvalue problems. *Linear Algebra and its Applications*, 493:556–572, 2016.
- Daniel Kressner, Bart Vandereycken, and Rik Voorhaar. Streaming tensor train approximation. *SIAM Journal on Scientific Computing*, 45(5):A2610–A2631, 2023.
- Ji Liu, Przemyslaw Musialski, Peter Wonka, and Jieping Ye. Tensor completion for estimating missing values in visual data. *IEEE transactions on pattern analysis and machine intelligence*, 35(1):208–220, 2012.
- Qiao Liu, Jiaze Xu, Rui Jiang, and Wing Hung Wong. Density estimation using deep generative neural networks. *Proceedings of the National Academy of Sciences*, 118(15):e2101344118, 2021.
- YP Mack and Murray Rosenblatt. Multivariate k-nearest neighbor density estimates. *Journal of Multivariate Analysis*, 9(1):1–15, 1979.
- Michael W Mahoney and Petros Drineas. Cur matrix decompositions for improved data analysis. *Proceedings of the National Academy of Sciences*, 106(3):697–702, 2009.
- Georgii S Novikov, Maxim E Panov, and Ivan V Oseledets. Tensor-train density estimation. In *Uncertainty in artificial intelligence*, pages 1321–1331. PMLR, 2021.
- Ivan Oseledets and Eugene Tyrtyshnikov. Tt-cross approximation for multidimensional arrays. *Linear Algebra and its Applications*, 432(1):70–88, 2010.
- Ivan V Oseledets. Tensor-train decomposition. *SIAM Journal on Scientific Computing*, 33(5):2295–2317, 2011.
- George Papamakarios, Theo Pavlakou, and Iain Murray. Masked autoregressive flow for density estimation. *Advances in neural information processing systems*, 30, 2017.
- Emanuel Parzen. On estimation of a probability density function and mode. *The annals of mathematical statistics*, 33(3):1065–1076, 1962.
- Yifan Peng, Yian Chen, E Miles Stoudenmire, and Yuehaw Khoo. Generative modeling via hierarchical tensor sketching. *arXiv preprint arXiv:2304.05305*, 2023.

- David Perez-Garcia, Frank Verstraete, Michael M Wolf, and J Ignacio Cirac. Matrix product state representations. *arXiv preprint quant-ph/0608197*, 2006.
- Danilo Rezende and Shakir Mohamed. Variational inference with normalizing flows. In *International conference on machine learning*, pages 1530–1538. PMLR, 2015.
- Dmitry Savostyanov and Ivan Oseledets. Fast adaptive interpolation of multi-dimensional arrays in tensor train format. In *The 2011 International Workshop on Multidimensional (nD) Systems*, pages 1–8. IEEE, 2011.
- David W Scott. On optimal and data-based histograms. *Biometrika*, 66(3):605–610, 1979.
- David W Scott. Averaged shifted histograms: effective nonparametric density estimators in several dimensions. *The Annals of Statistics*, pages 1024–1040, 1985.
- Richik Sengupta, Soumik Adhikary, Ivan Oseledets, and Jacob Biamonte. Tensor networks in machine learning. *European Mathematical Society Magazine*, (126):4–12, 2022.
- Tianyi Shi, Maximilian Ruth, and Alex Townsend. Parallel algorithms for computing the tensor-train decomposition. *SIAM Journal on Scientific Computing*, 45(3):C101–C130, 2023.
- Qingquan Song, Hancheng Ge, James Caverlee, and Xia Hu. Tensor completion algorithms in big data analytics. *ACM Transactions on Knowledge Discovery from Data (TKDD)*, 13(1):1–48, 2019.
- Yang Song and Stefano Ermon. Generative modeling by estimating gradients of the data distribution. *Advances in neural information processing systems*, 32, 2019.
- Edwin Stoudenmire and David J Schwab. Supervised learning with tensor networks. *Advances in neural information processing systems*, 29, 2016.
- Yiming Sun, Yang Guo, Charlene Luo, Joel Tropp, and Madeleine Udell. Low-rank tucker approximation of a tensor from streaming data. *SIAM Journal on Mathematics of Data Science*, 2(4):1123–1150, 2020.
- Xun Tang and Lexing Ying. Solving high-dimensional fokker-planck equation with functional hierarchical tensor. *arXiv preprint arXiv:2312.07455*, 2023.
- Xun Tang, Yoonhaeng Hur, Yuehaw Khoo, and Lexing Ying. Generative modeling via tree tensor network states. *arXiv preprint arXiv:2209.01341*, 2022.
- Benigno Uribe, Marc-Alexandre Côté, Karol Gregor, Iain Murray, and Hugo Larochelle. Neural autoregressive distribution estimation. *The Journal of Machine Learning Research*, 17(1):7184–7220, 2016.
- Haiyong Wang. How much faster does the best polynomial approximation converge than legendre projection? *Numerische Mathematik*, 147(2):481–503, 2021.
- Steven R White. Density-matrix algorithms for quantum renormalization groups. *Physical review b*, 48(14):10345, 1993.

Christopher Williams and Matthias Seeger. Using the nystrom method to speed up kernel machines. *Advances in neural information processing systems*, 13, 2000.

Adriano Z Zambom and Ronaldo Dias. A review of kernel density estimation with applications to econometrics. *International Econometric Review*, 5(1):20–42, 2013.

A Definitions and notations for the proof of Theorem 1

Before the proof, we introduce some definitions and notations that will be used in the main proof in Appendix B.

To begin with, we use $c^* \in \mathbb{R}^{n^d}$ to present the coefficient tensor of ground truth under a set of orthonormal basis functions $\{\phi_l^j\}_{l=1}^n$, whose entries are given by

$$c^*(l_1, \dots, l_d) = \langle p^*, \phi_{l_1}^1 \cdots \phi_{l_d}^d \rangle.$$

In the remainder of this appendix, we omit the superscripts on the basis functions unless they are needed to indicate the corresponding coordinate of dimensions. Based on the additive formulation of ground truth p^* in (38) and orthogonality of $\{\phi_l^j\}_{l=1}^n$, c^* can be expressed as

$$c^* = \mathbf{1}^d + c_1^* \otimes \mathbf{1}^{d-1} + \mathbf{1} \otimes c_2^* \otimes \mathbf{1}^{d-2} + \cdots + \mathbf{1}^{d-1} \otimes c_d^*, \quad (46)$$

where $\mathbf{1}^k \in \mathbb{R}^{n^k}$ represents the k times Kronecker product of $\mathbf{1} = [1, 0, \dots, 0]^T \in \mathbb{R}^n$. $c_j^* \in \mathbb{R}^n$ is a vector whose l -th coordinate is given by

$$c_j^*(l) = \int_0^1 \cdots \int_0^1 p^*(x_1, \dots, x_d) \phi_l(x_j) dx_1 \cdots dx_d. \quad (47)$$

We can further simplify the expression of c_j^* as follows. By the normalization condition of p^* , q_j^* in the expression of p^* satisfies $\sum_{j=1}^d \int_0^1 q_j^*(x_j) dx_j = 0$. Without loss of generality, we assume that

$$\int_0^1 q_j^*(x_j) dx_j = 0. \quad (48)$$

This further gives us

$$c_j^*(l) = \begin{cases} 0, & \text{if } l = 1; \\ \int_0^1 q_j^*(x_j) \phi_l(x_j) dx_j, & \text{if } 2 \leq l \leq n. \end{cases} \quad (49)$$

Definition 1. Let $\mathcal{B}_{s,d}$ be the s -cluster basis functions defined in (5). Define the s -cluster estimator

$$\hat{p}_s(x) := 1 + \sum_{\varphi_1 \in \mathcal{B}_{1,d}} \langle \hat{p}, \varphi_1 \rangle \varphi_1(x) + \cdots + \sum_{\varphi_s \in \mathcal{B}_{s,d}} \langle \hat{p}, \varphi_s \rangle \varphi_s(x) \quad (50)$$

The corresponding coefficient tensor $\hat{c}[s] \in \mathbb{R}^{n^d}$ of \hat{p}_s is

$$\hat{c}[s](l_1, \dots, l_d) = \langle \hat{p}_s, \varphi_{l_1} \cdots \varphi_{l_d} \rangle. \quad (51)$$

In this case, $\hat{c}[s]$ will be referred to as the s -cluster coefficient estimator of c^* .

Definition 2. Given matrix $A \in \mathbb{R}^{m \times n}$ and positive integer $r \leq \min\{m, n\}$, we define function $\text{SVD} : \mathbb{R}^{m \times n} \times \mathbb{Z}^+ \rightarrow \mathbb{O}^{m \times r}$ satisfying

$$\text{SVD}(A, r) = U \quad (52)$$

where $A = U \Sigma V^T$ is the top- r SVD of the matrix A .

B Proof of the main Theorem 1

In this proof, we simply denote $\hat{c}[K]$ as defined in (51) by \hat{c} .

Proof. Let $\hat{G}_{1:d}$ be the TT cores of \tilde{c} , to bound the error $\|c^* - \hat{G}_{1:d}\|_F$, we first use Lemma 4 to formulate it as

$$\begin{aligned} & \|c^* - \hat{G}_{1:d}\|_F^2 \\ &= \|\hat{G}_{1:d-1} \hat{G}_{1:d-1}^T c^{*(d-1)} - c^{*(d-1)}\|_F^2 \end{aligned} \quad (53)$$

$$+ \|\hat{G}_{1:d-1} \hat{G}_{1:d-1}^T \hat{c}^{(d-1)} - \hat{G}_{1:d-1} \hat{G}_{1:d-1}^T c^{*(d-1)}\|_F^2. \quad (54)$$

Later we will bound the above two terms by **Step 1** and **Step 2** respectively. Before elaborating these two steps, let us introduce two error estimates that will be used frequently in the proof of this theorem. With high probability, we have

$$\max_{k \in \{1, \dots, d\}} \|(U_{k-1}^{*T} \otimes I_n)(c^{*(k)} - \hat{c}^{(k)})V_k^*\|_F \leq C_1 \sqrt{\frac{n \log(dn) \|p^*\|_\infty}{N}}, \quad (55)$$

$$\|c^* - \hat{c}\|_F \leq C_2 \left(\sqrt{\frac{d^K n^{2K}}{N}} \right). \quad (56)$$

Their proofs are provided respectively by Lemma 11 and Lemma 12. In the above inequality, C_1, C_2 are two sufficiently large universal constants. U_k^* and V_k^* are orthogonal matrices such that $U_k^* U_k^{*T} \in \mathbb{R}^{n^k \times n^k}$ is the projection matrix onto the space $\text{Col}(c^{*(k)})$, and $V_k^* V_k^{*T} \in \mathbb{R}^{n^{d-k} \times n^{d-k}}$ is the projection matrix onto the space $\text{Row}(c^{*(k)})$. Due to the additive formulation (46) of c^* , U_k^* and V_k^* have analytical expressions, shown in Lemma 8.

(56) provides an upper bound of the gap between empirical and ground truth coefficient tensor, which scales as $O(d^{K/2})$ upon using K -cluster basis for the density estimator. Notably, with the projection U_k^* and V_k^* , this gap grows only at $O(\sqrt{d \log(dn)})$ under the Assumption 1 for $\|p^*\|_\infty$ as stated in (55). This is due to the 1-cluster structure of c^* , which is the key to make our error analysis sharp.

Step 1. To bound (53), we show by induction that for $k \in \{1, \dots, d-1\}$,

$$\|\hat{G}_{1:k} \hat{G}_{1:k}^T c^{*(k)} - c^{*(k)}\|_F^2 \leq C_3 \frac{n \log(dn) \|p^*\|_\infty \|c^*\|_F^2}{N} \sum_{j=1}^k \frac{1}{\sigma_2^2(c^{*(j)})} \quad (57)$$

for a universal sufficiently large constant C_3 with high probability, where $\sigma_2(c^{*(j)})$ is the second largest singular value of the unfolding matrix $c^{*(j)}$.

We prove $k=1$ first:

$$\|\hat{G}_1 \hat{G}_1^T c^{*(1)} - c^{*(1)}\|_F^2 = \|\hat{G}_1 \hat{G}_1^T c^{*(1)} - U_1^* U_1^{*T} c^{*(1)}\|_F^2 \leq \|\hat{G}_1 \hat{G}_1^T - U_1^* U_1^{*T}\|_2^2 \|c^*\|_F^2 \quad (58)$$

We use the matrix perturbation theory in Corollary 3 to bound $\|\hat{G}_1 \hat{G}_1^T - U_1^* U_1^{*T}\|_2$. The spectrum gap assumption in Corollary 3 holds since $\|\hat{c}^{(1)} - c^{*(1)}\|_F \leq O\left(\sqrt{\frac{d^K n^{2K}}{N}}\right)$ and $O\left(\sqrt{\frac{d^K n^{2K}}{N}}\right) \leq \sigma_2(c^{*(1)})$ by (56) and using a sufficiently large N such that (39) holds. Therefore, we have

$$\|\hat{G}_1 \hat{G}_1^T - U_1^* U_1^{*T}\|_2 \leq C_4 \left(\frac{\|(\hat{c}^{(1)} - c^{*(1)})V_1^{*T}\|_2}{\sigma_2(c^{*(1)})} + \frac{\|\hat{c}^{(1)} - c^{*(1)}\|_2^2}{\sigma_2^2(c^{*(1)})} \right). \quad (59)$$

for some universal constant C_4 . According to (55), the first term

$$\frac{\|(\hat{c}^{(1)} - c^{*(1)})V_1^{*T}\|_2}{\sigma_2(c^{*(1)})} \leq C_1 \sqrt{\frac{n \log(dn) \|p^*\|_\infty}{N \sigma_2^2(c^{*(1)})}} \quad (60)$$

and the second term can be bounded by the first term upon using sufficiently large N such that (39) holds. Therefore,

$$\|\hat{G}_1 \hat{G}_1^T c^{*(1)} - c^{*(1)}\|_F^2 \leq C_3 \frac{n \log(dn) \|p^*\|_\infty \|c^*\|_F^2}{N \sigma_2^2(c^{*(1)})} \quad (61)$$

for some universal constant C_3 .

Now suppose (57) holds for k . Then for $k+1$,

$$\begin{aligned} & \|\hat{G}_{1:k+1} \hat{G}_{1:k+1}^T c^{*(k+1)} - c^{*(k+1)}\|_F^2 \\ &= \|\hat{G}_{1:k+1} \hat{G}_{1:k+1}^T c^{*(k+1)} - (\hat{G}_{1:k} \otimes I_n)(\hat{G}_{1:k} \otimes I_n)^T c^{*(k+1)}\|_F^2 + \|\hat{G}_{1:k} \hat{G}_{1:k}^T c^{*(k)} - c^{*(k)}\|_F^2 \\ &\leq \|\hat{G}_{1:k+1} \hat{G}_{1:k+1}^T c^{*(k+1)} - (\hat{G}_{1:k} \otimes I_n)(\hat{G}_{1:k} \otimes I_n)^T c^{*(k+1)}\|_F^2 \end{aligned} \quad (62)$$

$$+ C_3 \frac{n \log(dn) \|p^*\|_\infty \|c^*\|_F^2}{N} \sum_{j=1}^k \frac{1}{\sigma_2^2(c^{*(j)})}. \quad (63)$$

where the equality follows from Lemma 3, and the inequality follows from induction (57). It suffices to bound (62). Note that

$$\begin{aligned} (62) &= \|(\hat{G}_{1:k} \otimes I_n) \hat{G}_{k+1} \hat{G}_{k+1}^T (\hat{G}_{1:k} \otimes I_n)^T c^{*(k+1)} - (\hat{G}_{1:k} \otimes I_n)(\hat{G}_{1:k} \otimes I_n)^T c^{*(k+1)}\|_F^2 \\ &= \|(\hat{G}_{1:k} \otimes I_n) [\hat{G}_{k+1} \hat{G}_{k+1}^T (\hat{G}_{1:k} \otimes I_n)^T c^{*(k+1)} - (\hat{G}_{1:k} \otimes I_n)^T c^{*(k+1)}]\|_F^2 \\ &\leq \|\hat{G}_{1:k} \otimes I_n\|_2^2 \|\hat{G}_{k+1} \hat{G}_{k+1}^T (\hat{G}_{1:k} \otimes I_n)^T c^{*(k+1)} - (\hat{G}_{1:k} \otimes I_n)^T c^{*(k+1)}\|_F^2 \\ &= \|\hat{G}_{k+1} \hat{G}_{k+1}^T (\hat{G}_{1:k} \otimes I_n)^T c^{*(k+1)} - (\hat{G}_{1:k} \otimes I_n)^T c^{*(k+1)}\|_F^2. \end{aligned} \quad (64)$$

Step 1A. Define the matrix formed by principal left singular vectors:

$$\tilde{G}_{k+1} = \text{SVD}((\hat{G}_{1:k} \otimes I_n)^T c^{*(k+1)}, 2) \in \mathbb{O}^{2n \times 2}. \quad (65)$$

where the SVD function is defined in (52). Since $\text{Rank}((\hat{G}_{1:k-1} \otimes I_n)^T c^{*(k)}) = 2$, it follows that

$$(\hat{G}_{1:k} \otimes I_n)^T c^{*(k+1)} = \tilde{G}_{k+1} \tilde{G}_{k+1}^T (\hat{G}_{1:k} \otimes I_n)^T c^{*(k+1)}. \quad (66)$$

Therefore by (64) and (66),

$$\begin{aligned} (62) &= \|\hat{G}_{k+1} \hat{G}_{k+1}^T (\hat{G}_{1:k+1} \otimes I_n)^T c^{*(k+1)} - \tilde{G}_{k+1} \tilde{G}_{k+1}^T (\hat{G}_{1:k} \otimes I_n)^T c^{*(k+1)}\|_F^2 \\ &\leq \|\hat{G}_{k+1} \hat{G}_{k+1}^T - \tilde{G}_{k+1} \tilde{G}_{k+1}^T\|_2^2 \|\hat{G}_{1:k} \otimes I_n\|_2^2 \|c^{*(k+1)}\|_F^2 \\ &= \|\hat{G}_{k+1} \hat{G}_{k+1}^T - \tilde{G}_{k+1} \tilde{G}_{k+1}^T\|_2^2 \|c^*\|_F^2. \end{aligned} \quad (67)$$

Perturbation of projection matrices $\|\hat{G}_{k+1} \hat{G}_{k+1}^T - \tilde{G}_{k+1} \tilde{G}_{k+1}^T\|_2$ will again be estimated using Corollary 3. More specifically, in Corollary 3, we consider $\hat{A} = (\hat{G}_{1:k} \otimes I_n)^T \hat{c}^{(k+1)}$ and $A = \hat{G}_{1:k} \otimes$

$I_n)^T c^{*(k+1)}$, and $\hat{G}_{k+1} \hat{G}_{k+1}^T$ and $\tilde{G}_{k+1} \tilde{G}_{k+1}^T$ are respectively the projection matrices of \hat{A} and A . In the subsequent **Step 1B**, we verify the conditions that should be satisfied in Corollary 3.

Step 1B. By the induction assumption (57), we have

$$\begin{aligned} \|\hat{G}_{1:k} \hat{G}_{1:k}^T c^{*(k)} - c^{*(k)}\|_F^2 &\leq C_3 \frac{n \log(dn) \|p^*\|_\infty \|c^*\|_F^2}{N} \sum_{j=1}^k \frac{1}{\sigma_2^2(c^{*(j)})} \\ &\leq \frac{C_3 n \log(dn) (1 + B^* d) C_c d}{N} \sum_{j=1}^d \frac{d}{c_\sigma^2 j (d-j)} \leq \frac{C_4 n d^2 \log^2(dn)}{N}, \end{aligned} \quad (68)$$

where C_4 is a universal constant, B^* is given in Assumption 1. The second inequality above follows from upper bound for $\|c^*\|_F^2$ in Corollary 2 and the lower bound for singular value in Lemma 10, and the third inequality follows from the fact that $\sum_{j=1}^d \frac{1}{j(d-j)} = O(\frac{\log(d)}{d})$. Consequently,

$$\|(\hat{G}_{1:k} \otimes I_n)(\hat{G}_{1:k} \otimes I_n)^T c^{*(k+1)} - c^{*(k+1)}\|_F^2 = \|\hat{G}_{1:k} \hat{G}_{1:k}^T c^{*(k)} - c^{*(k)}\|_F^2 \leq \frac{\sigma_2^2(c^{*(k+1)})}{4}, \quad (69)$$

where the inequality follows from the lower bound for the singular value $c^{*(k)}$ given in Lemma 10 and the assumption (39) on sample size N . Therefore, by Lemma 18,

$$\bullet \text{ Rank}((\hat{G}_{1:k} \otimes I_n)^T c^{*(k+1)}) = 2; \quad (70)$$

$$\bullet V_{k+1}^* V_{k+1}^{*T} \text{ is the projection matrix on to } \text{Row}((\hat{G}_{1:k} \otimes I_n)^T c^{*(k+1)}); \quad (71)$$

$$\bullet \sigma_2((\hat{G}_{1:k} \otimes I_n)^T c^{*(k+1)}) \geq \frac{\sigma_2(c^{*(k+1)})}{2}. \quad (72)$$

We start to apply Corollary 3 to \hat{G}_{k+1} and \tilde{G}_{k+1} , observe that

$$\begin{aligned} &\|(\hat{G}_{1:k} \otimes I_n)^T c^{*(k+1)} - (\hat{G}_{1:k} \otimes I_n)^T \hat{c}^{(k+1)}\|_F \leq \|\hat{G}_{1:k} \otimes I_n\|_2 \|c^{*(k+1)} - \hat{c}^{(k+1)}\|_F \\ &= \|\hat{c} - c^*\|_F \leq C_2 \left(\sqrt{\frac{d^K n^{2K}}{N}} \right) \leq 8\sigma_2(c^{*(k+1)}) \leq 4\sigma_2((\hat{G}_{1:k} \otimes I_n)^T c^{*(k)}), \end{aligned} \quad (73)$$

where the equality follows from the fact that $\hat{G}_{1:k} \otimes I_n \in \mathbb{O}^{n^{k+1} \times 2n}$, the second inequality follows from (56), the third inequality follows from (39), and the last inequality follows from (72). Since (73) and (71) hold, by Corollary 3

$$\begin{aligned} &\|\tilde{G}_{k+1} \tilde{G}_{k+1}^T - \hat{G}_{k+1} \hat{G}_{k+1}\|_2 \\ &\leq \frac{\|(\hat{G}_{1:k} \otimes I_n)^T (c^{*(k+1)} - \hat{c}^{(k+1)}) V_{k+1}^*\|_2}{\sigma_2((\hat{G}_{1:k} \otimes I_n)^T c^{*(k+1)})} \end{aligned} \quad (74)$$

$$+ \frac{\|(\hat{G}_{1:k} \otimes I_n)^T (c^{*(k+1)} - \hat{c}^{(k+1)})\|_2^2}{\sigma_2^2((\hat{G}_{1:k} \otimes I_n)^T c^{*(k+1)})^2} \quad (75)$$

We will bound (74) in **Step 1D** and (75) in **Step 1E**.

Step 1D. For (74), we have

$$\begin{aligned}
& \|(\hat{G}_{1:k} \otimes I_n)^T (c^{*(k+1)} - \hat{c}^{(k+1)}) V_{k+1}^* \|_2 \\
&= \|(\hat{G}_{1:k} \otimes I_n)(\hat{G}_{1:k} \otimes I_n)^T (c^{*(k+1)} - \hat{c}^{(k+1)}) V_{k+1}^* \|_2 \\
&= \|(\hat{G}_{1:k} \hat{G}_{1:k}^T \otimes I_n)(c^{*(k+1)} - \hat{c}^{(k+1)}) V_{k+1}^* \|_2 \\
&\leq \|(\{U_k^* U_k^{*T} - \hat{G}_{1:k} \hat{G}_{1:k}^T\} \otimes I_n)(c^{*(k+1)} - \hat{c}^{(k+1)}) V_{k+1}^* \|_2 \\
&+ \|(U_k^* U_k^{*T} \otimes I_n)(c^{*(k+1)} - \hat{c}^{(k+1)}) V_{k+1}^* \|_2.
\end{aligned} \tag{76}$$

$$\tag{77}$$

Note that

$$\begin{aligned}
(77) &= \|(U_k^* \otimes I_n)(U_k^* \otimes I_n)^T (c^{*(k+1)} - \hat{c}^{(k+1)}) V_{k+1}^* \|_2 \\
&= \|(U_k^* \otimes I_n)^T (c^{*(k+1)} - \hat{c}^{(k+1)}) V_{k+1}^* \|_2 \\
&\leq C_1 \sqrt{\frac{n \log(dn) \|p^*\|_\infty}{N}} \leq \frac{\sqrt{C_3}}{8} \sqrt{\frac{n \log(dn) \|p^*\|_\infty}{N}},
\end{aligned} \tag{78}$$

where the last inequality follows from (55) and we choose C_3 in (61) to be at least $64C_1^2$. In addition,

$$\begin{aligned}
(76) &\leq \| \{U_k^* U_k^{*T} - \hat{G}_{1:k} \hat{G}_{1:k}^T\} \otimes I_n \|_2 \|c^{*(k+1)} - \hat{c}^{(k+1)}\|_2 \|V_{k+1}^* \|_2 \\
&= \|U_k^* U_k^{*T} - \hat{G}_{1:k} \hat{G}_{1:k}^T\|_2 \|c^* - \hat{c}\|_2 \leq \|U_k^* U_k^{*T} - \hat{G}_{1:k} \hat{G}_{1:k}^T\|_2 C_2 \left(\sqrt{\frac{d^K n^{2K}}{N}} \right) \\
&\leq C_4 \frac{\sqrt{n \|p^*\|_\infty}}{\sigma_2(c^{*(k)})} \sqrt{\frac{d \log(dn)}{N}} C_2 \left(\sqrt{\frac{d^K n^{2K}}{N}} \right) \leq \frac{\sqrt{C_3}}{8} \sqrt{\frac{n \log(dn) \|p^*\|_\infty}{N}},
\end{aligned} \tag{79}$$

where the second inequality follows from (56), the third inequality in which C_4 is a universal constant follows from Lemma 5, and the last inequality holds for sufficiently large N in (39).

Therefore (76), (77), (78), and (79) together lead to

$$\|(\hat{G}_{1:k} \otimes I_n)^T (c^{*(k+1)} - \hat{c}^{(k+1)}) V_{k+1}^* \|_2 \leq \frac{\sqrt{C_3}}{4} \sqrt{\frac{n \log(dn) \|p^*\|_\infty}{N}}. \tag{80}$$

So by (80) and (72),

$$(74) \leq \frac{\sqrt{C_3}}{2} \frac{\sqrt{n \log(dn) \|p^*\|_\infty}}{\sqrt{N} \sigma_2(c^{*(k+1)})}. \tag{81}$$

Step 1E. Observe that

$$(75) \leq \frac{\|c^{*(k+1)} - \hat{c}^{(k+1)}\|_2^2}{\sigma_2^2((\hat{G}_{1:k} \otimes I_n)^T c^{*(k+1)})^2} \leq \frac{4C_2^2 d^K n^{2K}}{N \sigma_2^2(c^{*(k+1)})} \leq \frac{\sqrt{C_3}}{2} \frac{\sqrt{n \log(dn) \|p^*\|_\infty}}{\sqrt{N} \sigma_2(c^{*(k+1)})}, \tag{82}$$

where second inequality follows from (56) and (72), and the last inequality hold for sufficiently large N in (39). Consequently, (74), (75), (81), and (82) together lead to

$$\|\tilde{G}_{k+1} \tilde{G}_{k+1}^T - \hat{G}_{k+1} \hat{G}_{k+1}^T\|_2 \leq \sqrt{C_3} \frac{\sqrt{n \log(dn) \|p^*\|_\infty}}{\sqrt{N} \sigma_2(c^{*(k+1)})}. \tag{83}$$

Step 1F. We complete the induction in this step. Note that

$$(62) \leq \|\hat{G}_{k+1}\hat{G}_{k+1}^T - \tilde{G}_{k+1}\tilde{G}_{k+1}^T\|_F^2 \|c^*\|_F^2 \leq C_3 \frac{n \log(dn) \|p^*\|_\infty}{N \sigma_2^2(c^{*(k+1)})} \|c^*\|_F^2,$$

where the first inequality follows from (67), and the last inequality follows from (83). (62) and (63) together lead to

$$\|\hat{G}_{1:k+1}\hat{G}_{1:k+1}^T c^{*(k+1)} - c^{*(k+1)}\|_F^2 \leq C_3 \frac{n \log(dn) \|p^*\|_\infty \|c^*\|_F^2}{N} \sum_{j=1}^{k+1} \frac{1}{\sigma_2^2(c^{*(j)})}.$$

This completes the induction. Note that by induction

$$(53) = \|\hat{G}_{1:d-1}\hat{G}_{1:d-1}^T c^{*(d-1)} - c^{*(d-1)}\|_F^2 \leq C_3 \frac{n \log(dn) \|p^*\|_\infty \|c^*\|_F^2}{N} \sum_{j=1}^{d-1} \frac{1}{\sigma_2^2(c^{*(j)})}. \quad (84)$$

Step 2. We have

$$(54) = \|\hat{G}_{1:d-1}\hat{G}_{1:d-1}^T(\hat{c}^{(d-1)} - c^{*(d-1)})\|_F^2 \leq 2\|(\hat{G}_{1:d-1}\hat{G}_{1:d-1}^T - U_{d-1}^*U_{d-1}^{*T})(\hat{c}^{(d-1)} - c^{*(d-1)})\|_F^2 \quad (85)$$

$$+ 2\|U_{d-1}^*U_{d-1}^{*T}(\hat{c}^{(d-1)} - c^{*(d-1)})\|_F^2. \quad (86)$$

Note that

$$(85) \leq 2\|\hat{G}_{1:d-1}\hat{G}_{1:d-1}^T - U_{d-1}^*U_{d-1}^{*T}\|_2^2 \|\hat{c}^{(d-1)} - c^{*(d-1)}\|_F^2 = 2\|\hat{G}_{1:d-1}\hat{G}_{1:d-1}^T - U_{d-1}^*U_{d-1}^{*T}\|_2^2 \|\hat{c} - c^*\|_F^2 \leq C_5 \frac{n \|p^*\|_\infty}{\sigma_2^2(c^{*(d-1)})} \frac{d \log(dn)}{N} \|\hat{c} - c^*\|_F^2 \leq C_5 \frac{n \|p^*\|_\infty}{\sigma_2^2(c^{*(d-1)})} \frac{d \log(dn)}{N} C_2^2 \left(\frac{d^K n^{2K}}{N} \right) \leq C_6 \frac{n \log(dn) \|p^*\|_\infty}{N}, \quad (87)$$

where C_5, C_6 are universal constants. The second inequality follows from Lemma 5 given (84), the third inequality follows from (56), and the fourth inequality follows from (39). In addition,

$$(86) = 2\|(U_{d-1}^*U_{d-1}^{*T} \otimes I_n)(\hat{c}^{(d)} - c^{*(d)})\|_F^2 \leq 2C_1^2 \frac{n \log(dn) \|p^*\|_\infty}{N}. \quad (88)$$

where the inequality follows from (55).

Therefore

$$(54) \leq C_7 \frac{n \log(dn) \|p^*\|_\infty}{N} \leq 2C_7 \frac{n \log(dn) \|p^*\|_\infty \|c^*\|_F^2}{\sigma_2^2(c^{*(d-1)})N}, \quad (89)$$

for some universal constant C_7 , where the first inequality follows from (87) and (88), and the second inequality follows from the fact that $\sigma_2(c^{*(d-1)}) \leq \|c^{*(d-1)}\|_F = \|c^*\|_F$. At this point, we combine (84) and (89) and obtain the final estimation for the relative error:

$$\frac{\|c^* - \hat{G}_{1:d}\|_F}{\|c^*\|_F} = \text{O}_{\mathbb{P}} \left(\sqrt{\frac{n \log(dn) \|p^*\|_\infty}{N} \sum_{j=1}^{d-1} \frac{1}{\sigma_2^2(c^{*(j)})}} \right).$$

By further applying $\|p^*\|_\infty \leq 1 + B^*d$ from Assumption 1, we arrive at the results in Theorem 1. \square

C Some useful results for the proof of Theorem 1

C.1 TT-SVD

Lemma 2. Let $\hat{G}_{1:d}$ be the output tensor cores from Algorithm 1 with target rank r . Then $\hat{G}_{1:k} \in \mathbb{O}^{n^k \times r}$ for $k \in \{1, \dots, d-1\}$,

Proof. We proceed by induction. Since $\hat{G}_1 = \text{SVD}(\hat{c}^{(1)}, r) \in \mathbb{R}^{n \times r}$, it follows that $\hat{G}_1 \in \mathbb{O}^{n \times r}$. Assume $\hat{G}_{1:k-1} \in \mathbb{O}^{n^{k-1} \times r}$, by Lemma 20 we have

$$\hat{G}_{1:k} = (\hat{G}_{1:k-1} \otimes I_n) \hat{G}_k \in \mathbb{R}^{n^k \times r} \in \mathbb{O}^{n^k \times r}.$$

□

Lemma 3. Let $\hat{G}_{1:d}$ be the output tensor cores from Algorithm 1 with target rank r . For $k \in \{1, \dots, d-1\}$, it holds that

$$\begin{aligned} & \|\hat{G}_{1:k} \hat{G}_{1:k}^T c^{*(k)} - c^{*(k)}\|_F^2 \\ &= \|\hat{G}_{1:k} \hat{G}_{1:k}^T c^{*(k)} - (\hat{G}_{1:k-1} \otimes I_n) (\hat{G}_{1:k-1} \otimes I_n)^T c^{*(k)}\|_F^2 + \|\hat{G}_{1:k-1} \hat{G}_{1:k-1}^T c^{*(k-1)} - c^{*(k-1)}\|_F^2. \end{aligned}$$

Proof. Observe that

$$\begin{aligned} & \|\hat{G}_{1:k} \hat{G}_{1:k}^T c^{*(k)} - c^{*(k)}\|_F^2 \\ &= \|\hat{G}_{1:k} \hat{G}_{1:k}^T c^{*(k)} - (\hat{G}_{1:k-1} \otimes I_n) (\hat{G}_{1:k-1} \otimes I_n)^T c^{*(k)}\|_F^2 \\ &+ \|(\hat{G}_{1:k-1} \otimes I_n) (\hat{G}_{1:k-1} \otimes I_n)^T c^{*(k)} - c^{*(k)}\|_F^2 \end{aligned} \quad (90)$$

$$+ \langle \hat{G}_{1:k} \hat{G}_{1:k}^T c^{*(k)}, (\hat{G}_{1:k-1} \otimes I_n) (\hat{G}_{1:k-1} \otimes I_n)^T c^{*(k)} - c^{*(k)} \rangle. \quad (91)$$

$$- \langle (\hat{G}_{1:k-1} \otimes I_n) (\hat{G}_{1:k-1} \otimes I_n)^T c^{*(k)}, (\hat{G}_{1:k-1} \otimes I_n) (\hat{G}_{1:k-1} \otimes I_n)^T c^{*(k)} - c^{*(k)} \rangle. \quad (92)$$

Step 1. Note that

$$(\hat{G}_{1:k-1} \otimes I_n) (\hat{G}_{1:k-1} \otimes I_n)^T c^{*(k)} = \{(\hat{G}_{1:k-1} \hat{G}_{1:k-1}^T) \otimes I_n\} c^{*(k)} = \hat{G}_{1:k-1} \hat{G}_{1:k-1}^T c^{*(k-1)}.$$

Therefore (90) = $\|\hat{G}_{1:k-1} \hat{G}_{1:k-1}^T c^{*(k-1)} - c^{*(k-1)}\|_F^2$.

Step 2. By Lemma 2, $\hat{G}_{1:k-1} \in \mathbb{O}^{n^{k-1} \times r}$. Then the kronecker product of two orthogonal matrices is still orthogonal, $\hat{G}_{1:k-1} \otimes I_n \in \mathbb{O}^{n^k \times rn}$. The details are in Lemma 19. It follows that

$$\begin{aligned} & (\hat{G}_{1:k-1} \otimes I_n) (\hat{G}_{1:k-1} \otimes I_n)^T c^{*(k)} - c^{*(k)} = ((\hat{G}_{1:k-1} \otimes I_n) (\hat{G}_{1:k-1} \otimes I_n)^T - I_n) c^{*(k)} \\ &= (\hat{G}_{1:k-1} \otimes I_n)_\perp [(\hat{G}_{1:k-1} \otimes I_n)_\perp]^T c^{*(k)}. \end{aligned} \quad (93)$$

Therefore

$$(92) = \langle (\hat{G}_{1:k-1} \otimes I_n) (\hat{G}_{1:k-1} \otimes I_n)^T c^{*(k)}, (\hat{G}_{1:k-1} \otimes I_n)_\perp [(\hat{G}_{1:k-1} \otimes I_n)_\perp]^T c^{*(k)} \rangle = 0.$$

Step 3. By (93), it follows that

$$\begin{aligned} (91) &= \langle (\hat{G}_{1:k-1} \otimes I_n) \hat{G}_k \hat{G}_{1:k}^T c^{*(k)}, (\hat{G}_{1:k-1} \otimes I_n)_\perp [(\hat{G}_{1:k-1} \otimes I_n)_\perp]^T c^{*(k)} \rangle \\ &= \langle [(\hat{G}_{1:k-1} \otimes I_n)_\perp]^T (\hat{G}_{1:k-1} \otimes I_n) \hat{G}_k \hat{G}_{1:k}^T c^{*(k)}, [(\hat{G}_{1:k-1} \otimes I_n)_\perp]^T c^{*(k)} \rangle = 0. \end{aligned}$$

This immediately leads to the desired result. □

Lemma 4. Let $\hat{G}_{1:d}$ be the output tensor cores from Algorithm 1 with target rank r . Then

$$\|c^* - \hat{G}_{1:d}\|_F^2 = \|c^{*(d-1)} - \hat{G}_{1:d-1}\hat{G}_{1:d-1}^T c^{*(d-1)}\|_F^2 + \|\hat{G}_{1:d-1}\hat{G}_{1:d-1}^T c^{*(d-1)} - \hat{G}_{1:d-1}\hat{G}_{1:d-1}^T \hat{c}^{(d-1)}\|_F^2.$$

Proof. Since $\hat{G}_{1:d-1}\hat{G}_{1:d-1}^T \hat{c}^{(d-1)}$ is a reshape matrix of $\hat{G}_{1:d}$, we have

$$\|c^* - \hat{G}_{1:d}\|_F^2 = \|c^{*(d-1)} - \hat{G}_{1:d-1}\hat{G}_{1:d-1}^T \hat{c}^{(d-1)}\|_F^2.$$

It suffices to show that

$$\langle \hat{G}_{1:d-1}\hat{G}_{1:d-1}^T c^{*(d-1)} - c^{*(d-1)}, \hat{G}_{1:d-1}\hat{G}_{1:d-1}^T \hat{c}^{(d-1)} - \hat{G}_{1:d-1}\hat{G}_{1:d-1}^T c^{*(d-1)} \rangle = 0. \quad (94)$$

By Lemma 2, $\hat{G}_{1:d-1} \in \mathbb{O}^{n^{d-1} \times r}$. So

$$\hat{G}_{1:d-1}\hat{G}_{1:d-1}^T c^{*(d-1)} - c^{*(d-1)} = (\hat{G}_{1:d-1})_\perp (\hat{G}_{1:d-1})_\perp^T c^{*(d-1)}.$$

Therefore $(\hat{G}_{1:d-1})_\perp^T \hat{G}_{1:d-1} = 0$ and so

$$\begin{aligned} (94) &= \langle (\hat{G}_{1:d-1})_\perp (\hat{G}_{1:d-1})_\perp^T c^{*(d-1)}, \hat{G}_{1:d-1}\hat{G}_{1:d-1}^T (\hat{c}^{(d-1)} - c^{*(d-1)}) \rangle \\ &= \langle (\hat{G}_{1:d-1})_\perp^T c^{*(d-1)}, (\hat{G}_{1:d-1})_\perp^T \hat{G}_{1:d-1}\hat{G}_{1:d-1}^T (\hat{c}^{(d-1)} - c^{*(d-1)}) \rangle = 0. \end{aligned}$$

□

Lemma 5. Suppose all the conditions in Theorem 1 holds. Let $\hat{G}_{1:d}$ be the output tensor cores from Algorithm 1 with target rank $r = 2$. Suppose that

$$\|\hat{G}_{1:k}\hat{G}_{1:k}^T c^{*(k)} - c^{*(k)}\|_F^2 \leq C \frac{n \log(dn) \|p^*\|_\infty \|c^*\|_F^2}{N} \sum_{j=1}^k \frac{1}{\sigma_2^2(c^{*(j)})} \quad (95)$$

where C is a universal constant. Let U_k^* be defined as in Lemma 8. Note that by Lemma 8, $U_k^* U_k^{*T} \in \mathbb{R}^{n^k \times n^k}$ is the projection matrix onto the space $\text{Col}(c^{*(k)})$. Then

$$\|\hat{G}_{1:k}\hat{G}_{1:k}^T - U_k^* U_k^{*T}\|_2 \leq C' \frac{\sqrt{n} \|p^*\|_\infty}{\sigma_2(c^{*(k)})} \sqrt{\frac{d \log(dn)}{N}}, \quad (96)$$

where C' a universal constant.

Proof. Note that by Lemma 10, for $k \in \{1, \dots, d-1\}$, $\sigma_2^2(c^{*(k)}) \geq \frac{c_\sigma^2 k(d-k)}{d}$. In addition, by Corollary 2, $\|c^*\|_F^2 \leq C_c d$ where $C_c = B^* + 2$. Therefore by (95)

$$\|\hat{G}_{1:k}\hat{G}_{1:k}^T c^{*(k)} - c^{*(k)}\|_F^2 \leq C \frac{n \log(dn) \|p^*\|_\infty \|c^*\|_F^2}{N} \frac{d}{c_\sigma^2} \sum_{j=1}^k \frac{1}{j(d-j)} \leq C'' \frac{C_c n \|p^*\|_\infty d \log(dn)}{c_\sigma^2 N} \quad (97)$$

where we have used the fact that $\sum_{j=1}^d \frac{1}{j(d-j)} = O(\frac{\log(d)}{d})$ and C'' is some universal constant.

By Lemma 18, $\text{Rank}(\hat{G}_{1:k}\hat{G}_{1:k}^T c^{*(k)}) = 2$, and $\hat{G}_{1:k}\hat{G}_{1:k}^T$ is the projection matrix on $\text{Col}(\hat{G}_{1:k}\hat{G}_{1:k}^T c^{*(k)})$. Consequently,

$$\begin{aligned} \|\hat{G}_{1:k}\hat{G}_{1:k}^T - U_k^*U_k^{*T}\|_2 &\leq \frac{2\|\hat{G}_{1:k}\hat{G}_{1:k}^T c^{*(k)} - c^{*(k)}\|_2}{\sigma_2(c^{*(k)}) - \|\hat{G}_{1:k}\hat{G}_{1:k}^T c^{*(k)} - c^{*(k)}\|_2} \leq \frac{2\|\hat{G}_{1:k}\hat{G}_{1:k}^T c^{*(k)} - c^{*(k)}\|_2}{\frac{1}{2}\sigma_2(c^{*(k)})} \\ &\leq 4\frac{\sqrt{C''C_c n}\|p^*\|_\infty}{c_\sigma\sigma_2(c^{*(k)})} \sqrt{\frac{d\log(dn)}{N}}, \end{aligned} \quad (98)$$

where the first inequality follows from Theorem 3 and $\text{Rank}(c^{*(k)}) = 2$, the second inequality follows from the assumption on sufficiently large sample size N as stated in (39), and the last inequality follows from (97). Furthermore, by the expressions of C_c in Corollary 2 and c_σ in Lemma 10, we have $\frac{\sqrt{C_c}}{c_\sigma}$ can be bounded a universal constant, leading to the final estimation (96). \square

C.2 Ground truth density function

Lemma 6. *Under Assumption 1, let*

$$\tilde{p}(x_1, \dots, x_d) = \sum_{l_1=1}^n \cdots \sum_{l_d=1}^n c^*(l_1, \dots, l_d) \phi_{l_1}(x_1) \cdots \phi_{l_d}(x_d)$$

where $c^* \in \mathbb{R}^{n^d}$ is the coefficient tensor formulated as (46). There exists an absolute constant C such that

$$\|p^* - \tilde{p}\|_{L_2([0,1]^d)} \leq Cn^{-\beta_0} \sum_{j=1}^d \|q_j^*\|_{H^{\beta_0}([0,1])}.$$

Proof. Direct calculations show that

$$\tilde{p}(x_1, \dots, x_d) = 1 + \sum_{l_1=1}^n c_1^*(l_1) \phi_{l_1}(x_1) + \cdots + \sum_{l_d=1}^n c_d^*(l_d) \phi_{l_d}(x_d).$$

where $c_j^* \in \mathbb{R}^n$ is defined in (49). Therefore

$$\|p^* - \tilde{p}\|_{L_2([0,1]^d)} \leq \sum_{j=1}^d \left\| \sum_{l_j=1}^n c_j^*(l_j) \phi_{l_j} - q_j^* \right\|_{L_2([0,1])}.$$

Denote \mathcal{S}_n the class of polynomial up degree n on $[0, 1]$, and \mathcal{P}_n the projection operator from $L_2([0, 1])$ to \mathcal{S}_n respect to L_2 norm. Since Legendre polynomials are orthogonal, (49) and (48)

$$\sum_{l_j=1}^n c_j^*(l_j) \phi_{l_j} = \mathcal{P}_n(q_j^*). \quad (99)$$

By the Legendre polynomial approximation theory shown in the appendix of Khoo et al. (2024), it follows that

$$\left\| \sum_{l_j=1}^n c_j^*(l_j) \phi_{l_j} - q_j^* \right\|_{L_2([0,1])} \leq C\|q_j^*\|_{H^{\beta_0}([0,1])} n^{-\beta_0} \quad (100)$$

for some absolute constant C which does not depend on c_j^* or q_j^* . The desired result follows immediately. \square

Corollary 2. *Under Assumption 1, for sufficiently large n , there exists a constant C such that*

$$\|c^*\|_F^2 \leq C_c d, \quad \text{where } C_c = B^* + 2$$

where $c^* \in \mathbb{R}^{n^d}$ is the coefficient tensor formulated as (46).

Proof. Observe that

$$\begin{aligned} \|c^*\|_F^2 &= \|\mathbf{1}^d + c_1^* \otimes \mathbf{1}^{d-1} + \mathbf{1} \otimes c_2^* \otimes \mathbf{1}^{d-2} + \dots + \mathbf{1}^{d-1} \otimes c_d^*\|_F^2 \\ &= \|\mathbf{1}^d\|_F^2 + \|c_1^* \otimes \mathbf{1}^{d-1}\|_F^2 + \dots + \|\mathbf{1}^{d-1} \otimes c_d^*\|_F^2 = 1 + \sum_{j=1}^d \|c_j^*\|^2. \end{aligned}$$

where the first equality follows from (46), and the second equality follows from orthogonality. In addition, note that

$$\|c_j^*\| = \left\| \sum_{l_j=1}^n c_j^*(l_j) \phi_{l_j} \right\|_{L_2([0,1])} \leq \|q_j^*\|_{L_2([0,1])} + C_1 \|q_j^*\|_{H^{\beta_0}([0,1])} n^{-\beta_0} \leq B^* + 1,$$

where the first inequality follows from (100), and the last inequality follows from Assumption 1 and n being sufficiently large. The desired result follows immediately. \square

C.3 Row and column spaces of the coefficient tensor

Lemma 7. *Let $k \in \{1, \dots, d-1\}$. Let $c^{*(k)} \in \mathbb{R}^{n^k} \times \mathbb{R}^{n^{d-k}}$ be the k -th unfolding of the tensor coefficient c^* as in (46) for $k = 1, \dots, d-1$. The row and the column space of $c^{*(k)}$ are given by*

$$\text{Col}(c^{*(k)}) = \text{Span}\{\mathbf{1}^k, c_1^* \otimes \mathbf{1}^{k-1} + \mathbf{1} \otimes c_2^* \otimes \mathbf{1}^{k-2} + \dots + \mathbf{1}^{k-1} \otimes c_k^*\}, \quad (101)$$

$$\text{Row}(c^{*(k)}) = \text{Span}\{\mathbf{1}^{d-k}, c_{k+1}^* \otimes \mathbf{1}^{d-k-1} + \mathbf{1} \otimes c_{k+2}^* \otimes \mathbf{1}^{d-k-2} + \dots + \mathbf{1}^{d-k-1} \otimes c_d^*\}. \quad (102)$$

Consequently, $\text{Rank}(c^{*(k)}) \leq 2$. Furthermore, if $q_j^* \neq 0$ for all $j \in \{1, \dots, d\}$, $\text{Rank}(c^{*(k)}) = 2$.

Proof. It is direct to show that

$$\begin{aligned} c^{*(k)} &= (\mathbf{1}^k) \otimes \{\mathbf{1}^{d-k}\} + (c_1^* \otimes \mathbf{1}^{k-1}) \otimes \{\mathbf{1}^{d-k}\} + \dots + (\mathbf{1}^{k-1} \otimes c_k^*) \otimes \{\mathbf{1}^{d-k}\} \\ &\quad + (\mathbf{1}^k) \otimes \{c_{k+1}^* \otimes \mathbf{1}^{d-k-1}\} + \dots + (\mathbf{1}^k) \otimes \{\mathbf{1}^{d-k-1} \otimes c_d^*\}, \end{aligned} \quad (103)$$

where terms with $(\)$ are viewed as column vectors in \mathbb{R}^{n^k} , and terms with $\{\ \}$ are viewed as row vectors in $\mathbb{R}^{n^{d-k}}$. To show (101) holds for the column space, it suffices to rewrite

$$\begin{aligned} c^{*(k)} &= (\mathbf{1}^k) \otimes \{\mathbf{1}^{d-k} + c_{k+1}^* \otimes \mathbf{1}^{d-k-1} + \mathbf{1} \otimes c_{k+2}^* \otimes \mathbf{1}^{d-k-2} + \dots + \mathbf{1}^{d-k-1} \otimes c_d^*\} \\ &\quad + (c_1^* \otimes \mathbf{1}^{k-1} + \mathbf{1} \otimes c_2^* \otimes \mathbf{1}^{k-2} + \dots + \mathbf{1}^{k-1} \otimes c_k^*) \otimes \{\mathbf{1}^{d-k}\}. \end{aligned}$$

Therefore (101) holds. The justification of (102) is similar and omitted for brevity. \square

Lemma 8. Let c^* be coefficient tensor as in (46) and c_j^* be as in (49). Denote $e_1 = [1, 0]^T$, $e_2 = [0, 1]^T$ and let the matrices $U_k^* \in \mathbb{R}^{n^k \times 2}$ and $V_k^* \in \mathbb{R}^{n^{d-k} \times 2}$ be such that

$$U_k^* = \mathbf{1}^k \otimes e_1 + \frac{c_1^* \otimes \mathbf{1}^{k-1} + \mathbf{1} \otimes c_2^* \otimes \mathbf{1}^{k-2} + \dots + \mathbf{1}^{k-1} \otimes c_k^*}{\sqrt{\|c_1^*\|^2 + \dots + \|c_k^*\|^2}} \otimes e_2, \quad (104)$$

$$V_k^* = \mathbf{1}^{d-k} \otimes e_1 + \frac{c_{k+1}^* \otimes \mathbf{1}^{d-k-1} + \mathbf{1} \otimes c_{k+2}^* \otimes \mathbf{1}^{d-k-2} + \dots + \mathbf{1}^{d-k-1} \otimes c_d^*}{\sqrt{\|c_{k+1}^*\|^2 + \dots + \|c_d^*\|^2}} \otimes e_2. \quad (105)$$

Then $U_k^* U_k^{*T} \in \mathbb{R}^{n^k \times n^k}$ is the projection matrix onto the space $\text{Col}(c^{*(k)})$, and $V_k^* V_k^{*T} \in \mathbb{R}^{n^{d-k} \times n^{d-k}}$ is the projection matrix onto the space $\text{Row}(c^{*(k)})$.

Proof. Note that the set of vectors $\{\mathbf{1}^k, c_1^* \otimes \mathbf{1}^{k-1}, \mathbf{1} \otimes c_2^* \otimes \mathbf{1}^{k-2}, \dots, \mathbf{1}^{k-1} \otimes c_k^*\}$ are orthogonal. Direct calculations show that

$$U_k^{*T} U_k^* = e_1 \otimes e_1 + e_2 \otimes e_2 = I_2 \in \mathbb{R}^{2 \times 2}.$$

Therefore $U_k^* \in \mathbb{O}^{n^k \times 2}$. Since $\text{Col}(U_k^*) = \text{Col}(c^{*(k)})$, $U_k^* U_k^{*T} \in \mathbb{R}^{n^k \times n^k}$ is the projection matrix onto the space $\text{Col}(c^{*(k)})$. The justification of $V_k^* V_k^{*T}$ is similar and omitted for brevity. \square

For simplicity, in (104) and (105) we introduce the notations

$$u_k^* = \frac{c_1^* \otimes \mathbf{1}^{k-1} + \mathbf{1} \otimes c_2^* \otimes \mathbf{1}^{k-2} + \dots + \mathbf{1}^{k-1} \otimes c_k^*}{\sqrt{\|c_1^*\|^2 + \dots + \|c_k^*\|^2}} \in \mathbb{R}^{n^k}, \quad (106)$$

$$v_k^* = \frac{c_{k+1}^* \otimes \mathbf{1}^{d-k-1} + \mathbf{1} \otimes c_{k+2}^* \otimes \mathbf{1}^{d-k-2} + \dots + \mathbf{1}^{d-k-1} \otimes c_d^*}{\sqrt{\|c_{k+1}^*\|^2 + \dots + \|c_d^*\|^2}} \in \mathbb{R}^{n^{d-k}}. \quad (107)$$

Lemma 9. Let u_k^* and v_k^* be as in (106) and (107) respectively. Denote

$$\Phi_k^*(x_1, \dots, x_k) = \frac{\sum_{l_1=1}^n c_1^*(l_1) \phi_{l_1}(x_1) + \dots + \sum_{l_k=1}^n c_k^*(l_k) \phi_{l_k}(x_k)}{\sqrt{\|c_1^*\|^2 + \dots + \|c_k^*\|^2}}, \quad (108)$$

$$\Psi_k^*(x_{k+1}, \dots, x_d) = \frac{\sum_{l_{k+1}=1}^n c_{k+1}^*(l_{k+1}) \phi_{l_{k+1}}(x_{k+1}) + \dots + \sum_{l_d=1}^n c_d^*(l_d) \phi_{l_d}(x_d)}{\sqrt{\|c_{k+1}^*\|^2 + \dots + \|c_d^*\|^2}}. \quad (109)$$

Then u_k^* is the coefficient tensor of Φ_k^* , and v_k^* is the coefficient tensor of Ψ_k^* . Then

$$\|\Phi_k^*\|_{L_2([0,1]^k)} = \|u_k^*\|_F = 1 \quad \text{and} \quad \|\Psi_k^*\|_{L_2([0,1]^{d-k})} = \|v_k^*\|_F = 1.$$

In addition, suppose Assumption 1 holds. Then for sufficient large n such that

$$\|\Phi_k^*\|_\infty \leq C' \sqrt{k} \quad \text{and} \quad \|\Psi_k^*\|_\infty \leq C' \sqrt{d-k} \quad \text{where} \quad C' = \frac{4B^*}{b^*}.$$

Proof. To see that u_k^* is the coefficient tensor of $\Phi_k^*(x_1, \dots, x_k)$, it suffices to observe that the (l_1, \dots, l_k) -coordinate of u_k^* is $\langle \Phi_k^*, \phi_{l_1}^1 \dots \phi_{l_k}^k \rangle$. Since the coefficient tensor is distance preserving, it holds that

$$\|\Phi_k^*\|_{L_2([0,1]^k)} = \|u_k^*\|_F = 1.$$

Next, we bound $\|\Phi_k^*\|_\infty$. By (99) and Theorem 5, it follows that there exists a constant C_1 such that

$$\left\| \sum_{l_j=1}^n c_j^*(l_j) \phi_{l_j} \right\|_\infty = \|\mathcal{P}_n(q_j^*)\|_\infty \leq \|q_j^*\|_\infty + C_1 n^{-\beta_0}.$$

Therefore, the numerator of (108) is bounded by

$$\left\| \sum_{l_1=1}^n c_1^*(l_1) \phi_{l_1} + \cdots + \sum_{l_k=1}^n c_k^*(l_k) \phi_{l_k} \right\|_\infty \leq \sum_{j=1}^k \|q_j^*\|_\infty + C_1 k n^{-\beta_0} \leq 2k B^* \quad (110)$$

upon using Assumption 1 and sufficiently large n . Observe that

$$\|c_j^*\| = \left\| \sum_{l_j=1}^n c_j^*(l_j) \phi_{l_j} \right\|_{L_2([0,1])} = \|\mathcal{P}_n(q_j^*)\|_{L_2([0,1])} \geq \|q_j^*\|_{L_2([0,1])} - C_2 n^{-\beta_0} \geq b^* - C_2 n^{-\beta_0} \geq b^*/2$$

from some constant C_2 , where the second equality follows from (99), the first inequality follows from Corollary 4, the second inequality follows from the Assumption 1 that $\min_{j \in \{1, \dots, d\}} \|q_j^*\|_{L_2([0,1])} \geq b^*$, and the last inequality holds for sufficiently large n . Therefore, the denominator

$$\sqrt{\|c_1^*\|^2 + \cdots + \|c_k^*\|^2} \geq b^* \sqrt{k}/2 \quad (111)$$

Note that (110) and (111) immediately imply $\|\Phi_k^*\|_\infty \leq 4 \frac{B^*}{b^*} \sqrt{k}$. The analysis for $\|\Psi_k^*\|_\infty$ is the same and therefore omitted. \square

C.4 Singular Values of the reshaped coefficient tensor

Lemma 10. *Let c^* be defined as in (46). Denote*

$$a_k^* = \sum_{i=1}^k \|c_i^*\|^2 \quad \text{and} \quad b_k^* = \sum_{i=k+1}^d \|c_i^*\|^2.$$

Then the k -th unfolding of coefficient tensor c^ has the smallest singular value formulated as*

$$\sigma_2^2(c^{*(k)}) = \frac{1 + a_k^* + b_k^* - \sqrt{(1 + a_k^* + b_k^*)^2 - 4a_k^* b_k^*}}{2}$$

for $k = 1, \dots, d$. Suppose in addition that Assumption 1 holds, for sufficient large n , $\sigma_2(c^{(k)})$ is lower bounded by*

$$\sigma_2(c^{*(k)}) \geq c_\sigma \sqrt{\frac{k(d-k)}{d}} \quad \text{where} \quad c_\sigma = \sqrt{\frac{16B^{*4}}{1 + \frac{b^{*2}}{4}}} \quad (112)$$

Proof. Let $k \in \{1, \dots, d\}$. Denote

$$f_k^* = c_1^* \otimes \mathbf{1}^{k-1} + \mathbf{1} \otimes c_2^* \otimes \mathbf{1}^{k-2} + \cdots + \mathbf{1}^{k-1} \otimes c_k^*, \quad \text{and} \quad g_k^* = c_{k+1}^* \otimes \mathbf{1}^{d-k-1} + \cdots + \mathbf{1}^{d-k} \otimes c_d^*.$$

Then one can easily check that $a_k^* = \|f_k^*\|_F^2$ and $b_k^* = \|g_k^*\|_F^2$ due to orthogonality, and we can write

$$c^* = (\mathbf{1}^k) \otimes \{\mathbf{1}^{d-k} + g_k^*\} + (f_k^*) \otimes \{\mathbf{1}^{d-k}\}.$$

where terms with $(\)$ are viewed as column vectors in \mathbb{R}^{n^k} , and terms with $\{\ \}$ are viewed as row vectors in $\mathbb{R}^{n^{d-k}}$. Therefore

$$c^{*(k)} = \begin{bmatrix} \mathbf{1}^k & f_k^* \end{bmatrix} \begin{bmatrix} \mathbf{1}^{d-k} + g_k^* \\ \mathbf{1}^{d-k} \end{bmatrix}.$$

Observe that

$$c^{*(k)}(c^{*(k)})^T = \begin{bmatrix} \mathbf{1}^k & f_k^* \end{bmatrix} \begin{bmatrix} 1 + \|g_k^*\|_F^2 & 1 \\ 1 & 1 \end{bmatrix} \begin{bmatrix} \mathbf{1}^k \\ f_k^* \end{bmatrix} = \begin{bmatrix} \mathbf{1}^k & f_k^*/\|f_k^*\|_F \end{bmatrix} \begin{bmatrix} 1 + \|g_k^*\|_F^2 & \|f_k^*\|_F \\ \|f_k^*\|_F & \|f_k^*\|_F^2 \end{bmatrix} \begin{bmatrix} \mathbf{1}^k \\ f_k^*/\|f_k^*\|_F \end{bmatrix}$$

Note that $\begin{bmatrix} \mathbf{1}^k & f_k^*/\|f_k^*\|_F \end{bmatrix}$ is an orthogonal matrix in $\mathbb{O}^{n^k \times 2}$. Therefore the eigenvalues of $c^{*(k)}(c^{*(k)})^T$ coincide with the eigenvalues of $\begin{bmatrix} 1 + \|g_k^*\|_F^2 & \|f_k^*\|_F \\ \|f_k^*\|_F & \|f_k^*\|_F^2 \end{bmatrix} \in \mathbb{R}^{2 \times 2}$. Direct calculations show that

$$\sigma_2^2(c^{*(k)}) = \lambda_2(c^{*(k)}(c^{*(k)})^T) = \frac{1 + a_k^* + b_k^* - \sqrt{(1 + a_k^* + b_k^*)^2 - 4a_k^*b_k^*}}{2}.$$

For (112), note that by (100), there exists a constant C_1

$$\left\| \sum_{l_j=1}^n c_j^*(l_j)\phi_{l_j} - q_j^* \right\|_{L_2([0,1])} \leq C_1 n^{-\beta_0} \quad (113)$$

Since $\left\| \sum_{l_j=1}^n c_j^*(l_j)\phi_{l_j} \right\|_{L_2([0,1])} = \|c_j^*\|$, it follows that

$$\|q_j^*\|_{L_2([0,1])} - C_1 n^{-\beta_0} \leq \|c_j^*\| \leq \|q_j^*\|_{L_2([0,1])} + C_1 n^{-\beta_0}$$

It follows from Assumption 1 and (100) that

$$b^* \leq \|q_j^*\|_{L_2([0,1])} \leq B^*.$$

So for sufficiently large n , it follows that $\frac{b^*}{2} \leq \|c_j^*\| \leq 2B^*$. Consequently,

$$\frac{b^{*2}k}{4} \leq a_k^* \leq 4B^{*2}k \quad \text{and} \quad \frac{b^{*2}(d-k)}{4} \leq b_k^* \leq 4B^{*2}(d-k).$$

Therefore

$$\begin{aligned} \sigma_2^2(c^{*(k)}) &= \frac{1 + a_k^* + b_k^* - \sqrt{(1 + a_k^* + b_k^*)^2 - 4a_k^*b_k^*}}{2} \\ &= \frac{(1 + a_k^* + b_k^* - \sqrt{(1 + a_k^* + b_k^*)^2 - 4a_k^*b_k^*})(1 + a_k^* + b_k^* + \sqrt{(1 + a_k^* + b_k^*)^2 - 4a_k^*b_k^*})}{2(1 + a_k^* + b_k^* + \sqrt{(1 + a_k^* + b_k^*)^2 - 4a_k^*b_k^*})} \\ &\geq \frac{4a_k^*b_k^*}{4(1 + a_k^* + b_k^*)} \geq \frac{16B^{*4}k(d-k)}{1 + \frac{b^{*2}}{4}d} \geq \frac{16B^{*4}k(d-k)}{(1 + \frac{b^{*2}}{4})d} \end{aligned}$$

□

C.5 Variance of cluster basis estimators

Lemma 11. *Suppose Assumption 1 holds. Let c^* be the coefficient tensor of p^* , and \hat{c} be the s -cluster coefficient tensor estimator defined in Definition 1 with $s \geq 2$. Let U_k^* and V_k^* be defined as in Lemma 8. Then,*

$$\max_{k \in \{1, \dots, d\}} \|(U_{k-1}^{*T} \otimes I_n)(c^{*(k)} - \hat{c}^{(k)}[s])V_k^*\|_F = O_{\mathbb{P}} \left(\sqrt{\frac{n \log(dn) \|p^*\|_{\infty}}{N}} \right). \quad (114)$$

Proof. We suppose $s \geq 3$ in the proof, where the case of $s = 2$ is a simplified version from the same calculations. Given any positive number t , we have

$$\begin{aligned} & \mathbb{P} \left(\max_{k \in \{1, \dots, d\}} \|(U_{k-1}^{*T} \otimes I_n)(c^{*(k)} - \hat{c}^{(k)}[s])V_k^*\|_F^2 \geq 4nt^2 \right) \\ &= \mathbb{P} \left(\|(U_{k-1}^{*T} \otimes I_n)(c^{*(k)} - \hat{c}^{(k)}[s])V_k^*\|_F^2 \geq 4nt^2 \text{ for least one } k \in \{1, \dots, d\} \right) \\ &\leq \sum_{k=1}^d \mathbb{P} \left(\|(U_{k-1}^{*T} \otimes I_n)(c^{*(k)} - \hat{c}^{(k)}[s])V_k^*\|_F^2 \geq 4nt^2 \right) \quad (\text{by union bound}) \\ &= \sum_{k=1}^d \mathbb{P} \left((118) \geq 4nt^2 \right) \\ &\leq \sum_{k=1}^d \sum_{l=1}^n \mathbb{P} \left(|\langle p^* - \hat{p}, \Phi_{k-1}^* \phi_l^k \Psi_k^* \rangle| \geq t \right) + \mathbb{P} \left(|\langle p^* - \hat{p}, \phi_l^k \rangle| \geq t \right) \\ &\quad + \mathbb{P} \left(|\langle p^* - \hat{p}, \Phi_{k-1}^* \phi_l^k \rangle| \geq t \right) + \mathbb{P} \left(|\langle p^* - \hat{p}, \phi_l^k \Psi_k^* \rangle| \geq t \right). \end{aligned} \quad (115)$$

We now bound the four terms in the double sums above by Lemma 16, which is based on Bernstein inequality.

We first bound

$$\mathbb{P} \left(|\langle p^* - \hat{p}, \Phi_{k-1}^* \phi_l^k \Psi_k^* \rangle| \geq t \right).$$

Note that by Lemma 9, it holds that

$$\|\Phi_{k-1}^* \phi_l^k \Psi_k^*\|_{L_2([0,1]^d)} = \|\Phi_{k-1}^*\|_{L_2([0,1]^{k-1})} \|\phi_l\|_{L_2([0,1])} \|\Psi_{k+1}^*\|_{L_2([0,1]^{d-k})} = 1,$$

and that

$$\|\Phi_{k-1}^* \phi_l^k \Psi_k^*\|_{\infty} = \|\Phi_{k-1}^*\|_{\infty} \|\phi_l\|_{\infty} \|\Psi_{k+1}^*\|_{\infty} \leq C'^2 \sqrt{n(k-1)(d-k)},$$

where $C' = \frac{4B^*}{b^*}$. Therefore, by Lemma 16,

$$\begin{aligned} \mathbb{P} \left(|\langle p^* - \hat{p}, \Phi_{k-1}^* \phi_l^k \Psi_k^* \rangle| \geq t \right) &\leq 2 \exp \left(\frac{-Nt^2}{\|p^*\|_{\infty} \|\Phi_{k-1}^* \phi_l^k \Psi_k^*\|_{L_2([0,1]^d)}^2 + \|\Phi_{k-1}^* \phi_l^k \Psi_k^*\|_{\infty} t} \right) \\ &\leq 2 \exp \left(\frac{-Nt^2}{\|p^*\|_{\infty} + C'^2 \sqrt{n(k-1)(d-k)} t} \right) =: \frac{\epsilon}{4dn}. \end{aligned} \quad (116)$$

where we assume the right-hand side is $\frac{\epsilon}{4dn}$ for some sufficiently small constant ϵ . Solving the last line above yields the quadratic equation

$$Nt^2 - C'^2 \sqrt{n(k-1)(d-k)} \log\left(\frac{8dn}{\epsilon}\right)t - \log\left(\frac{8dn}{\epsilon}\right) \|p^*\|_\infty = 0,$$

whose larger root can be bounded by

$$\begin{aligned} t_+ &= \frac{C'^2 \sqrt{n(k-1)(d-k)} \log\left(\frac{8dn}{\epsilon}\right) + \sqrt{C'^4 n(k-1)(d-k) [\log\left(\frac{8dn}{\epsilon}\right)]^2 + 4N \log\left(\frac{8dn}{\epsilon}\right) \|p^*\|_\infty}}{2N} \\ &\leq C_\epsilon \sqrt{\frac{\log(dn) \|p^*\|_\infty}{N}} =: t_\epsilon \end{aligned}$$

upon choosing sufficiently large N . Here $C_\epsilon \sim \log(1/\epsilon)$ is some sufficiently large positive constant which only depends on ϵ . At this point, we have

$$\mathbb{P}\left(|\langle p^* - \hat{p}, \Phi_{k-1}^* \phi_l^k \Psi_k^* \rangle| \geq t_\epsilon\right) \leq \frac{\epsilon}{4dn}.$$

For the other three terms in the double sums, by Lemma 9 we have

$$\|\phi_l^k\|_\infty \leq \sqrt{n}, \quad \|\Phi_{k-1}^* \phi_l^k\|_\infty \leq \sqrt{n(k-1)}, \quad \|\phi_l^k \Psi_k^*\|_\infty \leq \sqrt{n(d-k)}.$$

Following the same calculations, we can show that with high probability

$$\begin{aligned} \mathbb{P}\left(|\langle p^* - \hat{p}, \phi_l^k \rangle| \geq t_\epsilon\right) &\leq \frac{\epsilon}{4dn} \\ \mathbb{P}\left(|\langle p^* - \hat{p}, \Phi_{k-1}^* \phi_l^k \rangle| \geq t_\epsilon\right) &\leq \frac{\epsilon}{4dn}, \\ \mathbb{P}\left(|\langle p^* - \hat{p}, \phi_l^k \Psi_k^* \rangle| \geq t_\epsilon\right) &\leq \frac{\epsilon}{4dn} \end{aligned}$$

with appropriate choice of N . Inserting the estimates above into (115), we conclude that

$$\mathbb{P}\left(\max_{k \in \{1, \dots, d\}} \|(U_{k-1}^{*T} \otimes I_n)(c^{*(k)} - \hat{c}^{(k)}[s])V_k^*\|_F^2 \geq 4nt_\epsilon^2\right) \leq \epsilon$$

for any given positive ϵ . This indicates that, with high probability,

$$\max_{k \in \{1, \dots, d\}} \|(U_{k-1}^{*T} \otimes I_n)(c^{*(k)} - \hat{c}^{(k)}[s])V_k^*\|_F \leq 2\sqrt{nt_\epsilon} = 2C_\epsilon \sqrt{\frac{n \log(dn) \|p^*\|_\infty}{N}}$$

□

Lemma 12. *Suppose Assumption 1 holds. Let c^* be the coefficient tensor of p^* , and \hat{c} be the s -cluster coefficient tensor estimator defined in Definition 1 with $s \geq 2$. Then*

$$\|c^* - \hat{c}\|_F = \mathcal{O}_{\mathbb{P}}\left(\sqrt{\frac{d^s n^{2s}}{N}}\right). \quad (117)$$

Proof. It suffices to show that

$$\mathbb{E}(\|c^* - \hat{c}\|_F^2) = \mathcal{O}\left(\frac{d^s n^{2s}}{N}\right).$$

To this end, let $\mathcal{B}_{j,d}$ be the j -cluster basis functions defined in (5). Then by

$$\mathbb{E}(\|c^* - \hat{c}\|_F^2) = \sum_{j=0}^s \left\{ \sum_{\varphi_0 \in \mathcal{B}_{1,d}} \mathbb{E}(\langle \hat{p} - p^*, \varphi_0 \rangle^2) + \cdots + \sum_{\varphi_s \in \mathcal{B}_{s,d}} \mathbb{E}(\langle \hat{p} - p^*, \varphi_s \rangle^2) \right\}$$

Let $g_s(x) = \prod_{k=1}^s \phi_{i_{j_k}}(x_{j_k})$ be a generic element in $\mathcal{B}_{s,d}$. Then since $\{\phi_l\}_{l=1}^\infty$ are Legendre polynomials, it follows that with $\|\phi_l\|_\infty \leq \sqrt{l}$ and therefore $\|g_s\|_\infty \leq n^{s/2}$. Consequently,

$$\begin{aligned} \mathbb{E}(\langle \hat{p} - p^*, g_s \rangle^2) &= \text{Var}\left(\frac{1}{N} \sum_{i=1}^N g_s(x^{(i)})\right) = \frac{\text{Var}(g_s(x^{(1)}))}{N} \\ &\leq \frac{\int g_s^2(x) p^*(x) dx}{N} \leq \frac{\|g_s\|_\infty^2 \int p^*(x) dx}{N} \leq \frac{n^s}{N}, \end{aligned}$$

where the last equality follows from the fact that p^* is a density and so $\int p^*(x) dx = 1$. Since the cardinality of $\mathcal{B}_{s,d}$ is at most $n^s d^s$, it follows that $\sum_{\varphi_s \in \mathcal{B}_{s,d}} \mathbb{E}(\langle \hat{p} - p^*, \varphi_s \rangle^2) \leq \frac{d^s n^{2s}}{N}$. Since s is a bounded integers, it follows that

$$\mathbb{E}(\|c^* - \hat{c}\|_F^2) \leq \sum_{j=1}^s \frac{d^j n^{2j}}{N} = \mathcal{O}\left(\frac{d^s n^{2s}}{N}\right).$$

□

Lemma 13. *Let c^* be the coefficient tensor of p^* , and $\hat{c}[s]$ be the s -cluster coefficient tensor estimator defined in Definition 1 with $s \geq 2$. Let U_k^* and V_k^* be defined as in (104) and (105) respectively. Φ_k^* and Ψ_k^* are defined as in (108) and (109) respectively. The following equalities hold:*

- If $s \geq 3$,

$$\begin{aligned} &\|(U_{k-1}^{*T} \otimes I_n)(c^{*(k)} - \hat{c}[s]^{(k)})V_k^*\|_F^2 \\ &= \sum_{l=1}^n \left(\langle p^* - \hat{p}, \phi_l^k \rangle^2 + \langle p^* - \hat{p}, \Phi_{k-1}^* \phi_l^k \rangle^2 + \langle p^* - \hat{p}, \phi_l^k \Psi_k^* \rangle^2 + \langle p^* - \hat{p}, \Phi_{k-1}^* \phi_l^k \Psi_k^* \rangle^2 \right); \end{aligned} \quad (118)$$

- If $s = 2$,

$$\|(U_{k-1}^{*T} \otimes I_n)(c^{*(k)} - \hat{c}[s]^{(k)})V_k^*\|_F^2 = \sum_{l=1}^n \left(\langle p^* - \hat{p}, \phi_l^k \rangle^2 + \langle p^* - \hat{p}, \Phi_{k-1}^* \phi_l^k \rangle^2 + \langle p^* - \hat{p}, \phi_l^k \Psi_k^* \rangle^2 \right). \quad (119)$$

Proof. For $l \in \{1, \dots, n\}$, denote $\chi_l \in \mathbb{R}^n$ be the l -th canonical basis. That is, for $k \in \{1, \dots, n\}$

$$\chi_l(k) = \begin{cases} 0, & \text{if } l \neq k; \\ 1, & \text{if } l = k. \end{cases}$$

Denote \mathcal{T} the reshaped $\mathbb{R}^{2 \times n \times 2}$ tensor of the matrix $(U_{k-1}^{*T} \otimes I_n)(c^{*(k)} - \hat{c}[s]^{(k)})V_k^*$. It follows from (104), (105), (106) and (107) that, for any $l \in \{1, \dots, n\}$ the (a, l, b) -coordinate of \mathcal{T} satisfies

$$\mathcal{T}_{a,l,b} = \begin{cases} \langle c^* - \hat{c}[s], \mathbf{1}^{k-1} \otimes \chi_l \otimes \mathbf{1}^{d-k} \rangle, & \text{if } a = 1, b = 1; \\ \langle c^* - \hat{c}[s], u_{k-1}^* \otimes \chi_l \otimes \mathbf{1}^{d-k} \rangle, & \text{if } a = 2, b = 1; \\ \langle c^* - \hat{c}[s], \mathbf{1}^{k-1} \otimes \chi_l \otimes v_k^* \rangle, & \text{if } a = 1, b = 2; \\ \langle c^* - \hat{c}[s], u_{k-1}^* \otimes \chi_l \otimes v_k^* \rangle, & \text{if } a = 2, b = 2. \end{cases}$$

By (108) and (109),

- $\mathbf{1}^{k-1} \otimes \chi_l \otimes \mathbf{1}^{d-k}$ is the coefficient tensor of $\phi_l(x_k) \in \text{Span}\{\mathcal{B}_{1,d}\}$;
- $u_{k-1}^* \otimes \chi_l \otimes \mathbf{1}^{d-k}$ is the coefficient tensor of $\Phi_{k-1}^*(x_1, \dots, x_{k-1})\phi_l(x_k) \in \text{Span}\{\mathcal{B}_{2,d}\}$;
- $\mathbf{1}^{k-1} \otimes \chi_l \otimes v_k^*$ is the coefficient tensor of $\phi_l(x_k)\Psi_k^*(x_{k+1}, \dots, x_d) \in \text{Span}\{\mathcal{B}_{2,d}\}$;
- $u_{k-1}^* \otimes \chi_l \otimes v_k^*$ is the coefficient tensor of $\Phi_{k-1}^*(x_1, \dots, x_{k-1})\phi_l(x_k)\Psi_k^*(x_{k+1}, \dots, x_d) \in \text{Span}\{\mathcal{B}_{3,d}\}$.

Step 1. Suppose $s \geq 3$. By Lemma 14,

- $\langle c^* - \hat{c}[s], \mathbf{1}^{k-1} \otimes \chi_l \otimes \mathbf{1}^{d-k} \rangle = \langle p^* - \hat{p}, \phi_l^k \rangle$;
- $\langle c^* - \hat{c}[s], u_{k-1}^* \otimes \chi_l \otimes \mathbf{1}^{d-k} \rangle = \langle p^* - \hat{p}, \Phi_{k-1}^* \phi_l^k \rangle$;
- $\langle c^* - \hat{c}[s], \mathbf{1}^{k-1} \otimes \chi_l \otimes v_k^* \rangle = \langle p^* - \hat{p}, \phi_l^k \Psi_k^* \rangle$;
- $\langle c^* - \hat{c}[s], u_{k-1}^* \otimes \chi_l \otimes v_k^* \rangle = \langle p^* - \hat{p}, \Phi_{k-1}^* \phi_l^k \Psi_k^* \rangle$.

This immediately leads to (118).

Step 2. Suppose $s = 2$. Note that $\Phi_{k-1}^* \phi_l^k \Psi_k^* \in \text{Span}\{\mathcal{B}_{3,d}\}$. By Lemma 14, $\langle p^* - \hat{p}, \Phi_{k-1}^* \phi_l^k \Psi_k^* \rangle = 0$. The rest of the calculations are the same as **Step 1**. \square

Lemma 14. *Suppose p^* satisfies (38), and $\hat{c}[s]$ is the s -cluster coefficient tensor estimator of p^* in Definition 1, where $2 \leq s \leq d$. Suppose $t \in \{1, \dots, d\}$ and $F : \mathbb{R}^d \rightarrow \mathbb{R}$ is any function such that $F \in \text{Span}\{\mathcal{B}_{t,d}\}$. Let $f \in \mathbb{R}^{n^d}$ be the coefficient tensor of F as*

$$f(l_1, \dots, l_d) := \langle F, \phi_{l_1}^1 \cdots \phi_{l_d}^d \rangle \quad \text{for } 1 \leq l_1, \dots, l_d \leq n.$$

Then

$$\langle c^* - \hat{c}[s], f \rangle = \begin{cases} 0, & \text{if } t > s; \\ \langle p^* - \hat{p}, F \rangle, & \text{if } t \leq s. \end{cases}$$

Proof. Observe that by orthogonality of $\{\mathcal{B}_{j,d}\}_{j=1}^d$

$$\begin{aligned}
\langle c^* - \hat{c}[s], f \rangle &= \sum_{l_1, \dots, l_d=1}^n (c^* - \hat{c}[s])(l_1, \dots, l_d) \cdot f(l_1, \dots, l_d) \\
&= \sum_{l_1, \dots, l_d=1}^n \langle p^* - \hat{p}_s, \phi_{l_1}^1 \cdots \phi_{l_d}^d \rangle \langle F, \phi_{l_1}^1 \cdots \phi_{l_d}^d \rangle \\
&= \sum_{\varphi_0 \in \mathcal{B}_{0,d}} \langle p^* - \hat{p}_s, \varphi_0 \rangle \langle F, \varphi_0 \rangle + \cdots + \sum_{\varphi_d \in \mathcal{B}_{d,d}} \langle p^* - \hat{p}_s, \varphi_d \rangle \langle F, \varphi_d \rangle \\
&= \sum_{\varphi_0 \in \mathcal{B}_{0,d}} \langle p^* - \hat{p}_s, \varphi_0 \rangle \langle F, \varphi_0 \rangle + \cdots + \sum_{\varphi_s \in \mathcal{B}_{s,d}} \langle p^* - \hat{p}_s, \varphi_s \rangle \langle F, \varphi_s \rangle. \tag{120}
\end{aligned}$$

where in the second equality, \hat{p}_s is defined in (50), the last equality follows the observation that $p^* \in \text{Span}\{\mathcal{B}_{j,d}\}_{j=0}^1$ and $\hat{p}_s \in \text{Span}\{\mathcal{B}_{j,d}\}_{j=0}^s$ with $s \geq 2$. Therefore,

- If $t > s$, then $\langle F, \varphi_s \rangle = 0$ when $\varphi_s \in \mathcal{B}_{s,d}$. So in this case (120) = 0;
- If $t \leq s$, then (120) = $\langle p^* - \hat{p}, F \rangle$ by Lemma 15.

□

Lemma 15. *Let Ω be a measurable set in arbitrary dimension. Let $\{\psi_k\}_{k=1}^\infty$ be a collection of orthonormal basis in $L_2(\Omega)$ and let \mathcal{M} be a m -dimensional linear subspace of $L_2(\Omega)$ such that*

$$\mathcal{M} = \text{Span}\{\psi_k\}_{k=1}^m.$$

Suppose $F, G \in \mathcal{M}$. Denote $\langle F, G \rangle = \int_\Omega F(x)G(x)dx$. Then

$$\langle F, G \rangle = \sum_{k=1}^m \langle F, \psi_k \rangle \langle G, \psi_k \rangle.$$

Proof. It suffices to observe that

$$\langle F, G \rangle = \sum_{k=1}^\infty \langle F, \psi_k \rangle \langle G, \psi_k \rangle = \sum_{k=1}^m \langle F, \psi_k \rangle \langle G, \psi_k \rangle,$$

where the first equality follows from the assumption that $\{\psi_k\}_{k=1}^\infty$ is a complete basis, and the second equality follows from the fact that $F \in \mathcal{M}$, and so $\langle F, \psi_k \rangle = 0$ if $k > m$. □

Lemma 16. *Suppose that $\{x^{(i)}\}_{i=1}^N$ are independently sampled from the density $p^* : \mathbb{R}^d \rightarrow \mathbb{R}^+$. Denote the empirical distribution $\hat{p}(x) = \frac{1}{N} \sum_{i=1}^N \delta_{x^{(i)}}(x)$. Let $\varphi : \mathbb{R}^d \rightarrow \mathbb{R}$ be any non-random function. Then*

$$\mathbb{P}(|\langle \hat{p} - p^*, \varphi \rangle| \geq t) \leq 2 \exp\left(\frac{-Nt^2}{\|p^*\|_\infty \|\varphi\|_{L_2([0,1]^d)}^2 + \|\varphi\|_\infty t}\right).$$

Proof. It suffices to apply the Bernstein's inequality to the random variable $\langle \hat{p} - p^*, \varphi \rangle$. Observe that $\langle \hat{p} - p^*, \varphi \rangle = \frac{1}{N} \sum_{i=1}^N [\varphi(x^{(i)}) - \mathbb{E}[\varphi(x^{(i)})]]$. Since

$$\mathbb{E}([\varphi(x^{(i)}) - \mathbb{E}[\varphi(x^{(i)})]]^2) = \text{Var}[\varphi(x^{(i)})] \leq \mathbb{E}(\varphi^2(x^{(i)})) = \int \varphi^2(x)p^*(x)dx \leq \|\varphi\|_{L_2([0,1]^d)}^2 \|p^*\|_\infty$$

and that $\|\varphi(x^{(i)}) - \mathbb{E}[\varphi(x^{(i)})]\|_\infty \leq 2\|\varphi\|_\infty$, the desired result follows immediately from the Bernstein's inequality. □

C.6 Orthonormal matrices

Lemma 17. *Suppose $M \in \mathbb{R}^{n \times m}$ and $V \in \mathbb{O}^{n \times a}$ in the sense that $V^T V = I_a$. Suppose in addition that $V^T M = U \Sigma W^T$ is the SVD of $V^T M$, where $U \in \mathbb{O}^{a \times r}$, $\Sigma \in \mathbb{R}^{r \times r}$ and $W \in \mathbb{O}^{r \times m}$. Then*

$$V V^T M = (V U) \Sigma W^T \quad (121)$$

is the SVD of $V V^T M$. In particular, $\text{Rank}(V^T M) = \text{Rank}(V V^T M)$ and $\sigma_j(V^T M) = \sigma_j(V V^T M)$ for all $1 \leq j \leq \text{Rank}(V^T M)$.

Proof. Note that

$$(V U)^T V U = U^T V^T V U = U^T I_a U = U^T U = I_r.$$

Therefore $V U \in \mathbb{O}^{n \times r}$. Consequently, (121) holds by the uniqueness of SVD. Since the singular values both $V^T M$ and $V V^T M$ are both determined by Σ , the desired results follow. \square

Lemma 18. *Suppose $M \in \mathbb{R}^{n \times m}$ such that $\text{Rank}(M) = r$. Suppose in addition that $U \in \mathbb{O}^{n \times r}$ and that $\sigma_r(M) > 2 \|U U^T M - M\|_F$. Then*

- $\text{Rank}(U U^T M) = \text{Rank}(U^T M) = r$;
- $\text{Row}(M) = \text{Row}(U U^T M)$;
- $\sigma_r(U^T M) = \sigma_r(U U^T M) \geq \frac{\sigma_r(M)}{2}$.
- $U U^T$ is the projection matrix onto $\text{Col}(U U^T M)$. In other words, the column vectors of U form a basis for $\text{Col}(U U^T M)$.

Proof. Note that $\text{Row}(U U^T M) \subset \text{Row}(M)$. In addition, by Theorem 2,

$$\sigma_r(U U^T M) \geq \sigma_r(M) - \|U U^T M - M\|_F > 0.$$

So $\text{Rank}(U U^T M) \geq r$. Therefore $\dim(\text{Row}(U U^T M)) \geq r$. Since $\text{Row}(U U^T M) \subset \text{Row}(M)$ and $\dim(\text{Row}(M)) = \text{Rank}(M) = r$, it follows that

$$\text{Row}(U U^T M) = \text{Row}(M) \quad \text{and} \quad \text{Rank}(U U^T M) = r.$$

By Lemma 17, $\text{Rank}(U^T M) = \text{Rank}(U U^T M) = r$. In addition,

$$\sigma_r(U^T M) = \sigma_r(U U^T M) \geq \sigma_r(M) - \|U U^T M - M\|_F \geq \frac{\sigma_r(M)}{2},$$

where the equality follows from Lemma 17, and the first inequality follows from by Theorem 2.

Denote $U = [u_1, \dots, u_r]$, where $\{u_k\}_{k=1}^r$ are orthogonal. Then

$$\text{Col}(U U^T M) \subset \text{Span}\{u_k\}_{k=1}^r.$$

Since $\dim(\text{Span}\{u_k\}_{k=1}^r) = \dim(\text{Col}(U U^T M)) = r$, it follows that $\text{Span}\{u_k\}_{k=1}^r = \text{Col}(U U^T M)$. Consequently $\{u_k\}_{k=1}^r$ form a basis for $\text{Col}(U U^T M)$. \square

Lemma 19. Let $m, n, r, s \in \mathbb{Z}^+$ be positive integers. Suppose $U \in \mathbb{O}^{m \times r}$ and $W \in \mathbb{O}^{n \times s}$. Then $U \otimes W \in \mathbb{O}^{mn \times rs}$.

Proof. It suffices to observe that

$$(U \otimes W)^T(U \otimes W) = (U^T \otimes W^T)(U \otimes W) = U^T U \otimes W^T W = I_r \otimes I_s = I_{rs}.$$

□

Lemma 20. Let $m, r, s \in \mathbb{Z}^+$ be positive integers. Suppose $U \in \mathbb{O}^{m \times r}$ and $V \in \mathbb{O}^{rn \times s}$. Then $(U \otimes I_n)V \in \mathbb{O}^{mn \times s}$.

Proof. It suffices to observe that

$$\begin{aligned} [(U \otimes I_n)V]^T(U \otimes I_n)V &= V^T(U^T \otimes I_n)(U \otimes I_n)V = V^T(U^T U \otimes I_n)V \\ &= V^T(I_r \otimes I_n)V = V^T I_{rn} V = I_s. \end{aligned}$$

□

Lemma 21. Let $l, m, n, r \in \mathbb{Z}^+$ be positive integers. Let $U \in \mathbb{O}^{m \times r}$ and $U_\perp \in \mathbb{O}^{m \times (n-r)}$ be the orthogonal complement matrix of U . Then

$$(U \otimes I_l)_\perp = U_\perp \otimes I_l.$$

Proof. It suffices to note that $U_\perp \otimes I_l \in \mathbb{O}^{ml \times (n-r)l}$ and that $\langle U \otimes I_l, U_\perp \otimes I_l \rangle = 0$.

□

C.7 Matrix perturbation bound

Theorem 2. Let A, \hat{A} and E be three matrices in $\mathbb{R}^{n \times m}$ and that $\hat{A} = A + E$. Then

$$|\sigma_r(A) - \sigma_r(\hat{A})| \leq \|E\|_2.$$

Proof. This is the well-known Weyl's inequality for singular values.

□

Theorem 3. Let A, \hat{A} and E be three matrices in $\mathbb{R}^{n \times m}$ and that $\hat{A} = A + E$. Suppose the SVD of A, \hat{A} satisfies

$$A = [U \quad U_\perp] \begin{bmatrix} \Sigma_1 & 0 \\ 0 & \Sigma_2 \end{bmatrix} \begin{bmatrix} V^T \\ V_\perp^T \end{bmatrix}, \quad \hat{A} = [\hat{U} \quad \hat{U}_\perp] \begin{bmatrix} \hat{\Sigma}_1 & 0 \\ 0 & \hat{\Sigma}_2 \end{bmatrix} \begin{bmatrix} \hat{V}^T \\ \hat{V}_\perp^T \end{bmatrix}.$$

Here $r \leq \min\{n, m\}$, and $\Sigma_1, \hat{\Sigma}_1 \in \mathbb{R}^{r \times r}$ contain the leading r singular values of A and \hat{A} respectively. If $\sigma_r(A) - \sigma_{r+1}(A) - \|E\|_2 > 0$, then

$$\|UU^T - \hat{U}\hat{U}^T\|_2 \leq \frac{2\|E\|_2}{\sigma_r(A) - \sigma_{r+1}(A) - \|E\|_2}.$$

Proof. This is the well-known Wedin's theorem.

□

Lemma 22. Let A , \hat{A} and E be three matrices in $\mathbb{R}^{n \times m}$ and that $\hat{A} = A + E$. Suppose the SVD of A , \hat{A} satisfies

$$A = [U \ U_{\perp}] \begin{bmatrix} \Sigma_1 & 0 \\ 0 & \Sigma_2 \end{bmatrix} \begin{bmatrix} V^T \\ V_{\perp}^T \end{bmatrix}, \quad \hat{A} = [\hat{U} \ \hat{U}_{\perp}] \begin{bmatrix} \hat{\Sigma}_1 & 0 \\ 0 & \hat{\Sigma}_2 \end{bmatrix} \begin{bmatrix} \hat{V}^T \\ \hat{V}_{\perp}^T \end{bmatrix}.$$

Here $r \leq \min\{n, m\}$, and $\Sigma_1, \hat{\Sigma}_1 \in \mathbb{R}^{r \times r}$ contain the leading r singular values of A and \hat{A} respectively. Denote

$$\alpha = \sigma_{\min}(U^T \hat{A} V), \quad \beta = \|U_{\perp}^T \hat{A} V_{\perp}\|_2, \quad z_{21} = \|U_{\perp}^T E V\|_2, \quad \text{and} \quad z_{12} = \|U^T E V_{\perp}\|_2,$$

If $\alpha^2 \geq \beta^2 + \min\{z_{21}^2, z_{12}^2\}$, then

$$\|UU^T - \hat{U}\hat{U}^T\|_2 \leq \frac{\alpha z_{21} + \beta z_{12}}{\alpha^2 - \beta^2 - \min\{z_{21}^2, z_{12}^2\}}.$$

Proof. See Theorem 1 of [Cai and Zhang \(2018\)](#). □

Corollary 3. Let A , \hat{A} and E be three matrices in $\mathbb{R}^{n \times m}$ and that $\hat{A} = A + E$. Suppose $\text{Rank}(A) = r$ and $\sigma_r(A) \geq 4\|E\|_2$. Write the SVD of A , \hat{A} as

$$A = [U \ U_{\perp}] \begin{bmatrix} \Sigma_1 & 0 \\ 0 & 0 \end{bmatrix} \begin{bmatrix} V^T \\ V_{\perp}^T \end{bmatrix}, \quad \hat{A} = [\hat{U} \ \hat{U}_{\perp}] \begin{bmatrix} \hat{\Sigma}_1 & 0 \\ 0 & \hat{\Sigma}_2 \end{bmatrix} \begin{bmatrix} \hat{V}^T \\ \hat{V}_{\perp}^T \end{bmatrix} \quad (122)$$

where $\Sigma_1, \hat{\Sigma}_1 \in \mathbb{R}^{r \times r}$ contain the leading r singular values of A and \hat{A} respectively. The for any $\tilde{U} \in \mathbb{O}^{n \times r}$, $\tilde{V} \in \mathbb{O}^{m \times r}$ such that

$$\tilde{U}\tilde{U}^T = UU^T \quad \text{and} \quad \tilde{V}\tilde{V}^T = VV^T,$$

there exists a universal constant C such that

$$\|\tilde{U}\tilde{U}^T - \hat{U}\hat{U}^T\|_2 \leq C \left(\frac{\|E\tilde{V}\|_2}{\sigma_r(A)} + \frac{\|E\|_2^2}{\sigma_r^2(A)} \right). \quad (123)$$

Proof. Let $\alpha, \alpha, z_{21}, z_{12}$ be defined as in Lemma 22. Observe that

$$\alpha = \sigma_{\min}(U^T \hat{A} V) = \sigma_r(U^T \hat{A} V) = \sigma_r(UU^T \hat{A} VV^T) = \sigma_r(UU^T (A + E) VV^T)$$

where the second equality follows from the fact that $U^T \hat{A} V \in \mathbb{R}^{r \times r}$, and the second equality follows from Lemma 17. So by Theorem 2,

$$|\alpha - \sigma_r(A)| \leq \|UU^T E VV^T\|_2 = \|E\tilde{V}\tilde{V}^T\|_2 = \|E\tilde{V}\|_2 \quad (124)$$

In addition, since $\text{Rank}(A) = r$, it holds that $U_{\perp}^T A V_{\perp} = 0$. Therefore,

$$\beta = \|U_{\perp}^T (A + E) V_{\perp}\|_2 = \|U_{\perp}^T E V_{\perp}\|_2 \leq \|E\|_2.$$

In addition, we have that $z_{12} \leq \|E\|_2$ and that

$$z_{21} \leq \|E V\|_2 = \|E V V^T\|_2 = \|E\tilde{V}\tilde{V}^T\|_2 = \|E\tilde{V}\|_2,$$

where the first and the last equality both follow from Lemma 17. Consequently

$$\begin{aligned}\alpha^2 - \beta^2 - \min\{z_{21}^2, z_{12}^2\} &\geq \frac{1}{2}\sigma_r^2(A) - 2\|E\tilde{V}\|_2^2 - \|E\|_2^2 - \|E\|_2^2 \\ &\geq \frac{1}{2}\sigma_r^2(A) - 4\|E\|_2^2 \geq \frac{1}{4}\sigma_r^2(A),\end{aligned}$$

where the first inequality follows from (124), the second inequality follows from $\|E\tilde{V}\|_2 \leq \|E\|_2$, and the last inequality follows from $\sigma_r(A) \geq 4\|E\|_2$. Therefore by Lemma 22,

$$\begin{aligned}\|\tilde{U}\tilde{U}^T - \hat{U}\hat{U}^T\|_2 &= \|UU^T - \hat{U}\hat{U}^T\|_2 \leq \frac{\alpha z_{21} + \beta z_{12}}{\alpha^2 - \beta^2 - \min\{z_{21}^2, z_{12}^2\}} \\ &\leq \frac{(\sigma_r(A) + \|E\tilde{V}\|_2)\|E\tilde{V}\|_2 + \|E\|_2^2}{\frac{1}{4}\sigma_r^2(A)} \leq \frac{4\|E\tilde{V}\|_2}{\sigma_r(A)} + \frac{8\|E\|_2^2}{\sigma_r^2(A)},\end{aligned}$$

where $\|E\tilde{V}\|_2 \leq \|E\|_2$ is used in the last inequality. \square

C.8 Polynomial Approximation Theory

Let $C^{\beta_0}([0, 1])$ denote the class of functions with continuous derivatives up to order $\beta_0 \geq 1$.

Theorem 4. *For any $f \in C^{\beta_0}([0, 1])$, there exists a polynomial p_f of degree at most n such that*

$$\|f - p_f\|_\infty \leq C\|f^{(\beta_0)}\|_\infty n^{-\beta_0}, \quad (125)$$

where C is an absolute constant which does not depend on f .

Proof. This is the well-known Jackson's Theorem for polynomial approximation. See Section 7.2 of DeVore and Lorentz (1993) for a proof. \square

Corollary 4. *Let $f \in C^{\beta_0}([0, 1])$. Denote \mathcal{S}_n the class of polynomial up degree n on $[0, 1]$, and \mathcal{P}_n the projection operator from $L_2([0, 1])$ to \mathcal{S}_n respect to L_2 norm. Then there exists a constant C which does not depend on f such that*

$$\|f - \mathcal{P}_n(f)\|_{L_2([0,1])} \leq C\|f^{(\beta_0)}\|_\infty n^{-\beta_0}.$$

Proof. Let p_f be the polynomial satisfying (125). Then

$$\|f - \mathcal{P}_n(f)\|_{L_2([0,1])} \leq \|f - p_f\|_{L_2([0,1])} \leq \|f - p_f\|_\infty \leq C\|f^{(\beta_0)}\|_\infty n^{-\beta_0}.$$

\square

Theorem 5. *Let $f \in C^{\beta_0}([0, 1])$. Denote \mathcal{S}_n the class of polynomial up degree n on $[0, 1]$, and \mathcal{P}_n the projection operator from $L_2([0, 1])$ to \mathcal{S}_n respect to L_2 norm. Then there exists an constant C only depending on f such that*

$$\|f - \mathcal{P}_n(f)\|_\infty \leq Cn^{-\beta_0}.$$

Proof. See Theorem 4.8 of Wang (2021). \square